ABSTRACT

Title of Document:	**A BAYESIAN FRAMEWORK FOR STRUCTURAL HEALTH MANAGEMENT USING ACOUSTIC EMISSION MONITORING AND PERIODIC INSPECTIONS**
	Masoud Rabiei, Ph.D., 2011
Directed By:	**Professor Mohammad Modarres, Department of Mechanical Engineering**

Many aerospace and civil infrastructures currently in service are at or beyond their design service-life limit. The ability to assess and predict their state of damage is critical in ensuring the structural integrity of such aging structures. The empirical models used for crack growth prediction suffer from various uncertainties; these models are often based on idealized theories and simplistic assumptions and may fail to capture the underlying physics of the complex failure mechanisms. The other source of uncertainty is the scarcity of relevant material-level test data required to estimate the parameters of empirical models.

To avoid in-service failure, the structures must be inspected routinely to ensure no damage of significant size is present in the structure. Currently, the structure has to be taken off line and partly disassembled to expose the critical areas for nondestructive inspection (NDI). This is an expensive and time-consuming process.

Structural health monitoring (SHM) is an emerging research area for online assessment of structural integrity using appropriate NDI technology. SHM could have a major contribution to the structural diagnosis and prognosis.

Empirical models, offline periodic inspections and online SHM systems can each provide an independent assessment of the structural integrity; in this research, a novel structural health management framework is proposed in which the Bayesian knowledge fusion technique is used to combine the information from all sources mentioned above in a systematic manner.

This work focuses on monitoring fatigue crack growth in metallic structures using acoustic emission (AE) technology. Fatigue crack growth tests with real-time acoustic emissions monitoring are conducted on CT specimens made of 7075 aluminum. Proper filtration of the resulting AE signals reveals a log-linear relationship between fracture parameters (da/dN and ΔK) and select AE features; a flexible statistical model is developed to describe the relationship between these parameters.

Bayesian regression technique is used to estimate the model parameters using experimental data. The model is then used to calculate two important quantities that can be used for structural health management: (a) an AE-based instantaneous damage severity index, and (b) an AE-based estimate of the crack size distribution at a given point in time, assuming a known initial crack size distribution.

Finally, recursive Bayesian estimation is used for online integration of the structural health assessment information obtained from various sources mentioned above. The evidence used in Bayesian updating can be observed crack sizes and/or crack growth

rate observations. The outcome of this approach is updated crack size distribution as well as updated model parameters. The model with updated parameters is then used for prognosis given an assumed future usage profile.

A BAYESIAN FRAMEWORK FOR STRUCTURAL HEALTH MANAGEMENT USING ACOUSTIC EMISSION MONITORING AND PERIODIC INSPECTIONS

By

Masoud Rabiei

Dissertation submitted to the Faculty of the Graduate School of the
University of Maryland, College Park, in partial fulfillment
of the requirements for the degree of
Doctor of Philosophy
2011

Advisory Committee:
Professor Mohammad Modarres, Chair
Professor Gregory Baecher
Professor Hugh Bruck
Dr. Paul Hoffman
Professor Ali Mosleh

Dedication

To my parents

for letting me pursue my dreams

for so long

so far away from home

&

To my wife

for giving me

new dreams to pursue

Acknowledgements

I would like to take this opportunity to thank all the people who have contributed, in one way or another, to the successful completion of this research effort. My sincere gratitude goes to my advisor, Dr. Mohammad Modarres, for his patience, guidance, and encouragement throughout my academic endeavor.

I would like to thank all the members of my dissertation committee for their suggestions along the way: Dr. Paul Hoffman for his detailed feedback and insightful discussions, which helped us define a challenging yet manageable multi-disciplinary research problem, Dr Ali Mosleh for his valuable feedback on an initial version of this work which resulted in great improvements in the final dissertation, Dr Hugh Bruck for his help and support with the experimental part of this dissertation, and Dr Gregory Baecher for reviewing the final dissertation.

I would also like to thank all the professors who taught me so much both inside and outside the classrooms; especially, I would like to thank Dr. Abhijit Dasgupta and Dr Hugh Bruck for being truly inspirational teachers.

I would like to extend my gratitude to all my friends and colleagues at the Center for Risk and Reliability, past and present, for their valuable technical and personal support. I also thank all my dear friends for their support and encouragements throughout this journey.

Most importantly, I would like to thank my wife, Masoumeh, for her love and support; without her continuous love and sacrifice, this achievement would not have been possible.

Table of Contents

List of Tables

List of Figures

List of Notations

Symbols[1]

a	Crack size
da/dN (also referred to as $\dot{a}$)	Crack growth rate
dc/dN	AE count rate feature
ΔK	Stress intensity factor range
K_{Ic}	Fracture toughness
$N(\mu, \sigma)$	Gaussian distribution with mean μ and standard deviation σ
ΔP	Fatigue loading range
R	Fatigue loading ratio
v_k	Observation noise in Kalman filter
w_k	Process noise in Kalman filter
x_k	Vector of state variables at time step k
X_k	$X_k = \{x_1, x_2, \ldots, x_k\}$
z_k	Vector of observations at time step k
Z_k	$Z_k = \{z_1, z_2, \ldots, z_k\}$

Abbreviations

AE	Acoustic emission
SHM	Structural health monitoring
NDI	Nondestructive inspection
RUL	Remaining useful life
PoE	Probability of exceedance
PFM	Probabilistic fracture mechanics
KF	Kalman filter
EKF	Extended Kalman filter

---

[1] This is not a comprehensive list; more notations will be introduced in the text as required. When local differences occur, they are clearly indicated in the text.

Chapter 1: Introduction

1.1. *A Hybrid Approach to Structural Health Management*

The presence of cracks can significantly reduce the strength of a structure. Large cracks usually form from small flaws that are initially present in the material and eventually grow, first as small cracks and then as large ones. Many aerospace and civil infrastructures currently in service are at or beyond their design fatigue service-life limit (Wang et al. 2009); it is also expected that these structures will remain in service for an extended period.

The current approaches to ensure the structural integrity of aerospace and ground structures as well as civil infrastructure have been successful in minimizing the risk of catastrophic structural failure. The mounting costs associated with such approaches, however, have become an ongoing concern.

The ability to assess and predict the state of damage (i.e. crack size) is critical in ensuring the structural integrity of aging structures. Nondestructive inspection (NDI) techniques are used to inspect safety-critical structures, at scheduled intervals, to ensure that there are no "large" cracks in the structure. The size of the critical crack that endangers the safety of the structure depends on the type of structure and its application.

NDI inspections, as currently performed, have some important shortcomings, some of which are listed below:

- In the way inspections are currently performed, the structure has to be taken off line and partly disassembled to expose the critical areas for inspection. This is an expensive and time-consuming process.

- The disassembly and reassembly of the structure may itself induce new damages to the structure.

- Inspection of a large number of critical locations is labor-intensive; for example, the lower wing in some large aircrafts can have as many as 22000 critical fastener holes that should be inspected (Rich 1977). This process is subject to human error due to boredom and loss of focus. Missing even one hole with a large crack—undetected large cracks are often referred to as "rogue" cracks—can cause a catastrophic failure (Wang et al. 2008).

- The inspection intervals must be selected such that an undetected flaw will not grow to critical size before the next inspection. Empirical crack growth models are used to predict the size of the crack based on estimated future usage profiles until the next inspection time. These intervals are often chosen very conservatively because of the uncertainties associated with the predictions of the empirical model as well as the sensitivity and reliability of the NDI technology being used.

Structural health monitoring (SHM) is an emerging research area for online assessment of structural integrity using appropriate NDI technology (Giurgiutiu 2008). Structural health monitoring systems installed on the aging infrastructures could insure increased safety and reliability by replacing scheduled maintenance with condition-based maintenance (CBM) based on the feedback from the SHM system.

SHM could also result in cost savings by avoiding unnecessary maintenance, on one hand, and preventing unscheduled maintenance on the other hand.

Structural health monitoring could make a major contribution to structural diagnosis and prognosis: when SHM is performed in coordination with existing offline NDI practices, the structural health monitoring data collected in between current inspection intervals would provide supplementary information that would help alleviate some the problems associated with conventional offline inspection practices.

Online SHM and offline NDI inspections can complement each other; the information provided by SHM in between the scheduled intervals can be used to reassess the state of structural health in real-time. For instance, if a rogue crack is missed during a routine inspection, the SHM system may be able to detect the crack (either directly or by detecting higher-than-expected crack growth rates) before it reaches a critical length. The structure can then be taken offline for more in-depth inspection.

The empirical models used for crack growth prediction suffer from various uncertainties; these models are often based on idealized theories and simplistic assumptions and may fail to capture the underlying physics of the complex failure mechanisms. For example, if a damage mechanism that was not modeled, such as corrosion, appears in a component, then the model developed for cracks would incorrectly quantify the damage.

The other source of uncertainty is the scarcity of relevant material-level test data required to estimate the parameters of empirical models. Using insufficient data in the parameter estimation process will result in wide uncertainty bounds over the parameters that will directly affect the model predictions.

The information provided by the SHM system could potentially be used to update the model parameters in real-time based on the feedback from the structure. For instance, if corrosion is present in a structure but has been ignored in modeling, the model parameters could be updated to reflect the higher crack growth rate due to corrosion-fatigue cracking. The SHM system could also improve the model prediction by providing more accurate inputs to the model. Empirical models are highly sensitive to the initial crack size; at any given time, if the current damage state of the structure were updated via SHM information, the input to the empirical model would be updated, and, therefore, the predicted crack size based on estimated future usage profile would be more accurate as well.

1.2. *Research Objectives and Methodology*

The primary objective of this research is to provide a hybrid framework for structural health management that takes advantage of all available sources of information, including offline periodic inspections, online structural health monitoring information, and empirical damage progression models.

In this research, focus will be solely on fatigue crack growth in metallic structures. Acoustic emission (AE) monitoring will also be used as the online NDI technique to monitor the crack growth. Most of the outcomes of this research and the developed methodology, however, are general and can be applied to other failure mechanisms and NDI monitoring techniques as well.

The objectives of this research are as follows:

1- Investigate the AE technique for fatigue crack growth monitoring: The first objective is to use laboratory experiments to assess the capability of this

4

technique to detect and quantify fatigue cracks in metallic structures. The next

objective is to develop a quantitative approach to describe important fatigue

crack growth parameters by monitoring the corresponding AE parameters.

2- Develop a probabilistic risk measure that indicates the severity of structural

damage due to existence of fatigue cracks, based on information from the AE

monitoring system.

3- Develop a probabilistic approach to estimate the crack size distribution at a

given time, based on structural health monitoring information provided by the

AE technique.

4- Develop a hybrid structural health management framework based on the

following sources of information:

    a. Empirical crack growth model

    b. Structural health monitoring

    c. Periodic NDI inspections

This framework should include a prognosis module to predict the remaining

useful life (RUL) and the risk associated with further use of the structure.

In the first part of this research, the problem of monitoring fatigue crack growth using

AE technique is investigated. The outcome of this part is a statistical model that

correlates important crack growth parameters, i.e., crack growth rate, da/dN, and

stress intensity factor range, ΔK, with select AE features.

In the second part of this research, this model will be used to calculate two important

quantities that can be used for structural health management: (a) an AE-based

instantaneous damage severity index, and (b) an AE-based estimate of the crack size distribution at a given point in time, assuming a known initial crack size distribution. Finally, the outcome of the statistical model described above will be used as direct "evidence" in a recursive Bayesian estimation framework to update the model parameters as well as the estimated crack size distribution (Figure 1.1).
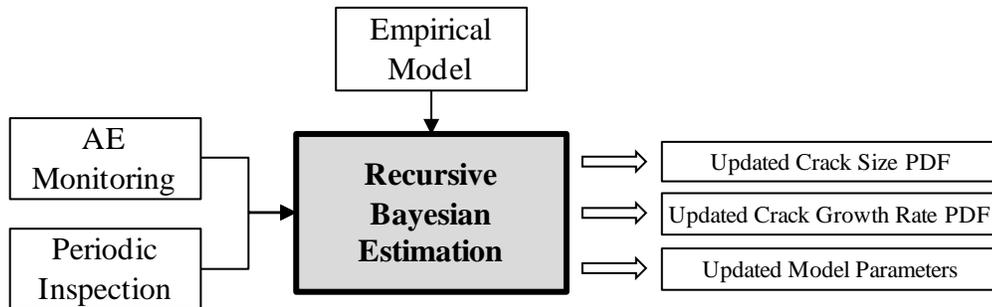
Figure 1.1 – Overview of the proposed methodology

1.3. *Scope of this Research*

Although NDI methods and practices have advanced remarkably in recent years, there are still key limitations that should be addressed. When NDI is used on actual structures, its sensitivity and reliability is determined in part by practical issues. Field inspection conditions may be quite different from standard laboratory tests; for instance, using AE monitoring in real-life applications (e.g. onboard an aircraft) is more challenging than in a laboratory due to significantly lower signal to noise ratios (SNR) and geometric complications.

This study recognizes the practical challenges that currently limit the application of AE monitoring in real-life field applications. The research objective, however, is twofold: (a) to propose practical ways to use AE technology in crack growth monitoring in a quantitative manner, and (b) to adopt the current state-of-the-art in

AE technology and demonstrate how it can play a role as an integrated part of a hybrid structural health management solution.

AE is rapidly emerging as a popular and powerful technique for structural health monitoring (Holford et al. 2009). As this technique becomes more mature and ready for fielded applications, advanced integration solutions, such as those developed in this dissertation, will become increasingly important.

1.4. *Outline of this Dissertation*

The remainder of this dissertation is organized into five chapters. In Chapter 2, a brief overview of the history and the theory of AE monitoring is first presented. Next, the application of AE technology for fatigue crack growth monitoring is investigated through laboratory experiments.

Chapter 3 details the statistical model development and Bayesian regression technique. The experimental data obtained in Chapter 2 is used in this chapter to estimate the model parameters.

Chapter 4 presents two practical ways for using AE monitoring in structural health management.

In Chapter 5, different pieces of the hybrid structural health management framework developed in previous chapters are fused together in a systematic way. First, details of recursive Bayesian estimation are covered in this chapter. Next, the fusion problem at hand is formulated as a state estimation problem where AE monitoring information and the periodic inspection findings are treated as noisy observations and are used to update the crack size estimates as well as the crack growth rate estimates.

Chapter 6 presents suggested future research and lists the key contributions of this work.

Chapter 2:   Crack Growth Monitoring using Acoustic Emission

2.1. *Overview*

This chapter will first review the history and the theory of AE monitoring. It will then focus on the application of the AE technique in crack growth monitoring. It will be shown that fatigue crack growth can be detected and characterized by monitoring the AE signals generated during crack growth. The experimental setup and procedure used to investigate the relationship between crack growth parameters and the AE parameters will be explained.

This chapter provides the foundation for the remainder of this dissertation. The results obtained here will be used in the following chapters to develop a statistical model to describe the average relationship between certain crack growth parameters and AE features. The experimental data generated in this chapter will then be used to infer the parameters of such model. Once the model is fully developed, it will be used to calculate a number of SHM-related quantities (e.g. the probability of transitioning from stable crack growth to unstable crack growth as a function of applied fatigue cycles) solely based on AE signals captured in real-time monitoring of the structure.

2.2. *History of Acoustic Emission*

Acoustic emission as a technology started in the early 1950s with the work of Joseph Kaiser (Kaiser 1950). Kaiser monitored the emissions of audible sound from materials subjected to external loads and used electronic instrumentation to detect the

acoustic waves produced by metals during deformation. He and his coworkers found out that many metals, such as zinc, steel, aluminum, lead and copper, produce elastic waves under applied stress. They also discovered that acoustic emission activity was irreversible: under static loading, the acoustic emissions were not generated during reloading until the previous stress level was exceeded. This phenomenon is now known as the Kaiser effect.

In the 1960s, researchers made great improvements in the instrumentation of the acoustic emission technique. They tried to overcome the excessive background noise problem by focusing on the signals with frequencies well above the audible range. With this improvement, acoustic emission found its way into studies related to materials research, structural evaluation and nondestructive testing.

In the 1970s and 1980s—the decades in which most papers on AE were published—efforts increased to understand the fundamental physics of acoustic emission. Topics of interest were the nature of the source event, the ways elastic waves propagate in metal and the ways the signals are detected using transducers. Scientists first tried to use the techniques from earthquake engineering to model acoustic emission sources. The problem was that those techniques were mainly applicable to semi-infinite geometries. In the case of a metal plate, the problem turned out to be much more complicated due to the reflections and interference of the signals. These difficulties discouraged scientists to some extent, but AE remained a popular qualitative NDI technique for industrial applications.

The acoustic emission technique is unique among other NDI methods; AE is a passive technique which detects the energy generated inside the material due to

deformation or damage propagation. Other NDI methods, such as ultrasonic testing and eddy-current testing (i.e., active techniques), first supply the energy to the structure and then capture the material's response.

In recent years, breakthroughs in electronics and computer technology have created new possibilities for AE as a promising NDI technique. New AE measurement systems and analysis tools have been developed that enable us to significantly improve the signal to noise ratio and also extract more useful information from the AE signals. Nevertheless, interpreting the AE signals and establishing a correlation between them and the source event remains a challenge and a topic for active research.

2.3. *Theory of Acoustic Emission*

Over the past 30 years, acoustic emission technology has been a promising and effective NDI technique capable of detecting, locating and monitoring fatigue cracks in a variety of composite and metal structures such as airframes (Boller 2001). Acoustic emissions are elastic stress waves generated by a rapid release of energy from localized sources within a material under stress (Mix 2005). Acoustic emissions often originate from defect-related sources such as permanent microscopic deformation within the material and fatigue crack extension.

When a load is applied to a solid structure (e.g. by internal pressure or by external mechanical means), it begins to deform elastically. Associated with this elastic deformation are changes in the structure's stress distribution and storage of elastic strain energy. As the load increases, some permanent microscopic deformation may occur, which is accompanied by a release of stored energy, partly in the form of

11

propagating elastic waves, termed acoustic emissions (Mix 2005). Such emissions can be detected and recorded with proper instrumentation. The recorded signals can then be processed to reveal information about the properties of the source event that generated them. This makes the AE technology an excellent candidate for nondestructive monitoring of structures with active damage—i.e., damage that continues to grow under applied stress.

A typical AE monitoring system consists of an active emission source (e.g. defect) inside the material and proper AE instrumentation for signal detection and conditioning. The required hardware typically includes sensors, pre-amplifiers, and data acquisition and signal processing equipment (Figure 2.1).
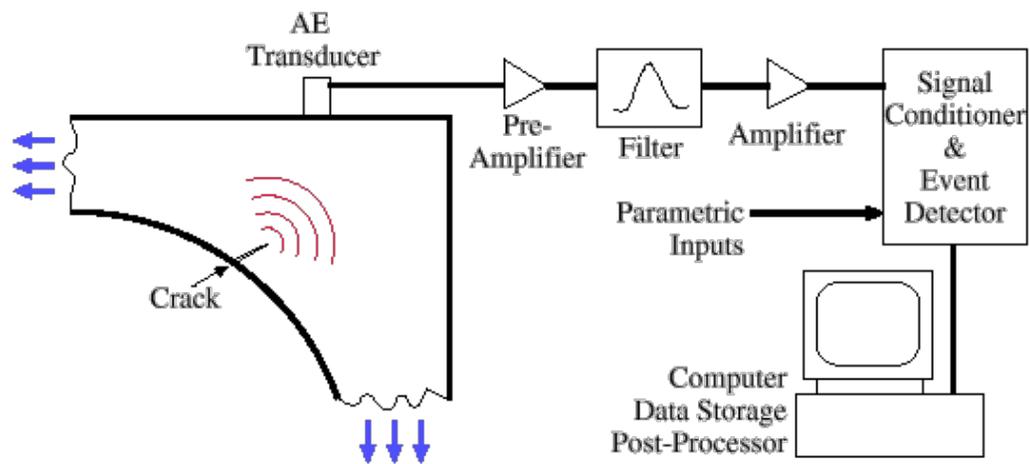
Figure 2.1 – A typical AE system (Huang et al. 1998)
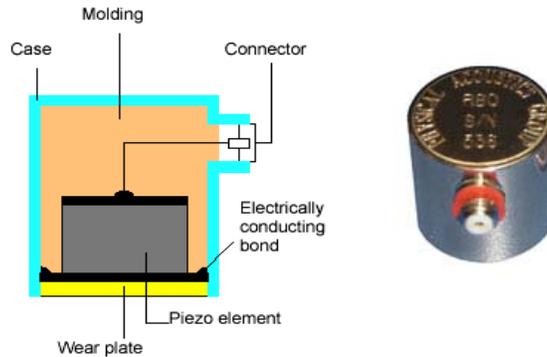
Figure 2.2 – Left: Schematic view of a typical AE sensor (Huang et al. 1998), Right: Wideband AE sensor from Physical Acoustics Corp[2].

The event at the source causes a release of energy which propagates in the form of a transient stress wave. This wave travels through the material until it reaches the sensor. The small surface displacements are captured by the sensor and converted into electric signals. The electric signal is transmitted to the pre-amplifier and subsequently to the signal processing unit. Based on the analysis techniques to be used, certain features of the signals and/or the complete waveforms are recorded.
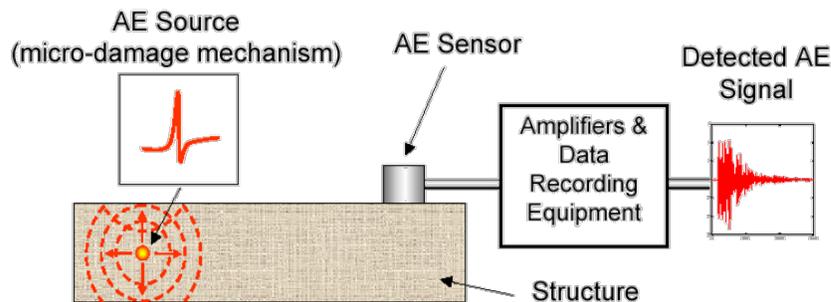
Figure 2.3 – AE burst travelling from source to sensor[3]

Considering the nature of the generating event, the acoustic emission waveform is generally considered to be a simple pulse at the source (Figure 2.3) and therefore contains a broad spectrum of frequencies. The frequency of the waves may range from tens of kHz up to tens of MHz, depending on the source (Pollock 1988; Miller

---

[2] Source: http://www.pacndt.com/index.aspx?go=products&focus=/sensors/wideband.htm
[3] Source: http://www.netcomposites.com/ikb/Topics/Defects/AE Defects Acoustic Emission/AE Brunel Modal Schematic_small.png

13

& McIntire 1987). In general, an AE signal detected by the sensor has a complex waveform (Figure 2.4). The shape of the waveform depends on both the characteristics of the AE source event and the wave propagation path (e.g. generated wave modes, wave velocity, attenuation, reflections, and signal interference). In addition to the wave propagation behavior, the waveform is also affected by the sensor response. When a sensor receives a broadband transient pulse, it is excited at its own natural frequencies of oscillation, which depend on the type of sensor used in an application. These two effects, i.e., the material response and sensor response, can cause the signals received by the sensor to be significantly different from the original pulses emitted by the source.

In recent years, AE research has focused on two main areas. The first area has to do with characterizing the wave propagation through complex geometries; due to all the complications described above, plus the fact that the AE source is not controlled by the operator, this has proved to be an extremely difficult problem. The second area of research is concerned with processing the AE waveforms in an intelligent way (depending on the application) in order to extract useful information that can be traced back to the source event (Holford et al. 2009). The approach in this chapter is in line with the second area; we first detect and isolate crack growth-related AE events and then attempt to establish a correlation between extracted AE features and fracture parameters. Figure 2.4 shows some important features that are typically extracted from AE signals.
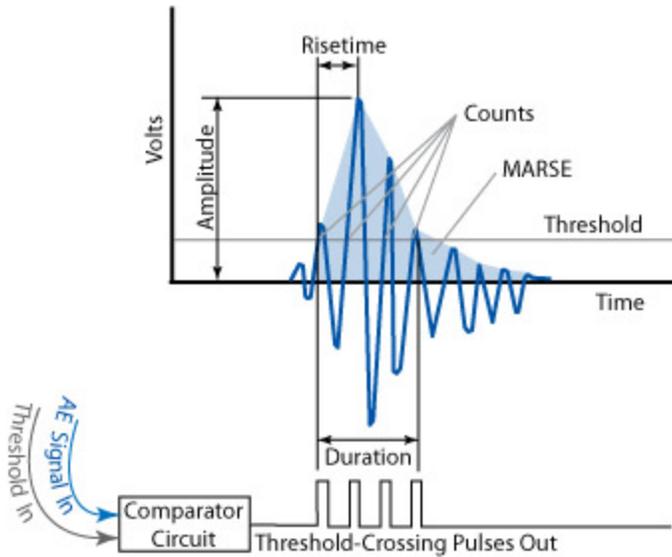
Figure 2.4 – Important features typically extracted from AE signals[4]

2.4. *AE Monitoring for Fatigue Crack Growth*

Fatigue crack growth is a well-known source of acoustic emission inside materials. If the crack-related AE signals (i.e. those that are directly attributed to gradual propagation of the crack tip) can be isolated from all other spurious sources of AE (e.g. friction between crack surfaces), it will be possible to use the information extracted from such signals to characterize the crack growth phenomenon.

Several researchers have studied the connection between fatigue crack growth behavior and the resulting acoustic emissions (Hamel et al. 1981; Bassim et al. 1994). Certain features of acoustic emission signals are stochastically correlated with key fatigue parameters, such as stress intensity factor range, ΔK, and crack growth rate, da/dN. Two of the most commonly used AE parameters in fatigue are the AE count c and its derivative, count rate dc/dN. For a given AE signal, c is defined as the number of times that the signal amplitude exceeds a predefined threshold value.

---

[4] Source: http://www.ndt-ed.org/EducationResources/CommunityCollege/OtherMethods/AE

15

Accordingly, dc/dN is defined as the derivative of c with respect to time (measured as elapsed fatigue cycles).

The following form has been proposed by (Bassim et al. 1994) for the relationship between dc/dN and ΔK:

$$\frac{dc}{dN} = A_1(\Delta K)^{A_2} \qquad (2.1)$$

where A_1 and A_2 are the model parameters, which mainly depend on material properties and should be determined experimentally.

Our goal is to use the AE parameter as the predictor to estimate the fatigue parameter; therefore, (2.1) is solved for ΔK as follows (Rabiei et al. 2009):

$$\Delta K = A_1^{-1/A_2}\left(\frac{dc}{dN}\right)^{1/A_2} \qquad (2.2)$$

Taking log from both sides of (2.2) yield a linear relationship:

$$\log \Delta K = \alpha_1 \log\left(\frac{dc}{dN}\right) + \alpha_2 \qquad (2.3)$$

where $\alpha_1 = A_1^{-1/A_2}$ and $\alpha_2 = 1/A_2$ are the new model constants to be estimated from data.

The significance of (2.3) is that once the model parameters are determined experimentally, this equation can be used to estimate ΔK by monitoring the acoustic emissions and extracting the dc/dN parameter from the observed signals—thus obviating the need for complex modeling and calculations used in fracture mechanics to calculate ΔK.

Stress intensity factor is a parameter that can be considered an aggregate driving force for fatigue crack growth. The fracture toughness, K_{Ic}, on the other hand, can be thought of as a measure of a material's resistance to stable crack propagation under

cyclic loading (T. L. Anderson 1994). The value of ΔK depends on the geometry, stress amplitude and the instantaneous size of the crack. For a given geometry, a large ΔK represents either a large crack size and/or a high stress amplitude range applied to the structure. The crack growth is stable as long as K_{max} is less than the fracture toughness of the material K_{Ic} (Figure 2.5).
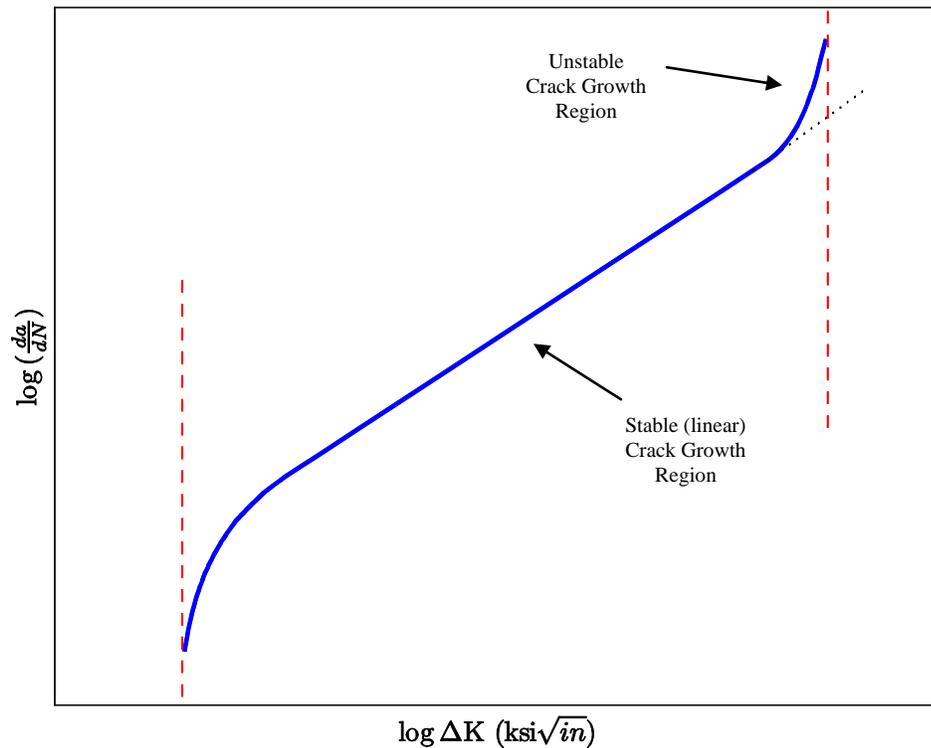
Figure 2.5 – Schematic of crack growth sigmoid curve showing both stable and unstable crack growth regions.

This fact will be used to define an AE-based measure of risk for transitioning from the stable to unstable crack growth regime and ultimately to failure.

The second parameter that will be estimated via AE monitoring is the crack growth rate, da/dN. Based on the well-known Paris equation (Paris & Erdogan 1963) in fracture mechanics, da/dN is expected to have a log-linear relationship with ΔK while the crack growth is in the stable region. According to (2.3), ΔK itself has a

log-linear relationship with AE parameter dc/dN, which results in the following equation:

$$\log\left(\frac{da}{dN}\right) = \beta_1 \log\left(\frac{dc}{dN}\right) + \beta_2 \qquad\qquad (\,2.4\,)$$

where β_1 and β_2 are the model parameters that describe the log-linear relationship between da/dN and dc/dN. From a structural monitoring perspective, this relationship means that on average, the rate of crack growth can be estimated solely based on features extracted from AE signals. This is a significant outcome because by knowing the rate of the crack growth and the initial crack size, the size of the crack can be estimated at any given time without knowing the applied load history or complex ΔK calculations. This fact will be used to develop an AE-based crack growth model that can predict the crack size as a function of observed AE signals. The outcome of this model will be used as evidence in a Bayesian updating process to obtain improved prognosis results.

To study the relationship between fatigue crack growth and the resulting acoustic emissions, a series of experiments were designed and performed in a controlled laboratory environment. In the next section, the experimental procedures, including fatigue testing, crack length measurement, AE monitoring and the required signal processing will be presented.

2.5. *Experimental Setup and Procedure*

In the previous section, the relationship between fatigue crack growth and the resulting acoustic emission signals was presented. Here we describe the experimental setup that was developed as part of this research to validate other findings in the literature (especially the proposed relationship in (2.1)) and also to generate the

experimental data that was required for fitting the statistical model that will be introduced in the next section.

The experimental procedure in this study consists of two parts: The first part is a standard fatigue crack growth test in which a notched aluminum specimen undergoes cyclic loading, which causes a crack to initiate from the notch and grow until fracture; the second part is real-time AE monitoring—on the same specimen and while the crack is growing—to capture the AE signals resulting from the propagation of the crack inside the material.

The two parts of the experiment should run in parallel, and the results need to be synchronized to allow for further analysis of the correlation between the events. In the following section, the details of fatigue testing and the employed crack measurement technique are given, and next, the hardware and the techniques used for AE monitoring are described.

2.5.1. Fatigue Testing

Fatigue tests were carried out on standard compact tension (CT) specimens (ASTM E647-08 2008) made of 7075 aluminum alloy with dimensions W=2.5 inch and B=0.125 inch (see Figure 2.6 for all dimensions). The test setup is shown in Figure 2.7.

Using a 5 kip MTS machine, the specimen was first fatigue pre-cracked using sinusoidal loading with amplitude $\Delta P = 270\ lbf$, a min-max loading ratio $R = 0.1$ and loading frequency $f = 30$ Hz. Loading cycles were applied until a fatigue crack of adequate length and straightness (in accordance with ASTM E647) was detected.

In the main crack growth test, the pre-cracked specimen was subjected to cyclic loading with similar settings as above with the exception of loading frequency, which was reduced to 10 Hz. The lower loading frequency made it easier to distinguish and process the AE events in post-processing of the collected data. Also, the error between the load command sent from the controller to the MTS machine and the actual load applied to the specimen (measured using the load cell on the MTS) is significantly bigger for higher loading frequencies. It is therefore advisable to run the test at lower frequencies when time allows.
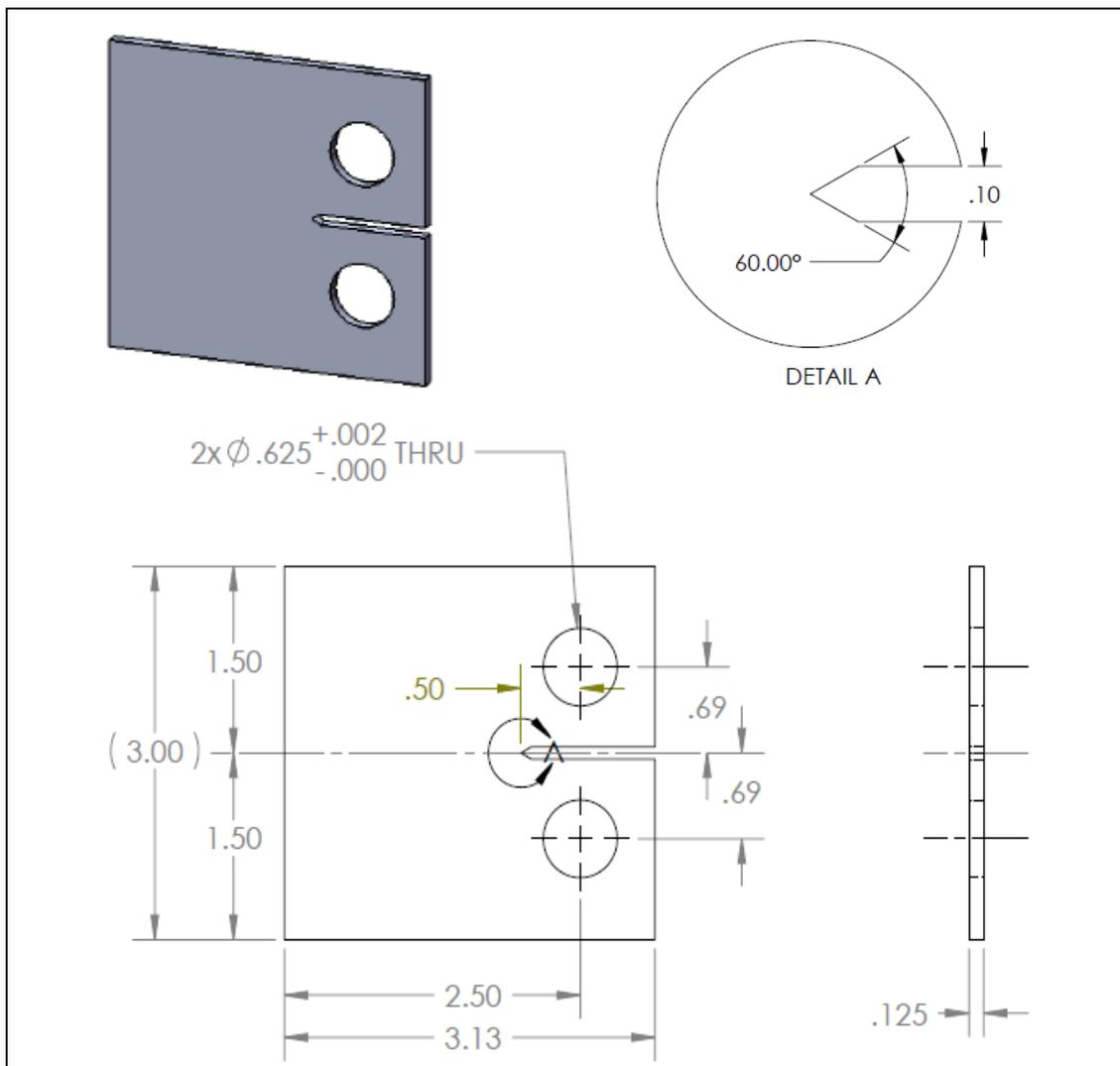
Figure 2.6 – Technical drawing of the CT specimen used in fatigue testing.
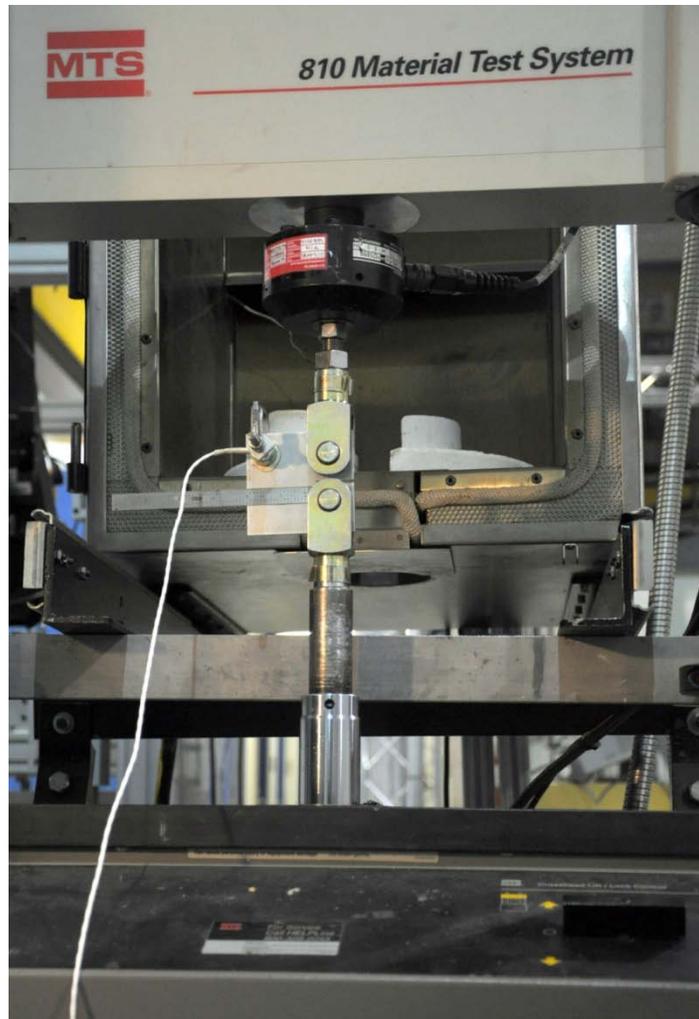
Figure 2.7 – Test setup: CT specimen instrumented with AE sensor and mounted on MTS machine.

The other important consideration in crack growth testing is to make sure that the specimen is perfectly aligned and the applied loading is symmetric so that the resulting crack will grow straight.

Crack Measurement using Digital Imaging

Throughout the experiment, macro digital photography was used for crack size measurement. In this approach, high resolution pictures of the specimen (with a scribed ruler attached to it) were automatically taken using a Digital Single-Lens

Reflex (DSLR) camera controlled by a computer (time-lapse photography technique). The complete setup is shown in Figure 2.8.

Figure 2.8 – Test setup for crack measurement using digital photography.

The time delay between taking pictures was set manually based on the rate of the crack growth; at the beginning of the test, pictures were taken every hundred cycles, whereas by the end of the test (as the crack growth rate increases) picture were taken every few cycles.

All the images are named based on the timestamp of when they were taken and stored on the computer for further processing. At the end of the experiment, all stored

images were post-processed in order to extract the length of the crack visible in each image.

As can be seen in Figure 2.9 (top), it was not very easy to pinpoint the tip of the crack in the resulting images. Therefore as the first step, all images were enhanced using the Image Processing Toolbox in MATLAB to make the crack tip in the images easier to distinguish. Using the Image Processing Toolbox, all images were first cropped such that only the crack and the ruler are visible in the image. Next, a combination of sharpening and edge detection filters were applied to the images. In the resulting image (Figure 2.9 (bottom)) the crack trajectory stands out from the background, and therefore it is much easier to pinpoint its tip and measure the length of the crack.

Once the tip of the crack was identified, the pixels in image were calibrated with respect to the ruler attached to the specimen. Taking advantage of the calibrated high-resolution images, the crack length could be measured with an accuracy of 0.01 inch. To perform the calibration and measure the size of the crack, we used a public domain Java-based image processing program called ImageJ[5]. ImageJ was developed at the National Institute of Health and is routinely used in biological image processing research applications. Using the software, the length and the angle at which the crack grew was easily recorded for each image. Table 2.1 shows an example of the crack measurement output from ImageJ.

---

[5] ImageJ can be downloaded at no charge from http://rsb.info.nih.gov/ij/
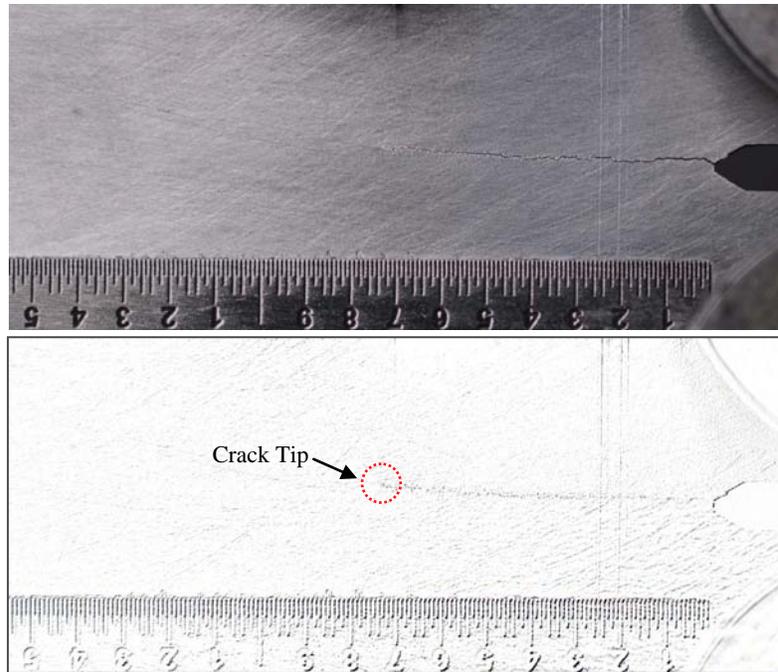
Figure 2.9 – Enhancing images via proper filtration for better detection of crack tip (Top: original, Bottom: filtered)

Table 2.1 – Example of crack measurement output from ImageJ

Measurement #	Label (time stamp)	Angle	Length (inch)
1	13-27-24.jpg	172.6	0.08
2	13-29-25.jpg	171.8	0.08
3	13-31-25.jpg	173.2	0.09
4	13-33-25.jpg	173.5	0.10
5	13-35-26.jpg	174.3	0.10
6	13-37-26.jpg	174.8	0.11
7	13-39-26.jpg	174.9	0.11
8	13-41-26.jpg	175.2	0.12
9	13-43-27.jpg	175.6	0.13
10	13-45-27.jpg	176.2	0.14

One advantage of this approach over other crack measurement techniques such as DCPD is that by taking pictures, the whole process of crack growth is captured in images and can be reviewed later if needed. For instance, a sudden change in AE activity may be attributed to a big jump in crack length or a sudden change in growth direction of the crack; it will be captured in images but lost in most other crack

measurement techniques. The approach also makes it possible to monitor the orientation of crack growth and make any necessary corrections to the crack size if the crack grows at an angle.

2.5.2. Acoustic Emission Monitoring

As mentioned before, the goal of the experiment was to record the AE signals generated by fatigue crack growth. To do so, we used a PCI-2 AE monitoring system supplied by Physical Acoustic Corporations[6] to monitor the CT specimen during the crack growth test described previously.

The AE monitoring system consists of three main parts: Sensors and amplifiers to collect and amplify the signals, a data acquisition module to perform front-end filtration and record the signals, and a software module to visualize the data and to perform the required analysis such as feature extraction and source location. In this experiment the crack location was assumed to be known, and no triangulation was necessary to locate the source of the signals; therefore, one sensor was enough to capture the signals.

The selection of the proper sensor for an application is the most important step towards successful AE monitoring. A large variety of sensors is available that can be used for AE monitoring in different applications. These sensors come in various sizes, shapes, frequency and temperature ranges, and packaging styles to meet the requirements of different applications and environments. For these experiments, we selected a high fidelity wide-band sensor manufactured by Physical Acoustics (model

---

[6] http://www.pacndt.com

WD). Table 2.2 shows the specifications of the available wideband sensors, including the selected WD model.

Table 2.2 – Specifications of wide-band sensor supplied by Physical Acoustics[7]

Model	Dimensions (dia x ht) mm	Weight (grams)	Operating Temperature (ºC)	Peak Sensitivity V/(m/s) [V/µbar] (dB)	Operating Frequency Range (kHz)
D9202B	18 x 17	**	-65 to 125	55$^+$ [-53]*	400 - 700
D9203B	18 x 17	**	-65 to 125	65$^+$ [-60]*	150 - 900
S9208	25 x 25	90	-54 to 121	45$^+$ [-85]*	200 - 1000
UT-1000	18 x 17	20	-65 to 177	64$^+$ [-73]*	100 - 950
WD	**18 x 17**	****	**-65 to 177**	**55$^+$ [-62.5]***	**100 - 900**
WDI	29 x 30	70	-35 to 75	96$^+$ [-25]*	200 - 900
WSa	19 x 21	32	-65 to 175	55$^+$ [-62]*	100 - 1000
Notes: + Denotes response to surface waves (angle of incidence transverse or parallel to face of sensor). * Denotes response to plane waves (angle of incidence normal to face of sensor). ** Sensor supplied with integral cable. Weight of sensor is not available.					

An essential requirement in mounting a sensor is sufficient acoustic coupling between the sensor and the surface of the structure. To increase the acoustic coupling, we used silicone grease as the coupling agent. It was important to make sure that the sensor's surface was smooth and clean, allowing for maximum couplant adhesion. The applied layer of couplant was also made as thin as possible while making sure that it filled the gaps caused by surface roughness to ensure good acoustic transmission. The sensor was held firmly to the testing surface at all times. To do so, custom-made C-clamps of the right size were used to hold the sensor firmly on the surface of the CT specimen during the experiment. (see Figure 2.10)

---

[7] Table adopted from Physical Acoustics website at:
http://www.pacndt.com/index.aspx?go=products&focus=sensors.htm
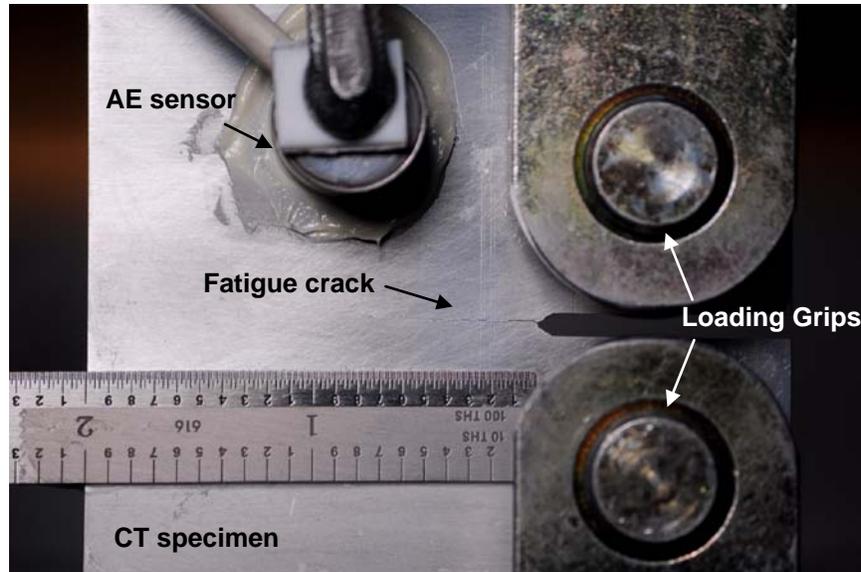
Figure 2.10 – Standard CT specimen with mounted AE sensor

Captured AE signals were first amplified using a 40 dB amplifier. Next, a 200 kHz high-pass filter was used to filter out the extraneous noise mostly from the MTS machine. Signals with amplitudes exceeding a threshold of 45 dB were transferred to a computer for feature extraction. The PCI-2 hardware was controlled via AEWin software. Many parameters were set in the software before starting data acquisition; a list of key parameters and their selected values in our experiment is given in Table 2.3.

Table 2.3 – AE Hardware settings

Parameter	Value
Preamplifier	40 dB
Peak Definition Time (PDT)	300 μs
Hit Definition Time (HDT)	500 μs
Hit Lock Time (HLT)	1000 μs
Threshold	45 dB
Sampling rate	5 MSPS
Pre-trigger length	100 μs
Hit length	614 μs
Analogue Filter (high-pass)	200 kHz
Analogue Filter (low-pass)	3 MHz

The recording of a waveform was triggered based on the selected threshold value, while the end point of a single AE hit was defined based on the parameters PDT, HDT and HLT (Figure 2.11). In other words, the end limit of each individual AE hit was defined by setting these parameters in a rather subjective manner. The proper values for these parameters are usually selected based on the specific application, using wave propagation formulae as well as trial and error using known sources of AE (such as pencil lead break). In our experiments, we consulted the experts at Physical Acoustics for proper values of these parameters based on their past experience.
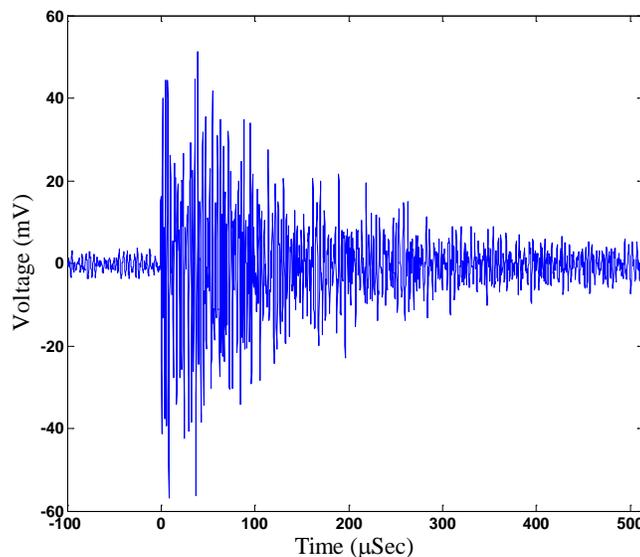
Figure 2.11 – A typical AE signal generated during fatigue crack growth

The AEWin software is capable of calculating various parameters (features) from the recorded AE signals. These features are often used to distinguish the AE signals based on their source event and are also useful in establishing correlations between AE events and other quantities of interest such as crack growth rate. Important time domain AE features include: AE hit time, AE count, amplitude, duration, energy and

28

the value of applied load when the AE hit was received. In the frequency domain, peak frequency and frequency centroid (a measure of average frequency) of the signal are the recorded features. In addition to the extracted features, the system also records full waveforms of the AE signals, which can be used for further offline processing.

2.5.3. Noise Filtration

Signals recorded during AE monitoring are often buried in noise from numerous sources. The source of the noise can be both internal (e.g., surface rubbing at loading pins, internal rubbing of crack surfaces) and external (e.g., noise from the hydraulic loading actuators).

The most crucial step in AE monitoring is to distinguish the AE signals originating from the source event of interest (e.g. crack tip) from extraneous noises. Researchers have proposed various de-noising techniques for AE signals due to crack growth (Fang & Berkovits 1993; Berkovits & Fang 1995). In these techniques, certain incoming signals are labeled as noise based on the value of some of their features. It is suggested in literature (Roberts & Talebzadeh 2003; Morton et al. 1973) that in fatigue crack growth, only events occurring near the maximum load in a cycle are associated directly with crack extension. This can be justified by the fact that the crack is much more likely to grow while the applied load is close to its maximum, and therefore the AE signals in that region are more likely to have been generated due to crack growth. In this study, the AE events occurring within the top 30% of the peak load were chosen as potential crack growth-related AE events.

The other filtration technique that was used to distinguish crack growth-related AE signals was based on the assumption that events occurring during the loading portion

of a cycle are more likely to be crack-related than those occurring during the unloading portion of the cycle.

AE features in frequency domain are also useful for blocking out unwanted signals. For instance, the hydraulic system of the MTS machine generates AE-like signals that can be filtered out based on their low frequency content. A typical crack-related AE signal is usually in the range above 200 kHz, whereas the MTS noise has lower frequency content. In our tests a 200 kHz high-pass filter was used to filter out the MTS noise. The optimal filtration threshold was determined experimentally by trial and error.

In order to make the filtration process easier and to make it possible to try other filters based on other AE features, a MATLAB GUI named AE-Discovery was developed (Figure 2.12).
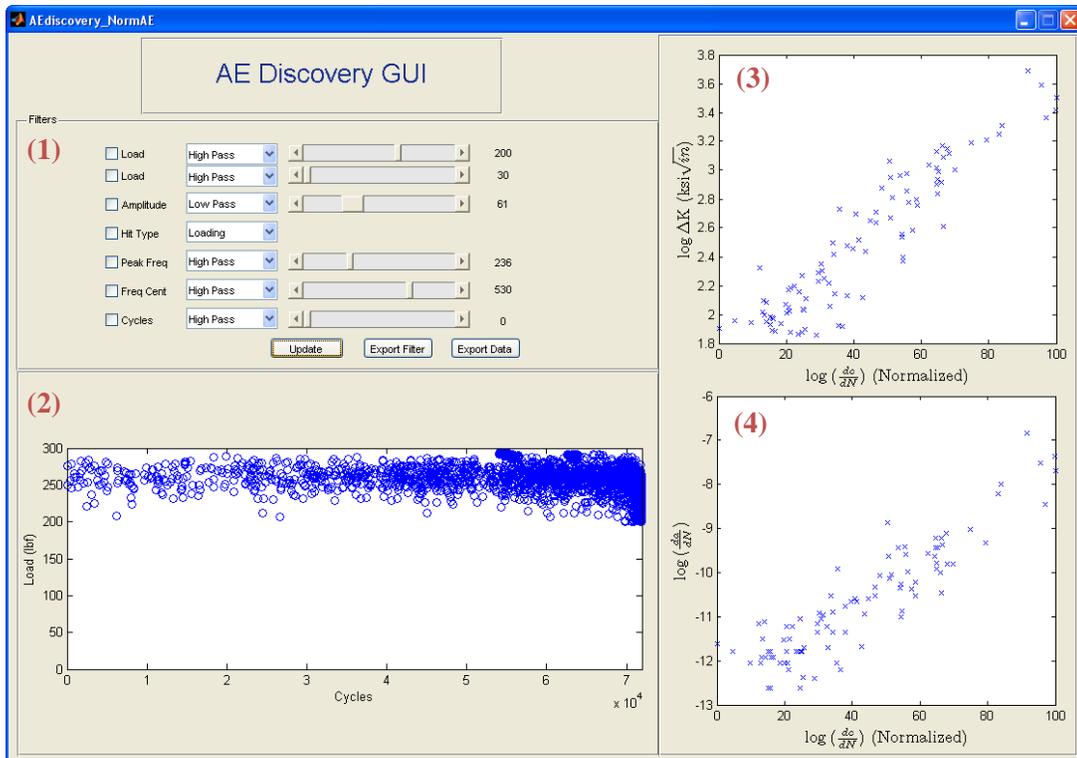
Figure 2.12 – AE Discovery GUI screenshot

The AE Discovery GUI consists of four sections: In section 1, a filter is defined by setting threshold values for different AE features and also selecting the type of the filter (i.e. high-pass or low-pass). There is also an option to filter out signals if they have been generated in the unloading portion of a cycle.

The result of applying the selected filter to the recorded AE signals is then plotted. In section 2, the load value and the cycle at which the AE hits are received are plotted. In sections 3 and 4, the correlation between AE feature, $\log dc/dN$, and crack growth features $\log \Delta K$ and $\log da/dN$ are plotted.

As mentioned previously, the AE feature $\log dc/dN$ is expected to have a linear correlation with both fatigue parameters $\log \Delta K$ and $\log da/dN$. This correlation cannot be seen unless the data is properly filtered so that we have reasonable confidence that the calculated features are in fact based on crack-induced AE signals. In this study, using the AE Discovery GUI, we selected a filter that resulted in high linear correlation between the aforementioned parameters. The selected thresholds and the type of the applied filters were consistent with recommendations previously cited from the literature.

2.5.4. Results and Discussion

The results from the experiment are presented in this section. In Figure 2.13, a short, two-second snapshot of the test is given showing the applied load for 20 cycles (blue line). The figure also shows the AE hits received in that short interval (red star). The AE hits can be categorized in three groups based on their corresponding load values. The AE hits in the first group have a load value close to the maximum, and as discussed before, are more likely to be from a crack growth-related event. The AE

hits in group 2 are more likely to have been caused by crack closure events because their load values show that these events occurred in the middle of the cycle and during the unloading portion of it (when the crack surfaces touch each other to close). The AE events in group 3 are most likely due to the noise generated by the crack surfaces rubbing on each other at the end of each cycle (Talebzadeh & Roberts 2001).
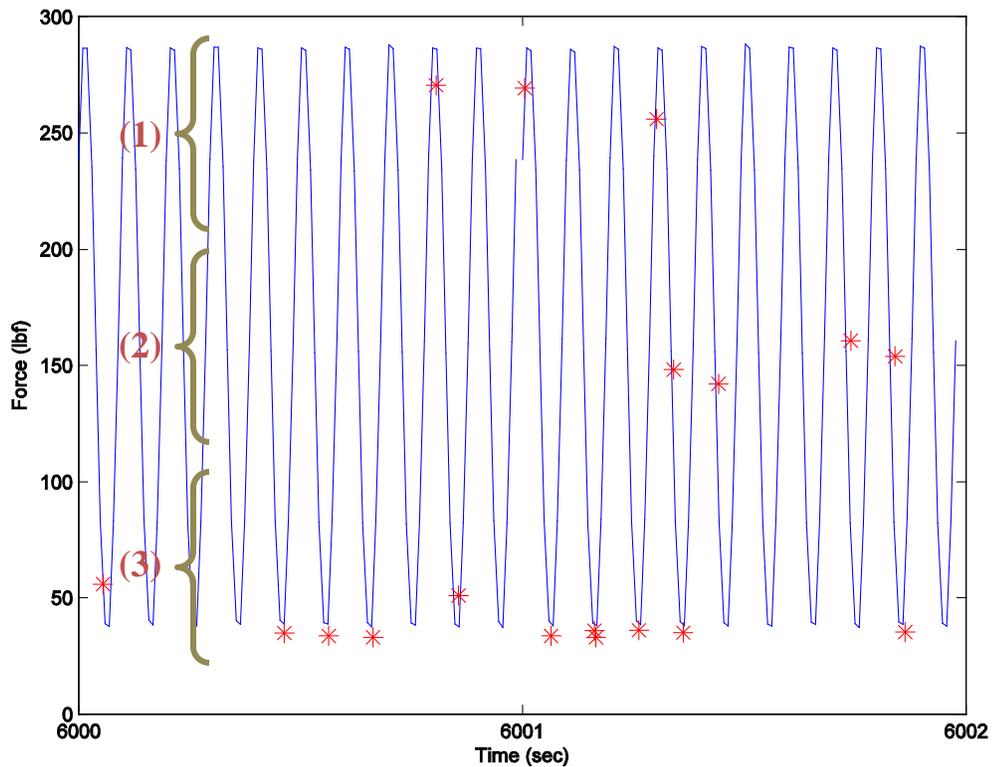
Figure 2.13 – Snapshot of 20 loading cycles along with corresponding AE hits

In Figure 2.14, the AE hits received during a complete crack growth test are presented. The red crosses are the hits during the loading portion of the cycle, whereas the blue dots represent the hits during the unloading portion of the cycle. It is obvious from this figure that in fact the majority of the AE hits happened during unloading and therefore can be considered as noise. The red points in this plot seem to belong to two distinct groups based on their load values: the ones with higher load

32

values are consistent with the conclusion from Figure 2.13 and are most likely related to crack growth; the hits with load values close to the minimum are harder to categorize as loading or unloading hits and are most likely from noise.
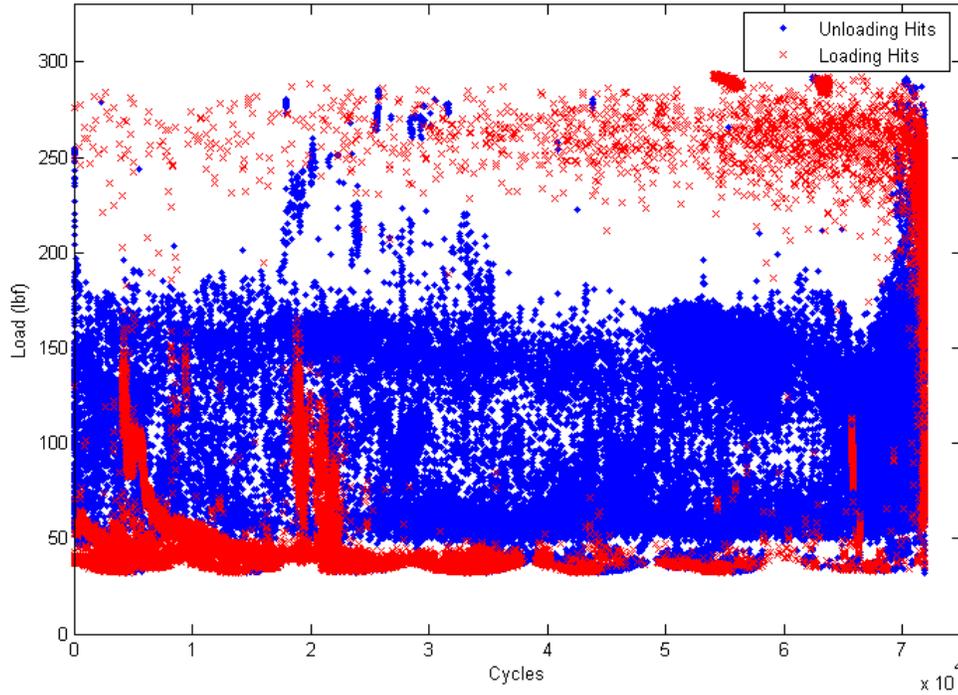
Figure 2.14 – AE hits from fatigue testing filtered based on hit type (loading / unloading)

Figure 2.15 shows the AE hits captured during the same experiment but this time filtered based on their peak frequency values; AE hits with peak frequency value less than 250 kHz are shown here. A comparison of Figure 2.15 with Figure 2.14 shows that the AE hits categorized as noise according to Figure 2.14 are in fact the ones with the lowest peak frequency values. This is consistent with the fact that crack growth-related AE hits are often very high-frequency signals.
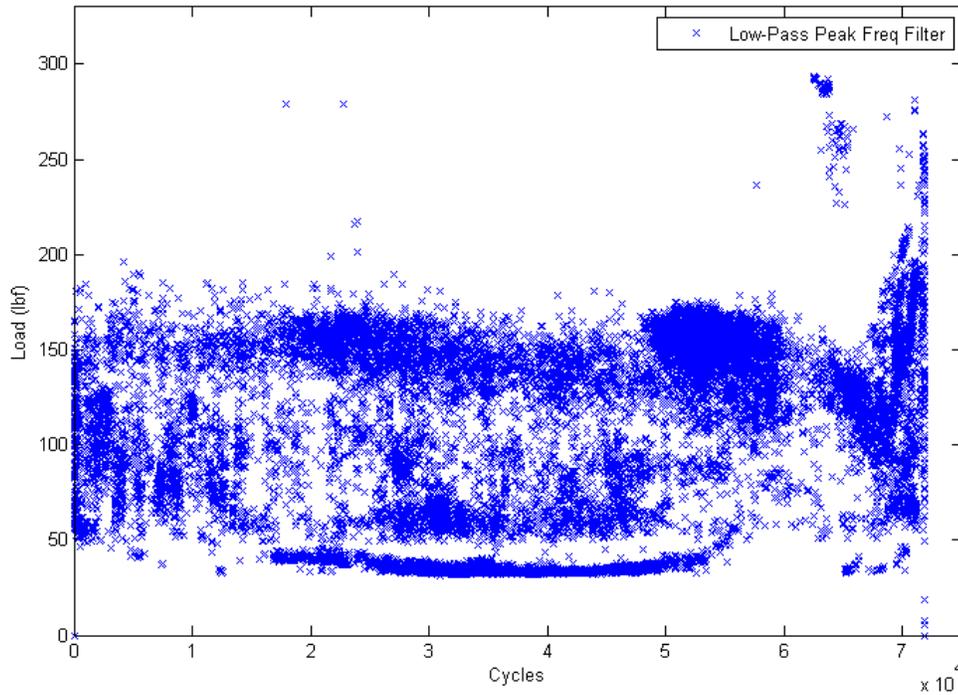
Figure 2.15 – AE hits from fatigue testing filtered based on peak frequency

Once proper filtration has been applied to the signals, the correlation between AE and

crack growth parameters can be seen. In Figure 2.16, both the crack size and the

cumulative AE count rate are plotted against elapsed cycles on the left-hand side. The

graph on the right-hand side shows that the increasing trend in crack size has a linear

relationship with the cumulative AE count rate (on a log scale) for cracks larger than

0.6 inches. This means that in theory, the crack size can be measured by monitoring

the cumulative AE count rate, if the relationship between the two is fully

characterized and modeled.
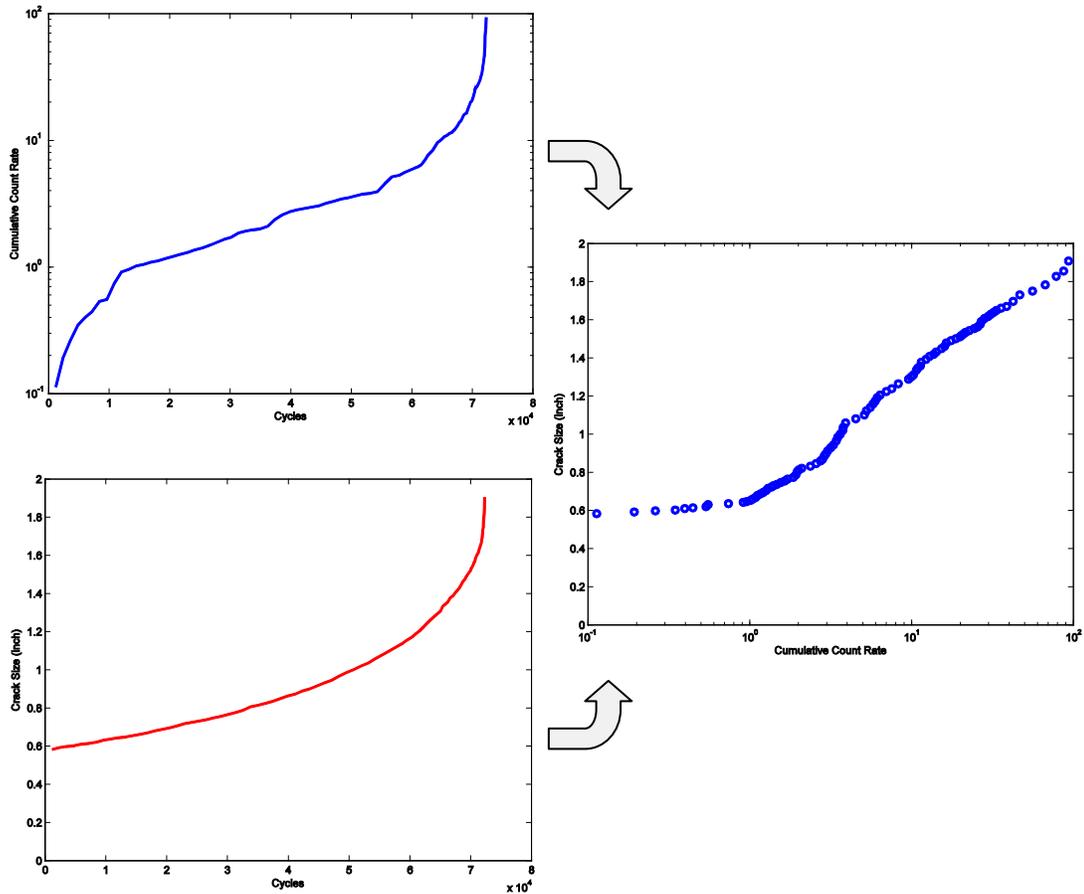
Figure 2.16 – Cumulative AE count rate versus crack size

Another way to explore the correlation between AE and crack growth parameters is by considering their derivatives. Figure 2.17 shows the correlation between the AE parameter, dc/dN, and the fatigue parameter, da/dN, on a log-log scale. These are the same data shown in Figure 2.16 but presented here in terms of derivatives. It is evident from this figure that these two parameters are (on average) linearly correlated with each other.

Since the physical interpretation of the AE parameter dc/dN has minimal significance, the values of $\log dc/dN$ were normalized (between 0 and 100) before plotting throughout this dissertation.
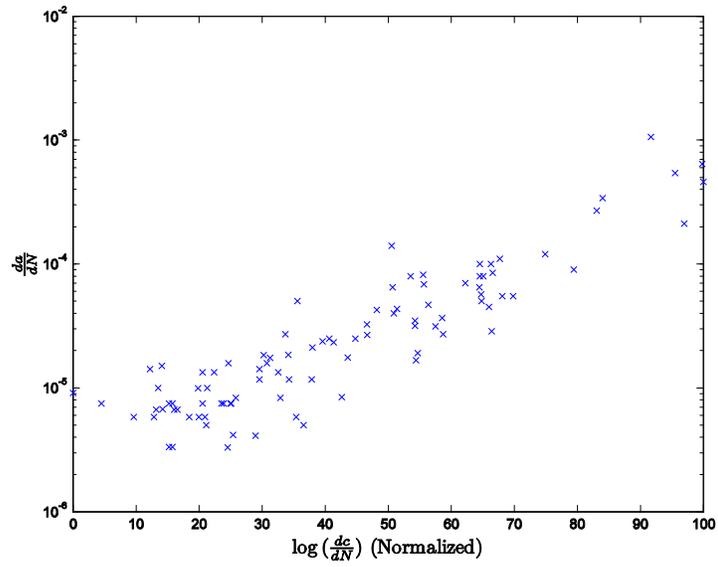
Figure 2.17 – The linear correlation observed between crack growth rate and AE count rate resulting from fatigue crack growth.

As discussed before, a similar correlation is expected between the AE count rate and the stress intensity factor range, ΔK. Using the same experimental data as above, the relation between these two parameters is depicted in Figure 2.18.
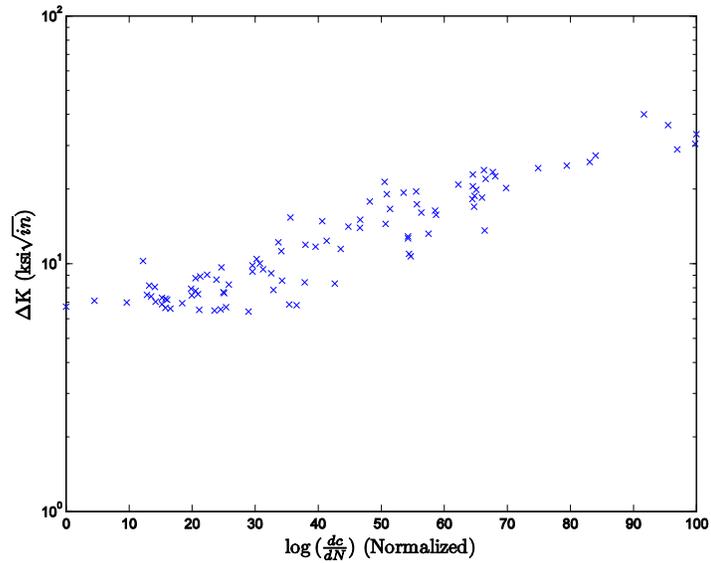
Figure 2.18 – The linear correlation observed between ΔK and AE count rate resulting from fatigue crack growth.

Figure 2.19 shows that there is no evident correlation between these parameters before appropriate filtration, since the calculated AE parameters in that case are contaminated with noise and do not represent actual crack growth-related events.
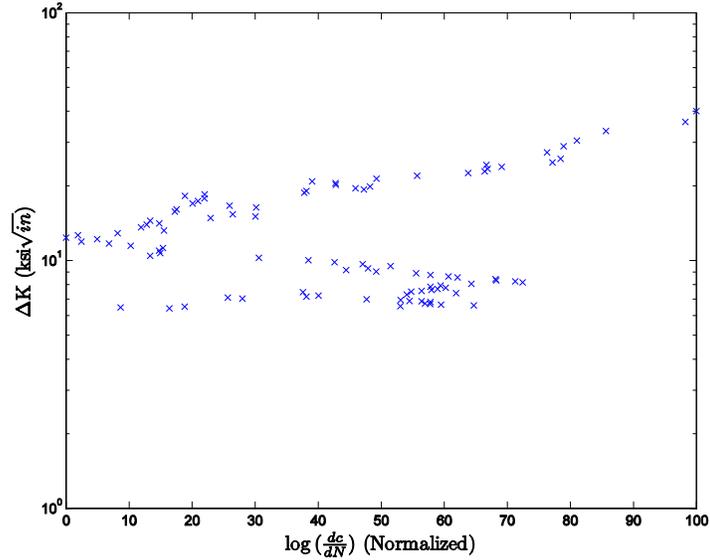
Figure 2.19 – Scatter plot of ΔK versus AE count rate data points before filtration.

The dataset collected using the experimental procedure described in this section will be used in the remainder of this dissertation to build a statistical model that can be used for AE-based structural health management.

2.6. *Summary*

In this chapter, the application of the AE technique in crack growth monitoring was presented. It was shown through experiment that fatigue crack growth can be detected and characterized by monitoring the AE signals generated during crack growth.

Details of the experimental setup and procedure were explained; specifically, the processes for identifying extraneous AE noise as well as effective filtration techniques were presented. The results obtained in this chapter suggest that features

extracted from properly filtered AE signals can be correlated with fracture parameters and can therefore be used to develop an AE-based SHM solution for crack growth monitoring.

Chapter 3:   Statistical Model Development

3.1. *Overview*

It was shown previously that on average, a log-linear relationship can be assumed between fracture parameters (da/dN or ΔK) and AE parameter (dc/dN). In this chapter, a statistical model is developed to describe the relationship between these parameters. Next, the Bayesian parameter estimation technique is used to infer the unknown model parameters based on the experimental data obtained in previous chapter.

3.2. *Model development*

In statistics, regression analysis is used for modeling and analyzing random variables when the focus is on the relationship between a dependent variable Y and one or more independent variables X. Here X represents dc/dN as the independent variable, and Y represents either da/dN or ΔK as the dependent variable that we are interested in estimating.

Regression analysis estimates the conditional expectation of the dependent variable given the independent variable — that is, the average value of the dependent variable when the independent variable is fixed. This is usually formalized as

$$E(Y|X) = \phi(X; \Theta) \tag{3.1}$$

where $\phi(\cdot)$ is known as the regression function parameterized by vector of parameters Θ.

Another way of looking at this problem is to partition the dependent variable Y into a deterministic component given by function $\phi(\cdot)$ of the independent variable X, plus a random component, ϵ, that follows a particular probability distribution. That is,

$$Y = \phi(X; \Theta) + \epsilon \qquad\qquad\qquad (3.2)$$

The addition of the random term makes the above relationship a statistical model, meaning that the functional relationship between the response variable Y and the predictor variable X holds only in an average sense, not for every data point.

The random error is the difference between the observed data and the prediction of the mathematical function at a given X, conditioned on the set of parameters Θ. The error is an unobserved random variable that is assumed to follow a particular probability distribution which describes its aggregate behavior. The probability distribution of an (un-biased) error term has a mean of zero and an unknown standard deviation σ that should be estimated (along with the rest of model parameters) based on observed data.

To carry out regression analysis, the form of the function ϕ must be specified. The general form of the regression function is either known ahead of time (e.g., based on the underlying physics of the phenomenon being modeled) or should be identified and verified using available data.

Based on the findings from previous sections (our experimental results along with findings of other researchers as cited), it seems reasonable to assume a linear form for the regression function $\phi(\cdot)$ where $\Theta = (\alpha_1, \alpha_2)$ when Y represents ΔK and $\Theta = (\beta_1, \beta_2)$ when Y represents da/dN.

To complete the model, the error term ϵ must be fully specified as well. Here we adopt the classic regression assumption that the errors are independent and identically-distributed (i.i.d.) random variables and follow a normal probability distribution:

$$\epsilon \sim N(0, \sigma) \tag{3.3}$$

The mean of the error distribution is zero, and its standard deviation is the unknown quantity parameter σ.

Another classic assumption in regression analysis is that the error has a constant variance for all observations regardless of the value of independent variable X. This assumption, however, does not hold in all cases[8]; it is reasonable to assume that a small crack is harder to measure, and as the crack becomes larger, the measurement of its length becomes more accurate. Accordingly, the da/dN and ΔK values associated with data points coming from smaller cracks could be less accurate than those from larger cracks.

One way to account for this effect is to release the constant variance assumption and allow σ to change as a function of the independent variable X. This will result in a flexible model that can capture any change in the error distribution based on the available data. Here, we choose a flexible two-parameter exponential relationship to capture the potential trend in σ,

$$\sigma = \gamma_1 \exp(\gamma_2 X) \tag{3.4}$$

---

[8] A classic example where the assumption of constant variance does not hold is income versus expenditure on meals. A poorer person tends to spend a small and rather constant amount of money on food, whereas a wealthier person may occasionally buy inexpensive food and at other times eat expensive meals.

This function can capture both increasing and decreasing trends of σ for positive and negative values of γ_2, respectively. It also reduces to the standard constant variance case if γ_2 is equal to zero. It is important to note that it is not necessary to have any prior knowledge about the trend of σ; γ_1 and γ_2 are in fact treated as additional unknown parameters and will be estimated using the observed data.

Once the model is developed, the next step is to use experimental data to estimate its unknown parameters. This will be presented in the following section.

3.3. *Bayesian Parameter Estimation*

In this section the experimental data obtained in the previous section will be used to find the unknown parameters of the statistical model. Numerous procedures have been developed for parameter estimation and inference in linear regression. These methods differ in computational simplicity of algorithms, presence of a closed-form solution, robustness and theoretical assumptions. In this dissertation, we adopt a Bayesian approach to parameter estimation often referred to as *Bayesian regression*.

Rather than relying solely on the best estimate of the parameters and the corresponding confidence intervals, as is the common practice when using Maximum Likelihood Estimation (MLE) and traditional regression techniques, in Bayesian estimation the model parameters are treated as unknown random variables and their uncertainty is characterized by calculating their joint probability distribution. By doing so, the available information in the scatter of the data is preserved in the resulting posterior probability distribution over the model parameters.

In addition, the Bayesian inference technique provides a framework for incorporating any additional sources of knowledge that may be available about the parameters

(Figure 3.1). Possible sources of such information include past experiments, handbook data and expert judgment (Azarkhail and Modarres, 2007).
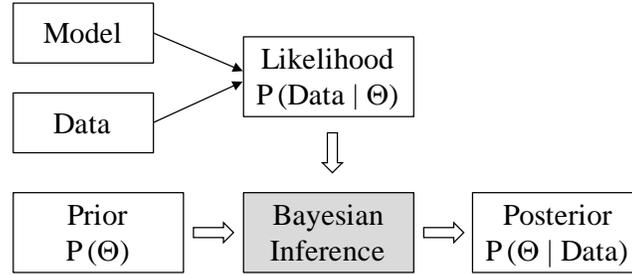
Figure 3.1 – Bayesian Inference Framework

In Bayesian inference, the initial belief about the distribution of the parameters (*a priori* distribution) is systematically updated according to Bayes' theorem (3.5), based on some kind of evidence or available observations.

$$p(\Theta|D) = \frac{p(D|\Theta)p(\Theta)}{p(D)}$$
(3.5)

The terms in Bayes' theorem are defined as follows:

- Θ is the vector of model parameters to be estimated. In the current problem, $\Theta = \{\alpha_1, \alpha_2, \gamma_1, \gamma_2\}$.

- $p(\Theta)$ is the *a priori* distribution of model parameters.

- D denotes the set observations to be used in the updating process. Here our observations consist of n data points obtained from experiments such that $D = \{(x_i, y_i)|\ x_i = \log(dc/dN)_i, y_i = \log \Delta K_i\}_{i=1}^{n}$

- $p(D)$ is the marginal probability of D, and acts as a normalizing constant.

- $p(D|\Theta)$ is referred to as the likelihood function, as it describes the conditional probability (likelihood) of observed data given the model parameters.

- $p(\Theta|D)$ is the *a posteriori* probability of the model parameters given the observations.

To obtain the posterior distribution, $p(\Theta|D)$, the initial belief about the distribution of model parameters, $p(\Theta)$, is updated according to the likelihood of the new observed data, $p(D|\Theta)$, and then normalized based on the marginal distribution of data, $p(D)$.

3.3.1. The Likelihood Function

The likelihood function is defined based on the model that was developed in the previous section. This model is a linear regression function with flexible variance that is defined in the following form:

$$Y = \alpha_1 X + \alpha_2 + \epsilon$$

where

$$\epsilon \sim N(0, \sigma),$$

$$\sigma = \gamma_1 \exp(\gamma_2 X)$$

(3.6)

All variables are defined as in (3.2) - (3.4). The results presented here are for the case where Y represents ΔK and X represents dc/dN. A similar estimation process can be used for the da/dN versus dc/dN data as well.

In the Bayesian approach to regression, the degree of fitness of the model to the data is represented in terms of the probability of occurrence or likelihood of the data given the model parameters – a larger value of the likelihood function shows a better fit of the model to the data.

To define the likelihood function, a mathematical relationship is needed that defines the probability of observing every observed data point assuming a model structure according to (3.6) and based on the set of parameters $\Theta = \{\alpha_1, \alpha_2, \gamma_1, \gamma_2\}$.

The likelihood can be defined based on the distribution of the error term, ϵ. To do so, the error $\epsilon_i = y_i - (\alpha_1 x_i + \alpha_2)$ for every data point (x_i, y_i) is calculated. Next, the likelihood of each data point can be defined according to $\epsilon_i \sim N(0, \gamma_1 \exp(\gamma_2 x_i))$.

An equivalent way of defining the likelihood function is to assume that the dependent variable has a normal distribution where both its mean and standard deviation are defined as functions of the dependent variable, X. That is, for every data point (x_i, y_i) we have,

$$y_i \sim N(\mu_i, \sigma_i)$$
$$\mu_i = \alpha_1 x_i + \alpha_2 \qquad (3.7)$$
$$\sigma_i = \gamma_1 \exp(\gamma_2 x_i)$$

This can be written explicitly as,

$$p(D|\alpha_1, \alpha_2, \gamma_1, \gamma_2) = \prod_{i=1}^{n} \frac{1}{\sqrt{2\pi}\sigma} \exp\left(-\frac{1}{2}\left(\frac{y_i - (\alpha_1 x_i + \alpha_2)}{\gamma_1 \exp(\gamma_2 x_i)}\right)\right) \qquad (3.8)$$

The likelihood (3.8) is based on the assumption that the data points are independent and therefore the likelihood for dataset D is simply the multiplication of the likelihood function for every data point (x_i, y_i).

3.3.2. *Defining the* **a priori** *Distribution*

The next term in (3.5) that needs to be defined is the prior distribution over the parameters, $p(\Theta)$. This study began with no past experience, and therefore no prior information about the distribution of parameters was available. Therefore non-informative (uniform) prior distributions for all parameters $\alpha_1, \alpha_2, \gamma_1$ and γ_2 were chosen.

An informative prior distribution can be used instead if additional information such as similar test results or prior estimates of the model parameters become available; this will affect the posterior distribution of parameters accordingly. When uniform priors are used for the parameters, both Bayesian and MLE approaches will result in the same best estimate for the parameters, but the coverage of the uncertainty over the

parameters could be different. The uncertainty bounds in MLE are estimated using the Fisher information matrix with the underlying assumption of normal distribution for the parameters, whereas in the Bayesian approach the uncertainty bounds are derived from the posterior joint distribution of the parameters.

3.3.3. Calculation of the a posteriori Distribution

So far the likelihood function and the prior distribution of the parameters have been defined; the only other term in (3.5) that remains to be defined is $p(D)$. As stated before, the denominator in Bayes' theorem is the marginal distribution of data, which acts as a normalization factor to make sure that the posterior function is in fact a probability density function and its integral is equal to 1. Therefore $p(D)$ can be written as,

$$p(D) = \int p(D|\Theta)p(\Theta)d\Theta \qquad (3.9)$$

The integration in (3.9) is in fact a four-dimensional integral since $\Theta = \{\alpha_1, \alpha_2, \gamma_1, \gamma_2\}$.

For complex likelihood functions with a large number of parameters it may be very difficult and sometimes impossible to calculate such integrals analytically. Therefore in practice, numerical approaches such as Monte Carlo-based methods are used to calculate these multidimensional integrals.

For this dissertation, WinBUGS software (Cowles 2004) was used to obtain the posterior distribution. WinBUGS is a software package for Bayesian analysis of complex statistical models using Markov chain Monte Carlo (MCMC) methods.

Monte Carlo methods are a class of computational algorithms that rely on repeated random sampling to compute their results. One of the typical applications of Monte

Carlo methods is numerical calculation of multi-dimensional integrals. MCMC methods are a class of algorithms for sampling from probability distributions based on constructing a Markov chain that has the desired distribution as its equilibrium distribution. The state of the chain after a large number of steps is used as a sample from the desired distribution.

To use WinBUGS for parameter estimation, the user should provide a *model file* as well as a *data file*. The model file contains the definition of the likelihood function as well as the prior distribution over the parameters. Other than defining the model using text statements, the user can also use the internal graphical interface called DoodleBUGS to define the model graphically via Directed Acyclic Graphs (DAG). In a DAG, stochastic nodes (representing a random variable) are shown as ellipses, and constant and logical nodes are shown as squares. The arrows that connect the different nodes together define the structure of the model. Figure 3.2 shows the DAG of the model in (3.7) created in WinBUGS.
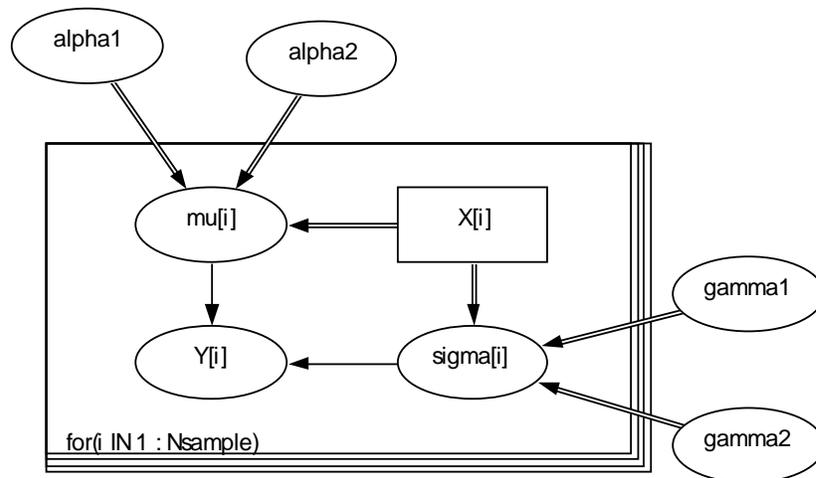
Figure 3.2 – Directed Acyclic Graphs (DAG) of the model in (3.7) created via DoodleBUGS.

After defining the model, the user must also provide a *data file* that contains all the data points used to fit the model and estimate the unknown parameters. The next step is to identify and select the unknown parameters to be estimated through the MCMC simulation. Once the model and data are specified, WinBUGS automatically selects and implements the appropriate sampling algorithms for the selected unknown model parameters.

The latest version of WinBUGS is version 1.4.3, released in August 2007. Further development is now focused on OpenBUGS, an open source version of the package. Interested readers can refer to (Ntzoufras 2009) for a good reference on Bayesian modeling using WinBUGS. For further reading on MCMC methods in general, see (Hastings 1970; Gilks et al. 1996; Gelman et al. 2003; Gamerman & Lopes 2006).

3.3.4. Posterior Predictive Distribution

Once the posterior distribution $p(\Theta|D)$ is calculated, the inference process is complete. The next step is to use the developed model (with known joint distribution of model parameters) for prediction purposes using unobserved data. In other words, the model (with posterior parameters) will be used to calculate the distribution of dependent variable Y for a given input X.

The posterior *predictive distribution* is the distribution of unobserved observations (prediction) conditional on the observed data. Let D be the observed data, Θ be the vector of parameters, and D_{pred} be the unobserved data; the posterior predictive distribution is defined as follows,

$$p(D_{pred}|D) = \int p(D_{pred}, \Theta|D)d\Theta$$

$$= \int p(D_{pred}|\Theta, D)p(\Theta|D)d\Theta \qquad (\,3.10\,)$$

Assuming that given Θ the observed and unobserved data are conditionally independent, (3.10) can be further simplified as,

$$p(D_{pred}|D) = \int p(D_{pred}|\Theta)p(\Theta|D)d\Theta \qquad (\,3.11\,)$$

So based on (3.11), the posterior predictive distribution is an integral of the likelihood function $p(D_{pred}|\Theta)$ with respect to the posterior distribution $p(\Theta|D)$. Note that again, we are dealing with a multi-dimensional integral that should be calculated numerically. The same MCMC procedure described above can be used to generate samples from the posterior predictive distribution based on draws from the posterior distribution of Θ.

3.3.5. Results and Discussion

In this section, the parameter estimation results are presented as well as the calculated predictive distribution that will later be used for prediction.

The results presented here are calculated via the MCMC procedure described above using WinBUGS. To facilitate the calculations, the problem was set up such that the data preprocessing was done in MATLAB first, after which WinBUGS was called as a standalone engine to perform the MCMC simulation. The simulation result was then passed into MATLAB for further processing and plotting. The model file was manually created as separate text file, whereas the data file was generated automatically using MATLAB for a given dataset. Both files were passed to

WinBUGS before running. The interface between MATLAB and WinBUGS was facilitated by MATBUGS[9].

The first dataset used for parameter estimation was the ΔK versus dc/dN data obtained from the experiment, i.e., $D = \{(x_i, y_i)|\ x_i = \log(dc/dN)_i\,, y_i = \log \Delta K_i\}_{i=1}^{n}$. ($x_i$ values are normalized as described in Chapter 2:2.5.4)

The output of the MCMC procedure is samples from the posterior joint distribution of $\Theta = \{\alpha_1, \alpha_2, \gamma_1, \gamma_2\}$, which is a four-dimensional distribution. To plot this distribution, the variables that are correlated with each other are grouped, and their 2D joint PDF is plotted.

Figure 3.3 shows the posterior distribution of parameters α_1 and α_2. The contour plot of the joint PDF (bottom) shows that these two parameters are highly correlated (Correlation coefficient[10] $\rho = -0.88$). Similar results are presented in Figure 3.4 for the parameters γ_1 and γ_2. These variables are also highly correlated ($\rho = -0.89$), which highlights the importance of considering their joint PDF (rather than marginal PDFs) when using them for prediction. In Figure 3.5 the contour plot for joint PDF of α_1 and γ_1 is presented, which shows that these variables are uncorrelated with each other ($\rho = 0.06$).

---

[9] MATBUGS is a free MATLAB script that can be downloaded from:
http://code.google.com/p/matbugs/.

[10] Correlation coefficient is a measure of correlation (linear dependence) between two random variables and is defined as $\rho_{X,Y} = cov(X,Y)/\sigma_X\sigma_Y$. It is easily shown that $-1 \le \rho \le +1$ with values closer to +1 and -1 indicating higher positive and negative correlations, respectively.

Figure 3.3 – Posterior distribution of parameters α_1 and α_2. Marginal PDF plots (top) and contour plot of the joint PDF (bottom).

Figure 3.4 – Posterior distribution of parameters γ_1 and γ_2. Marginal PDF plots (top) and contour plot of the joint PDF (bottom).
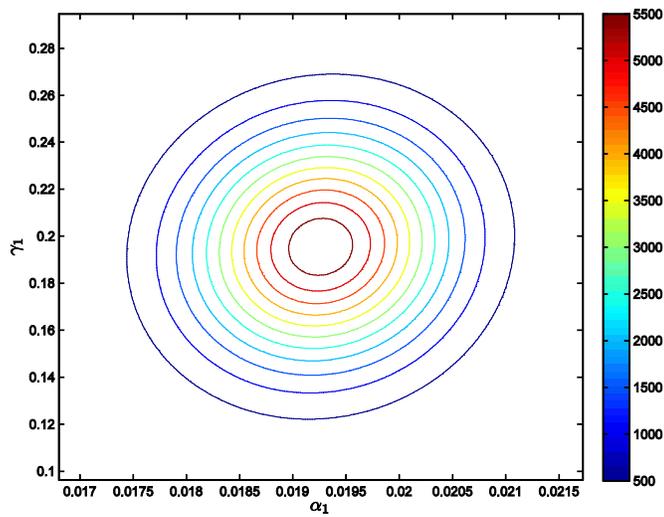
Figure 3.5 – Contour plot of the joint PDF of α_1 and γ_1 showing the lack of correlation between these random variables.

The PDFs plotted in the above figures are not smooth because they are in fact generated using the samples of the posterior distribution obtained via the MCMC process.

It was previously described that the flexible model in (3.4) was used to define the standard deviation of the dependent variable Y. For any given input X, one can calculate the corresponding distribution of σ by knowing the joint distribution of γ_1 and γ_2. The joint distribution γ_1 and γ_2 was one of the outcomes of the parameter estimation process (see Figure 3.4). To estimate the distribution of σ, it was defined as an additional unknown stochastic node (random variable) in WinBUGS. Through the MCMC process—as samples from the posterior densities of unknown parameters are being generated—WinBUGS also generates samples from the distribution of σ for different values of independent variable X. The result is shown in Figure 3.6. Note that for this particular dataset, the median value of σ is relatively constant (it has a slight decreasing trend) over the range of values of $\log dc/dN$. This is consistent with the fact that the estimated value of γ_2 is close to zero (see Figure 3.4), which means that the relationship in (3.4) reduces to a constant variance case where $\sigma_{\Delta K} \approx \gamma_1$. Notice the change in the calculated bounds of σ over the range of $\log dc/dN$. The tighter bounds in the middle of the range are due to a higher density of data points in this region, which results in a more confident estimate in this range.
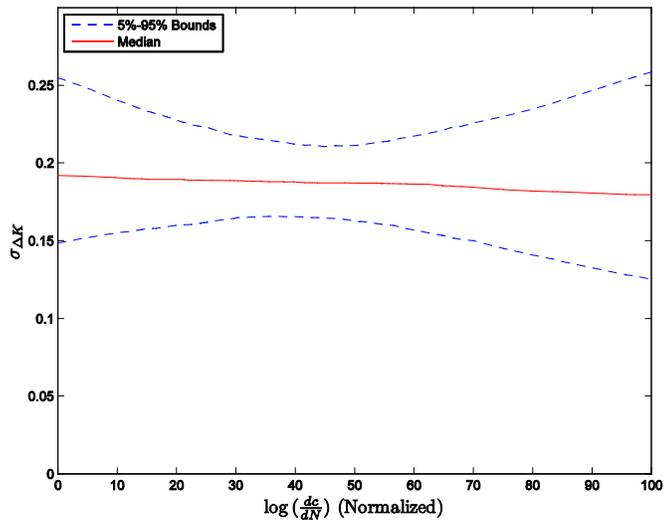
Figure 3.6 – Distribution of $\sigma_{\Delta K}$ as a function of the independent variable $\log dc/dN$

Once all the model parameters are estimated (i.e. the joint distribution $p(\Theta|D)$ is known), equation (3.11) can be used to calculate the posterior predictive distribution for the dependent variable $\log \Delta K$ as a function of the independent variable $\log dc/dN$, given past observations, D. The integral in (3.11) should be calculated numerically, as it is defined over a four-dimensional space of parameters. Once again, WinBUGS was used to calculate this integral using Monte Carlo simulation.

The result is presented in Figure 3.7 where the posterior distribution is shown by its median and the 5% and 95% prediction bounds. The data D used to fit the model is also plotted in this figure. Notice that the distribution of $\log \Delta K$ has a relatively constant variance, which is consistent with the estimated posterior distribution of parameters γ_1 and γ_2 (where $\gamma_2 \approx 0$) and the resulting variance function plotted in Figure 3.6.
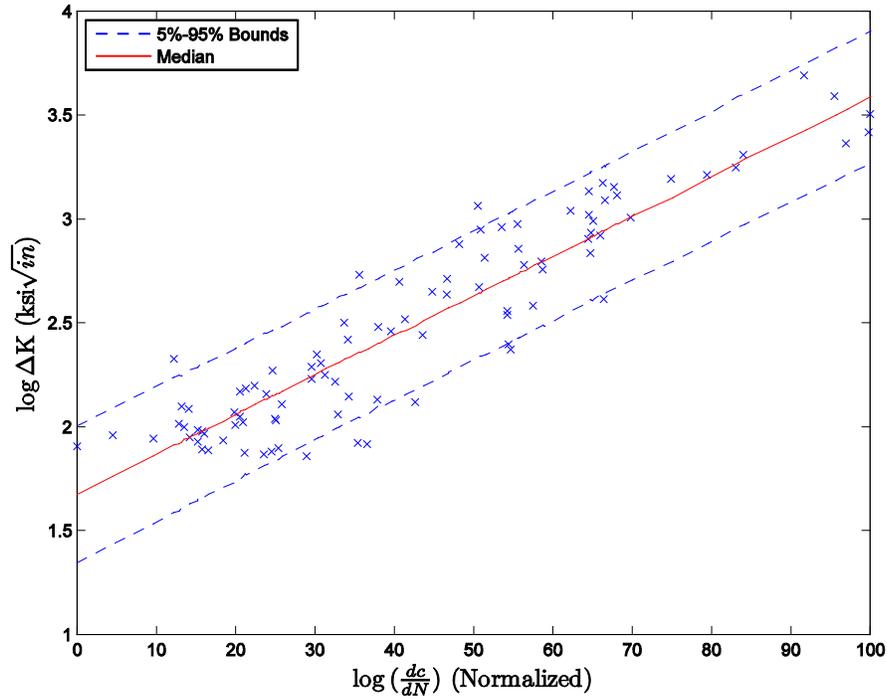
Figure 3.7 – Posterior predictive distribution of $\log \Delta K$ as a function of $\log dc/dN$.

The procedure described above can be repeated to fit the model (3.7) to the $\log da/dN$ versus $\log dc/dN$ dataset as well. Figure 3.8 shows the posterior distribution for two of the model parameters β_1 and β_2, while the posterior predictive distribution for $\log da/dN$ as a function of $\log dc/dN$ is plotted in Figure 3.9.

The models developed in this section provide a quantitative means for relating the crack growth parameters to the AE parameters. In the remainder of this dissertation, this concept will be used to develop a complete SHM solution based on AE monitoring.
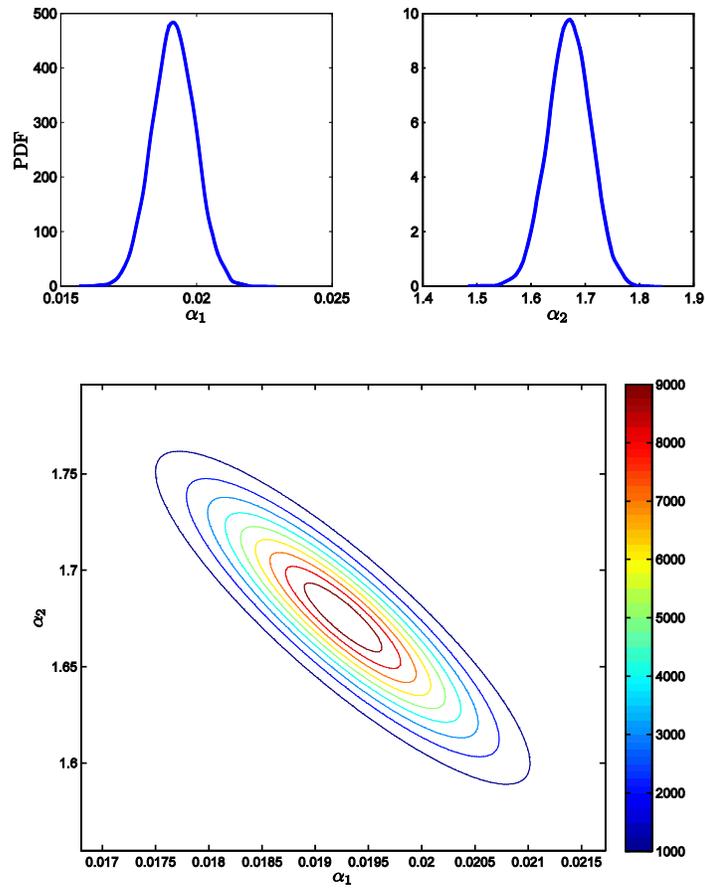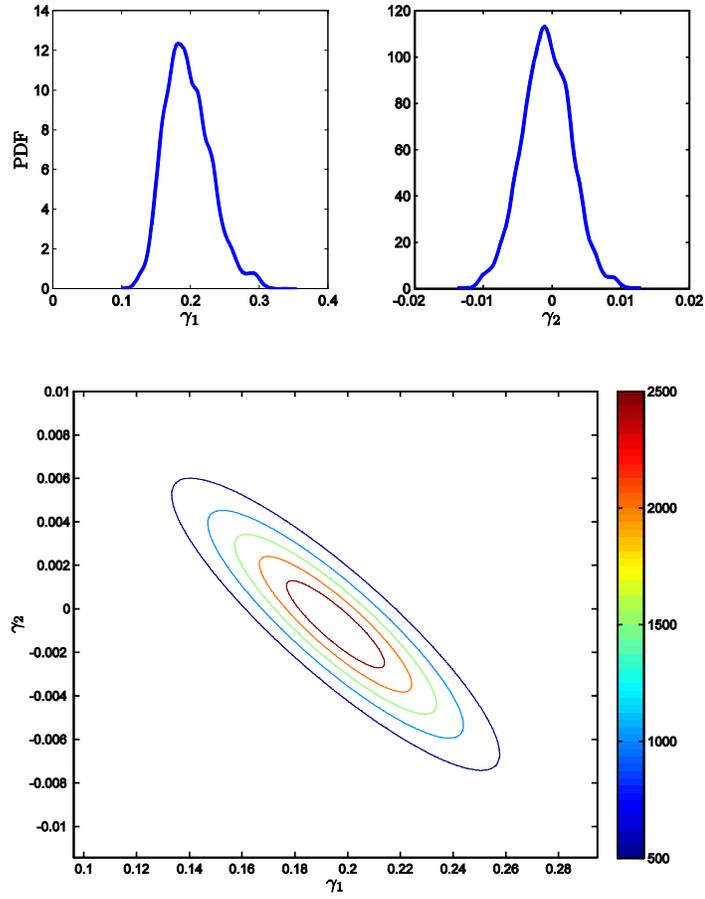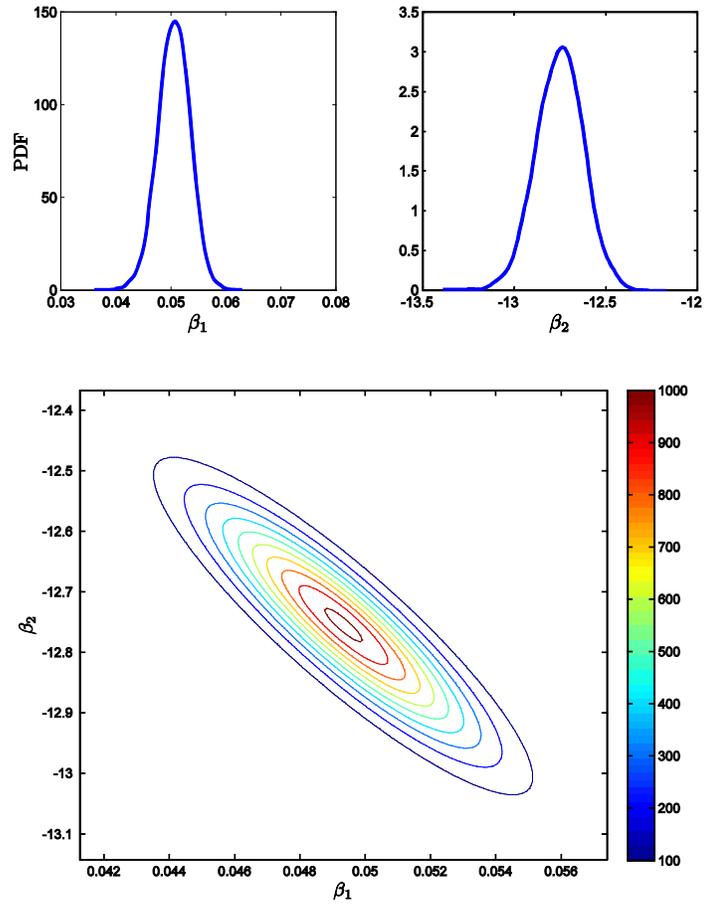
Figure 3.8 – Posterior distribution of parameters β_1 and β_2. Marginal PDF plots (top) and contour plot of the joint PDF (bottom).
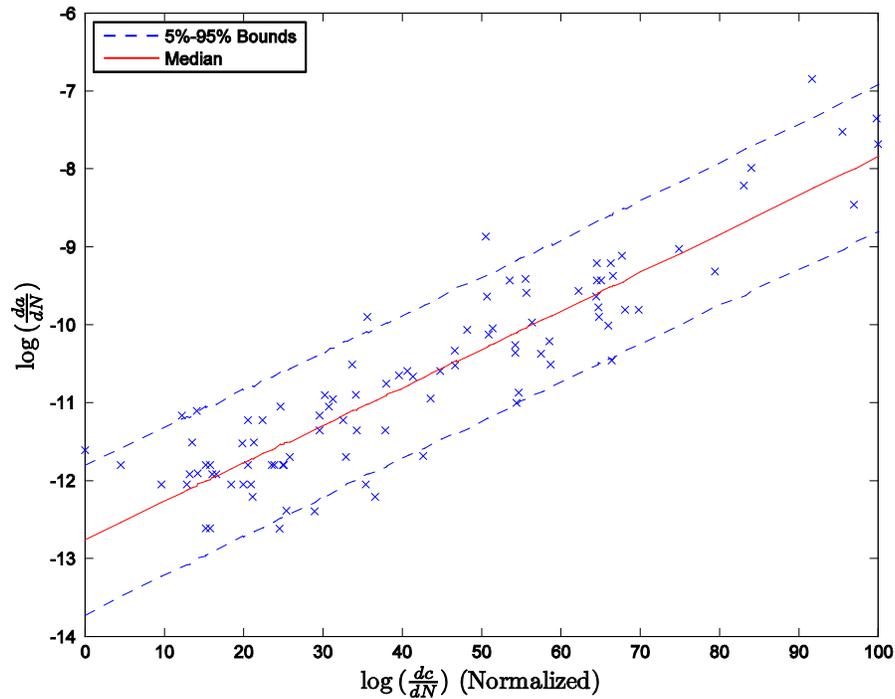
Figure 3.9 – Posterior predictive distribution of $\log da/dN$ as a function of $\log dc/dN$.

3.4. *Summary*

In this chapter, a flexible model was developed to describe the relationship between fracture parameters and AE features. Bayesian estimation was used to infer unknown model parameters based on experimental data. In this approach, the uncertainty in the data is preserved in the distribution of model parameters and will directly influence the outcome of the model, which results in a more realistic prediction of fracture parameters.

Once the model is calibrated for an application—i.e. its parameters are estimated based on experimental data—it can be used to calculate the distribution of fracture parameters da/dN and ΔK as a function of AE features obtained from real-time monitoring.

Chapter 4: Methods for Structural Health Management using AE monitoring

4.1. *Overview*

In this chapter, two novel approaches are proposed for structural health management using AE monitoring. In both of these approaches, the statistical model developed in the previous chapter will be utilized to calculate system health parameters (such as probability of structural failure and crack size distribution) solely based on AE monitoring data.

4.2. *AE-based Risk Factor*

In this section, we will calculate the probability of structural failure (as defined here) due to crack growth using AE monitoring data.

As a crack grows larger in a structure, the value of the stress intensity factor ΔK associated with it increases as well. For a standard CT specimen, this relationship is defined as follows (ASTM E647-08 2008):

$$
\begin{aligned}
\Delta K &= f(a) \\
&= \frac{\Delta P}{B\sqrt{W}} \frac{2\alpha}{(1-\alpha)^{3/2}} (0.886 + 4.64\alpha - 13.32\alpha^2 + 14.72\alpha^3 \\
&\quad - 5.6\alpha^4)
\end{aligned}
\tag{4.1}
$$

where ΔP is the range of the applied force cycles, W and B are the width and thickness of the CT specimen, respectively, and α is the dimensionless crack size defined as a/W.

Equation (4.1) shows that ΔK, in general, depends on the geometry of the structure, amplitude of the applied load cycles and the instantaneous size of the crack. For a given structure, assuming that the geometry is fixed, a large ΔK represents either a large crack size and/or high load amplitude applied to the structure. ΔK can therefore be considered a criticality parameter that describes the potential of the crack for further growth at any given point in time.

On the other hand, the resistance of a material to stable crack propagation under cyclic loading is characterized by its fracture toughness, K_{Ic} (T. L. Anderson 1994). At any point during the crack growth, if the stress intensity exceeds the fracture toughness of the material, the crack growth transitions from stable to non-stable/rapid growth regime where failure is imminent (see Figure 2.5). In other words, the crack growth is stable as long as K_{max} is less than the fracture toughness of the material, K_{Ic}. This fact is used to define an AE-based measure of risk, R_{AE}, as follows,

$$R_{AE} = p(K_{max} > K_{Ic}) \qquad\qquad (4.2)$$

where K_{max} is defined according to (4.1) for $\Delta P = P_{max}$.

As stated before, the objective is to assess the health of the structure based only on AE monitoring. To do so, the statistical model developed in the previous chapter is used in the following way:

Step 1: Estimate the model parameters (Θ) using experimental data for a given structure,

Step 2: Monitor the structure using the AE technique and extract the dc/dN parameter from the observed signals,

Step 3: At any given time, use equation (3.11) to calculate the posterior predictive distribution of ΔK as a function of instantaneous AE parameter, dc/dN.

Step 4: Use equation (4.2) to calculate R_{AE} (noting that $K_{max} = \Delta K/(1 - R)$ for constant amplitude loading with loading ratio R).

Figure 4.1 shows the outcome of the above procedure for steps 1-3.
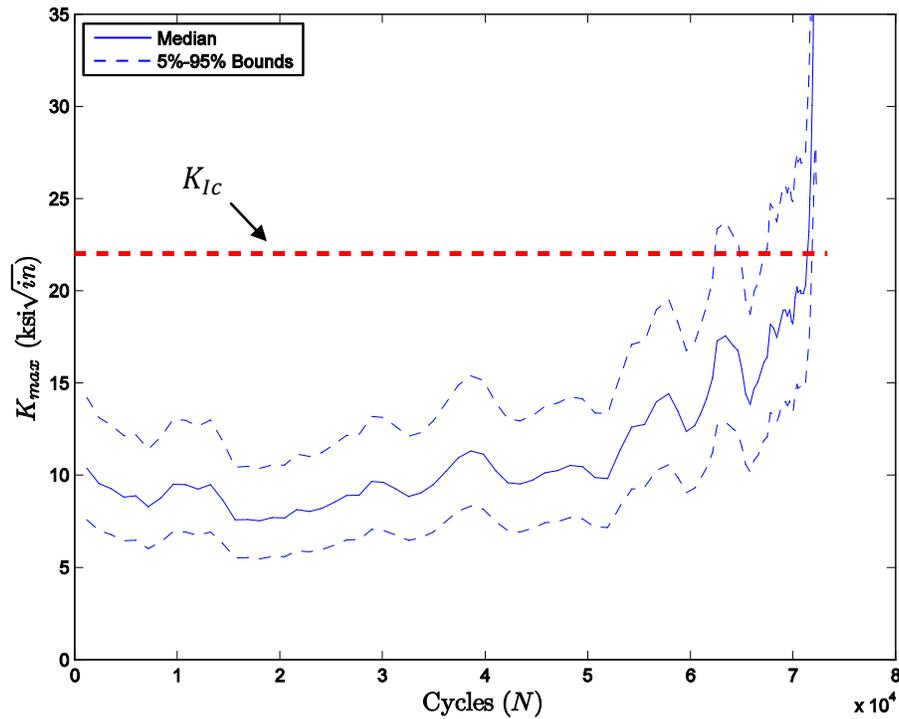
Figure 4.1 – Probability distribution of K_{max} as a function of applied fatigue cycles, N.

Here the calibrated model presented in Figure 3.7 is used to calculate the posterior predictive distribution of K_{max} from the beginning to the end of a crack growth test. To do so, the structure is monitored using the AE technique, and the dc/dN feature is extracted from the signals at different values of elapsed cycles, N (in practice, $\Delta c/\Delta N$ is calculated for consecutive intervals). Therefore, at a given cycle N, equation (3.11) can be used to calculate the posterior predictive distribution as a function of the instantaneous AE feature, dc/dN.

60

As the number of cycles increases, the crack continues to grow, and therefore, the distribution of K_{max} gradually shifts towards larger values. The dashed red line in Figure 4.1 shows a threshold value based on fracture toughness of the material where the crack growth is expected to transition to the unstable regime. Here, a nominal value of $K_{Ic} = 22 \ ksi$ for 7075 aluminum[11] was used.

Following step 4 in the procedure described above, R_{AE} can be calculated for any given cycle N according to (4.2). The result is shown in Figure 4.2.
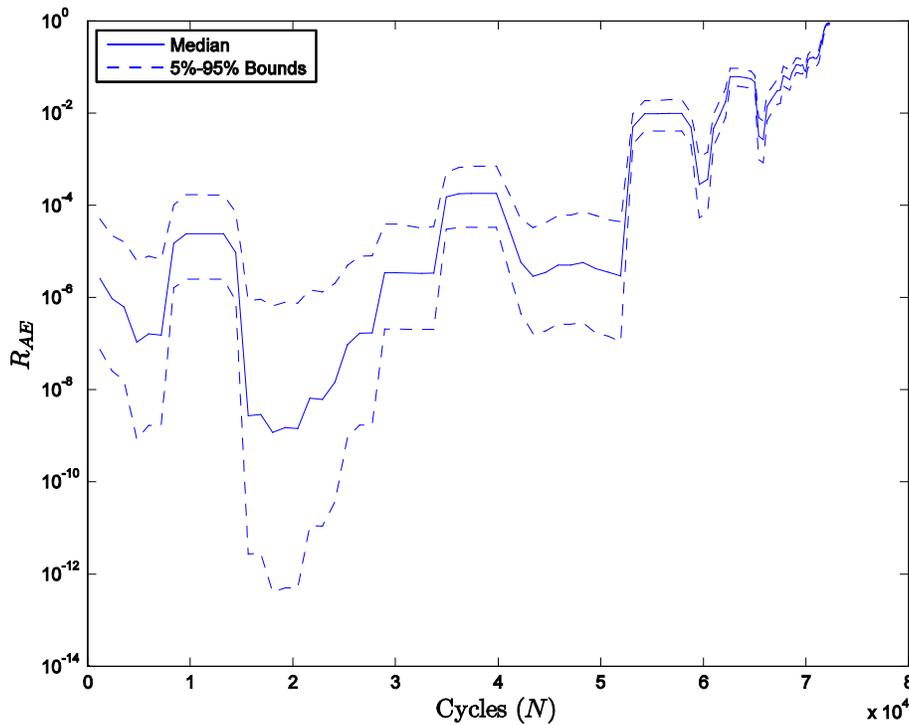
Figure 4.2 – AE-based risk factor, R_{AE}, calculated as a function of applied fatigue cycles, N.

As shown in Figure 4.2, R_{AE} increases (non-monotonically) throughout the experiment. The fluctuations in this figure are in fact a direct result of the fluctuations in the input AE feature, dc/dN, which also matches the trend in Figure 4.1. The AE-

---

[11] In reality, material properties such as K_{Ic} should not be treated as fixed values and are best describes as random variables. This is due to various sources of aleatory and epistemic uncertainty (Modarres et al. 1999) involved in the process of measuring such material properties.

based risk factor defined here is an *instantaneous* exceedance probability calculated based on the average value of dc/dN for any given interval. The AE feature has an overall increasing trend that may fluctuate due to instantaneous dynamics of the crack growth. So the best way to interpret the result in Figure 4.2 is to treat it as a red/green warning mechanism to alert the decision-maker in real-time about the increased risk factor at a given cycle based on the current AE readings.

4.3. *AE-based Crack Growth Model*

In this section, a new approach is proposed for estimating the crack size distribution as a function of applied fatigue cycles using AE monitoring.

To use an NDI technique for crack size estimation some features (specific to each NDI method) are needed that can be correlated with either the crack size or the crack growth rate.

For a given initial crack size, if the rate of crack growth can be estimated, then the crack size itself can be easily calculated by a summation over crack size increments starting from the known initial size. This is in fact the logic behind most crack growth models. In these models, however, the rate of crack growth is usually calculated based on its empirical relationship with the ΔK parameter, which itself has a complex derivation even for simple geometries.

The idea here is to estimate the rate of crack growth directly from AE monitoring using the statistical model that was developed earlier in this dissertation. This process is depicted in Figure 4.3. In this dissertation, this approach is called an AE-based crack growth model.
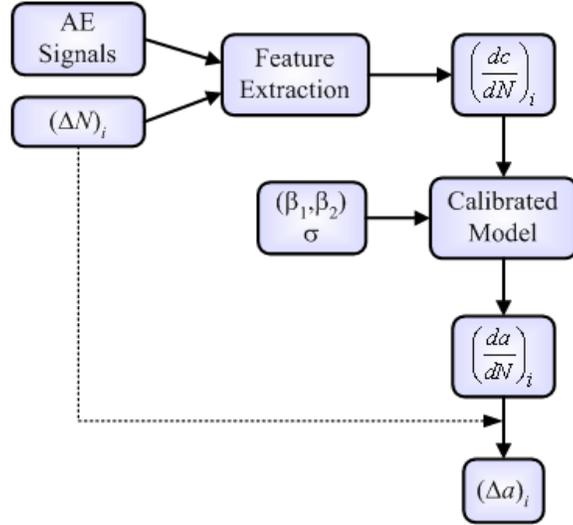
Figure 4.3 – Flowchart of the AE-based crack growth model (Rabiei et al. 2010)

The process starts by finding the parameters of the model (3.7), where $Y = \log da/dN$ and $X = \log dc/dN$, based on relevant experimental data. The resulting posterior predictive distribution for the crack growth test on a CT specimen was presented in Figure 3.9. Once the model is calibrated (i.e. its parameters are estimated), it can be used to estimate the distribution of da/dN for any given input dc/dN.

Consider a crack growth experiment where crack growth-related AE signals are recorded throughout the test. For any given interval of elapsed cycles, ΔN_i, the corresponding average AE feature $(\Delta c/\Delta N)_i$ can be calculated. Figure 4.4 shows the feature extracted from such data during crack growth in a CT specimen. The probability distribution of the crack extension Δa_i corresponding to the interval ΔN_i can be calculated using equation (3.11). This is shown in Figure 4.5 using the input AE data shown in Figure 4.4 and the calibrated model shown in Figure 3.9.
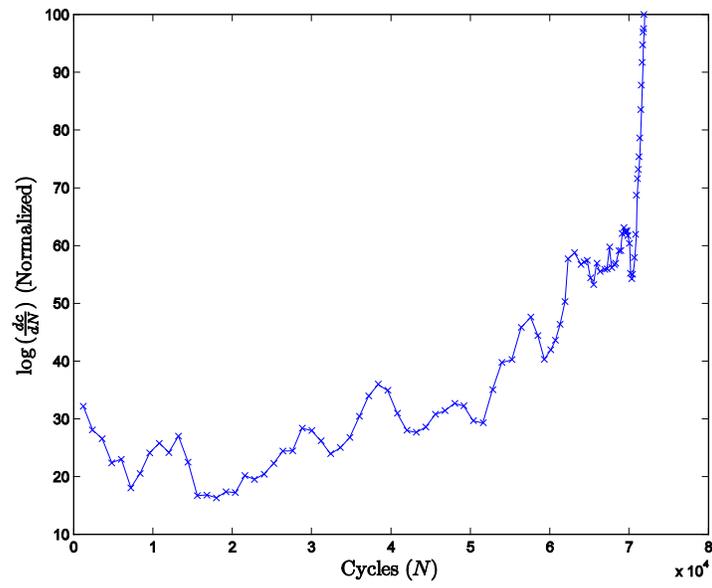
Figure 4.4 – The AE count rate feature extracted from signals obtained during crack growth
in a CT specimen
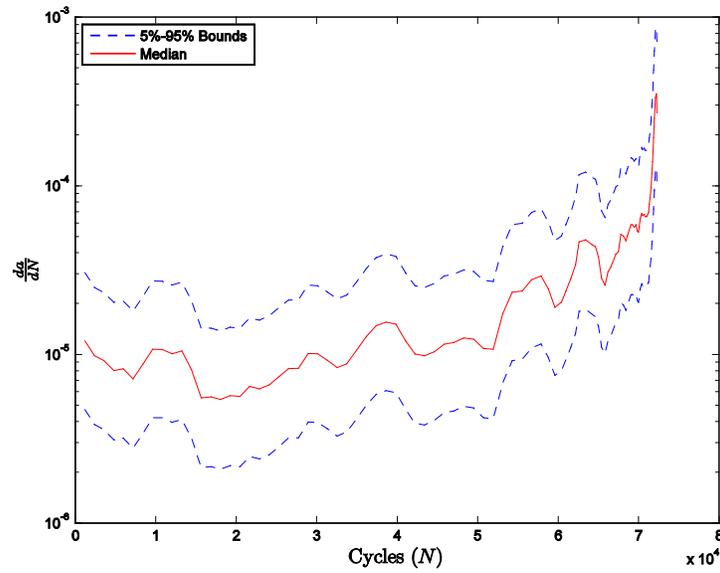
Figure 4.5 – Crack growth rate as a function of applied fatigue cycles predicted via AE
monitoring

If the crack size is known at the beginning of the interval, a probability distribution for the crack size at the end of the interval can be easily obtained. By repeating this process for consecutive intervals, multiple crack growth trajectories can be generated, as shown in Figure 4.6.
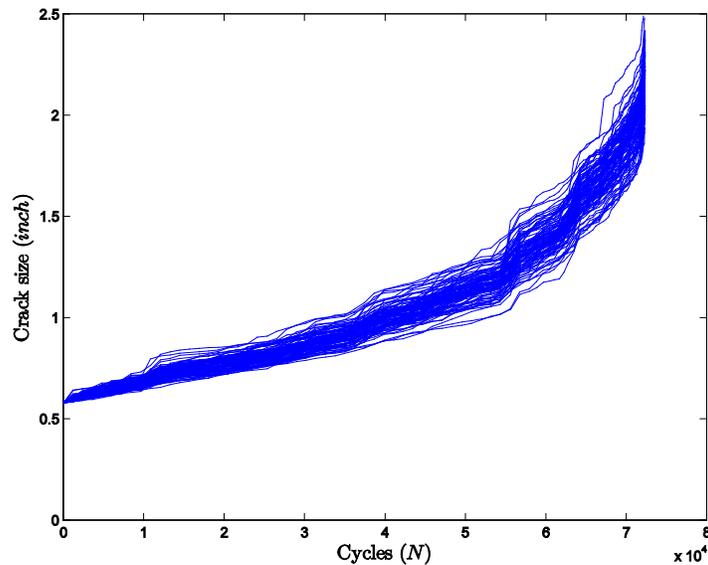
Figure 4.6 – Crack growth trajectories obtained via AE-based crack growth model

The main feature of the AE-based crack growth model presented above is that the rate of crack growth is determined experimentally, and therefore, there is no need to have any information about the amplitude of the applied loading cycles to the structure. This approach, however, relies heavily on a calibrated statistical model that should describe the relationship between an NDI feature of interest ($\log dc/dN$ in this case) and the crack growth rate. Developing a robust model that can capture this relationship with minimum uncertainty is a difficult task that is still a topic of continued research.

The performance of the proposed approach in one experiment is shown in Figure 4.7, in which the model prediction is compared against the actual crack growth trajectory

65

as measured in the test. This figure shows a rather poor performance of the model in this particular case, as the crack size is consistently over-estimated throughout the test.
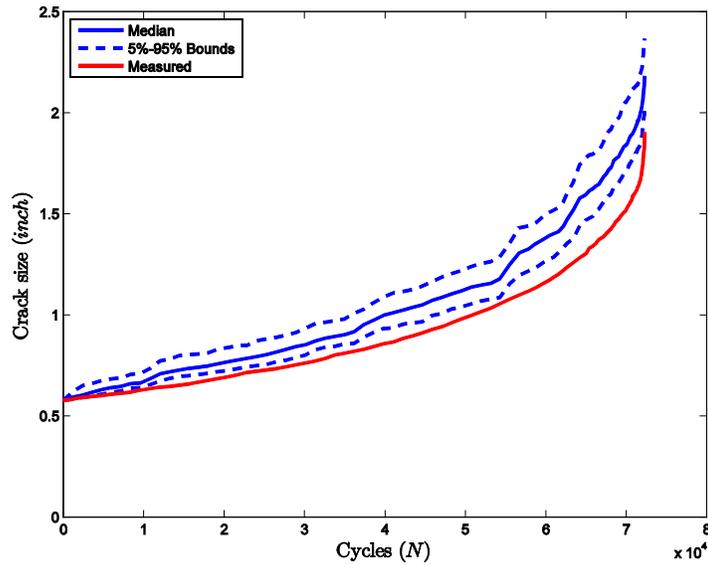
Figure 4.7 – Comparison of the outcome of AE-based crack growth model with actual crack measurements

The difference between the measured crack size and the output of the AE-based crack growth model is due to several sources of uncertainty that affect the model.

The first source of uncertainty is due to the statistical nature of the model being used in this approach; the linear relationship between the AE and fatigue parameters being used here only holds in an average sense: i.e., it is not valid for every single data point. In other words, the wider the distribution of Θ and the larger the value of σ is in (3.7) , the less accurate the outcome of the crack growth model will be.

The second source of uncertainty in the prediction results is the fact that when the model is being used, the input AE feature is calculated in an average sense over (typically) large intervals of elapsed cycles, ΔN. This will result in a coarser (and

therefore more uncertain) estimate from the model. The cumulative effect of these uncertainties could result in a mismatch between the true crack size and the model estimate. Reducing any of these sources of uncertainty will improve the model prediction.

4.4. *Probabilistic Empirical Crack Growth Model*

In this section, a probabilistic crack growth model is developed based on conventional fracture mechanics calculations. The model's performance will be tested based on the data from the crack growth tests described in Chapter 2. The primary objective of this chapter is to present a procedure to characterize the different sources of uncertainty present in a crack growth process and to develop a probabilistic model for fatigue crack growth. As will be shown here, despite all efforts to capture various sources of uncertainty, the final outcome of the model could still be far from reality. The outcome of this section, along with what was presented in section 4.3, will be used as inputs to the Bayesian fusion process that will be presented in the next chapter.

Fatigue crack growth, which is the main failure mechanism in structures experiencing dynamic loading, has been extensively researched for almost 170 years (Schütz 1996). Since the early 1960's when Paris (Paris & Erdogan 1963) initially proposed the relationship between fatigue crack growth rate and the stress intensity factor range, several researchers (including Forman (Forman et al. 1997) and Walker (Walker 1970), among others) have proposed different models of varying complexity to describe the crack growth phenomenon. A more comprehensive list of such models is presented in Table 4.1.

All these models are fundamentally similar in that they all use ΔK to calculate da/dN; their differences are in the way that each model accounts for other important parameters such as applied loading ratio, R.

Table 4.1 – Partial list of proposed fatigue crack growth models in literature (Shantz 2010)

Equation	Author
$\dfrac{da}{dN} = C \, (\Delta K \,)^n$	Paris
$\dfrac{da}{dN} = C \, (\Delta K \,)^n \left(1 - \dfrac{\Delta K_{th}}{\Delta K}\right)^p$	Mod. Paris
$\dfrac{da}{dN} = C \left(\dfrac{\Delta K}{(1-R)^{1-p}}\right)^m$	Walker
$\dfrac{da}{dN} = C \left(\dfrac{\Delta K^m}{(1-R)K_c - \Delta K}\right)$	Forman
$\dfrac{da}{dN} = C \left[\left(\dfrac{1-f}{1-R}\right)\Delta K\right]^n \left[\left(1 - \dfrac{\Delta K_{th}}{\Delta K}\right)^p / \left(1 - \dfrac{K_{max}}{K_c}\right)^q\right]$	FNK/ NASGRO
$\dfrac{da}{dN} = \dfrac{C_1}{\Delta K^{n1}} + \dfrac{C_2}{\Delta K^{n2}} - \dfrac{C_2}{[K_c(1-R)]^{n2}}$	Saxena
$\dfrac{da}{dN} = C(\Delta K - K_{th})^2 \left(1 + \dfrac{\Delta K}{K_c - K_{max}}\right)$	McEvily
$\dfrac{da}{dN} = C\left(\Delta K^p \Delta K_{max}^q\right)$	Roberts/Klesnil
$\dfrac{da}{dN} = C\left(K_{max}^2 - K_{min}^2\right)^m$	Arad
$\dfrac{da}{dN} = C(\Delta G)^m$	Mostovoy

To demonstrate the process of constructing a probabilistic crack growth model, the Paris equation in its original form[12] will be used as shown in (4.3). The process presented here, however, is applicable to any of the more sophisticated models as well.

---

[12] It should be noted that the goal of this section is not to develop a sophisticated crack growth model but rather to present the practical steps required to characterize the uncertainties involved in the modeling process and to show that despite every effort made at the time of modeling, the outcome of the empirical models could differ from reality because of various unknown/unpredicted factors that could affect the performance of any individual structure in real-life application.

For a given material and set of test conditions, the crack growth behavior can be described by the relationship between cyclic crack growth rate da/dN and stress intensity range ΔK as follows,

$$\frac{da}{dN} = C(\Delta K)^m \qquad\qquad (4.3)$$

where C and m are both constants that depend only on material properties and a set of test conditions, such as loading ratio, frequency and environment (Dowling 1998). The fact that these constants do not depend on the specific geometry of a component enables us to use the results obtained from standard fatigue tests on simple specimens to predict the crack growth behavior in more complex structures.

A crack growth model predicts the instantaneous size of a crack by simulating its growth trajectory starting from a known or assumed initial crack size. The required inputs to a crack growth model are the following:

- Initial crack size, a_0

- Applied load amplitude, ΔP

- Stress intensity factor range, ΔK (this is a function of instantaneous crack size, load amplitude and the specific geometry of the component)

- Model parameters C, m (obtained from fatigue tests performed on standard components with similar material and in the same testing condition)

Probabilistic Fracture Mechanics (PFM) is gaining popularity as a method for realistic evaluation of fracture response and reliability of cracked structures (Rahman & Rao 2002). Fracture mechanics and probability theory are implemented within the PFM framework to account for both mechanistic and stochastic aspects of the fracture

problem by considering the input variables as random rather than having deterministic values.

All the inputs to the fatigue problem suffer from some level of uncertainty, which if ignored, could lead to inaccurate predictions. Early work in PFM mainly focused on capturing the inherent random nature of the applied loads in structural components (Yang & Trapp 1974; Shinozuka & Yang 1969). In more recent works, various fracture mechanics inputs (such as initial crack size, material properties, and service conditions) are treated as random variables (Besuner 1987; Provan 1987).

The initial crack size, for instance, is often not known in advance and should be assumed based on past experience and best engineering judgment. a_0 is usually modeled as a lognormal random variable.

The applied load amplitude is also subject to uncertainty. In real-world applications where we deal with random amplitude loading, this uncertainty becomes much more problematic. The uncertainty over applied loading amplitudes exists even in a controlled laboratory environment and for simple constant amplitude loading conditions.

In the experiments conducted as part of this research, the main source of uncertainty in input loading was improper sensor calibration on the test frame. For higher loading frequencies, there may also be a mismatch between the force command signal sent to the test frame from the controller and the actual force applied to the specimen. Figure 4.8 shows the histogram of the applied load cycles in a constant amplitude test where the command signals for the minimum and the maximum loads were set to

30 lbf and 300 lbf, respectively. ΔP can be represented as a normal random variable with its mean and variance calculated from the following equations:

$$\mu_{\Delta P} = \mu_{P_{max}} - \mu_{P_{min}}$$
$$\sigma^2_{\Delta P} = \sigma^2_{P_{max}} + \sigma^2_{P_{min}}$$

(4.4)

Mean and variance of the minimum and maximum load can be easily calculated using the recorded loading history.
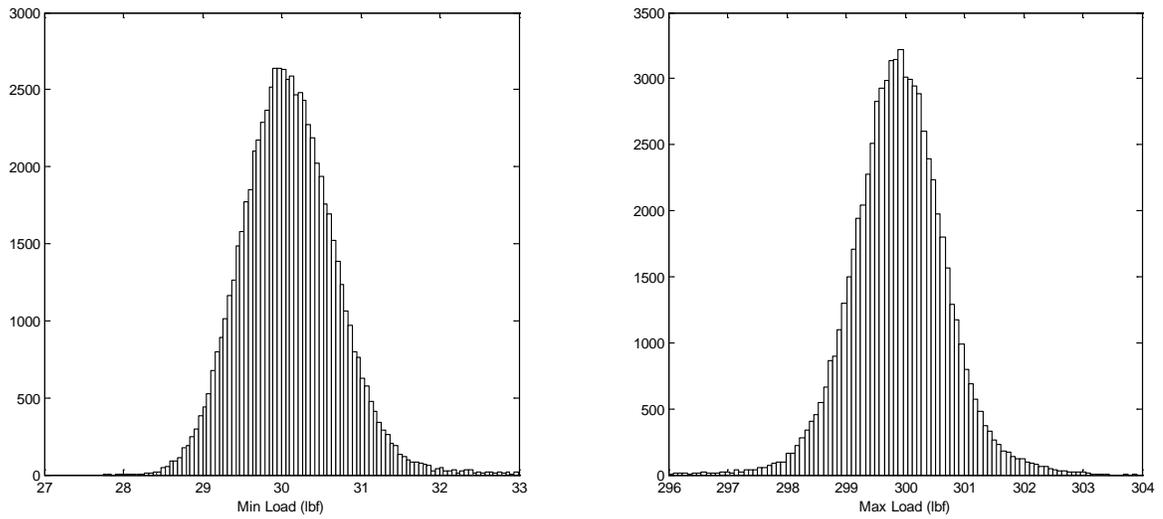
Figure 4.8 – The scatter in the minimum and maximum applied load in a constant amplitude fatigue test using the MTS machine.

Several researchers have introduced using stochastic parameters in empirical crack growth models (N. R. Moore et al. 1992; Yang et al. 1983; Provan 1987). By using experimental data to fit model parameters to distribution functions, the uncertainties in model parameters can be quantified.

So far this dissertation has discussed quantities such as a_0 and ΔP that can be modeled as independent random variables. When it comes to model parameters, C and m, the independence assumption of random variables no longer holds; C and m are in fact the intercept and slope of a line calculated in a curve fitting process and are

71

highly correlated. To capture this effect, the joint distribution of these parameters should be characterized and used in PFM.

To establish the joint distribution of parameters C and m, multiple tests should be carried out on standard specimens made of the same material and under the same test conditions (e.g., similar loading ratios and loading frequencies). The resulting data are scattered due to the uncertainties associated with each of the tests and specimens—the specimens may seem to be identical at the macro scale, while their microstructure could be significantly different. As proposed by Paris (Paris & Erdogan 1963), da/dN and ΔK have a (partial) linear relationship when plotted on log-log scale. C and m are the parameters of the line fitted to this data.

To develop a probabilistic crack growth model for this research, we obtained raw crack growth data from tests previously performed by NAVAIR on CT specimens with similar material (7075 aluminum) and under a comparable test condition (R=0.1). These data are shown in Figure 4.9.

Next, Bayesian regression (as described in section 3.3) will be used to find the model parameters. The advantage of using Bayesian estimation as opposed to conventional linear regression is that in the Bayesian approach, the information in the scattered test data (Figure 4.9) is captured via the distribution of model parameters. In other words, instead of suppressing the uncertainty in the test data (by using point estimates for the parameters), it will be retained in the model parameters and will affect the uncertainty of the outcome of the crack growth model. This is an important step towards constructing a more realistic crack growth model.
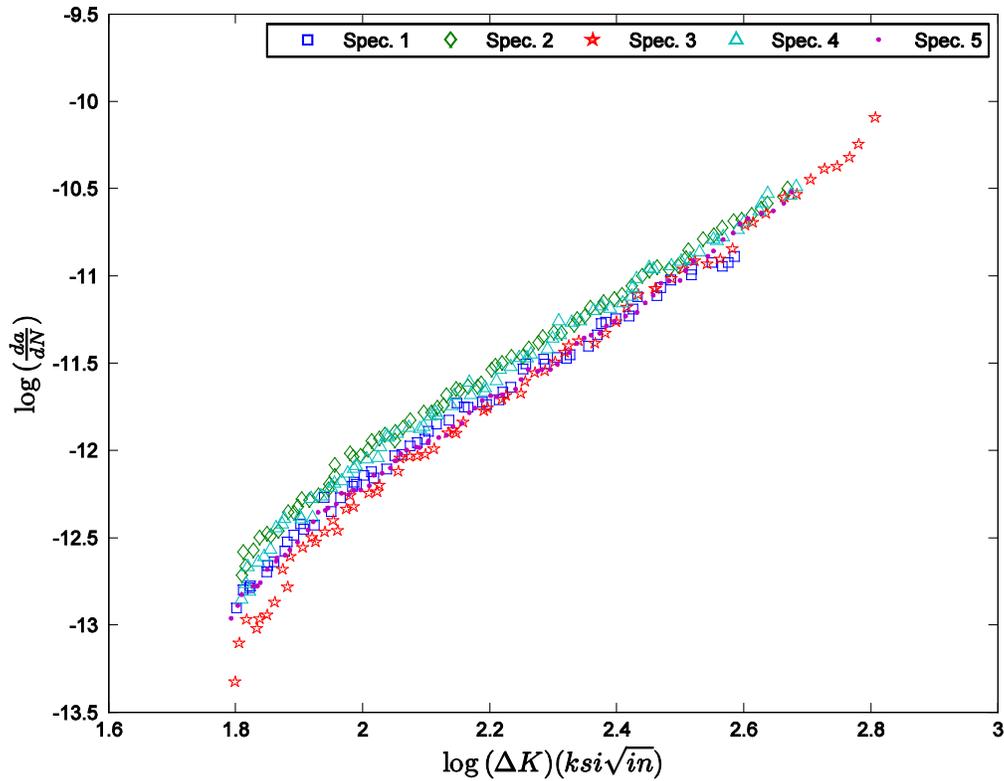
Figure 4.9 – Fatigue crack growth results for multiple CT specimens made of 7075 aluminum and tested at R=0.1

Figure 4.10 (top) shows the estimated marginal distributions of the model parameters. The distributions shown in this figure are not smooth, as they have been estimated using MCMC. Here, similar to the results in previous chapters, we have used WinBUGS to perform the Bayesian estimation. The contour plot of the joint distribution of parameters is presented in Figure 4.10 (bottom).
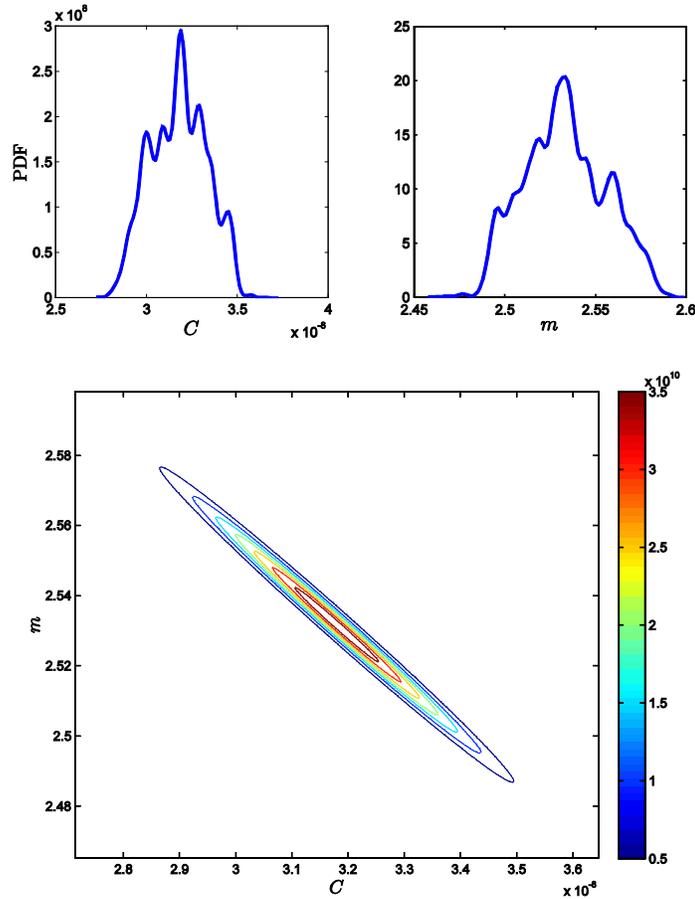
Figure 4.10 – Bayesian estimation results for parameters C and m of Paris equation based on experimental data

It is evident from the figure above that C and m are strongly correlated. Figure 4.11 shows the regression result along with 5% and 95% bounds for cases where C and m are treated as dependent and independent random variables. When the variables are considered dependent, the bivariate distribution shown in Figure 4.10 (bottom) will be used as $p(\Theta|D)$ in (3.11), whereas if the dependence between the variables is ignored, the product of the marginal distributions (Figure 4.10 (top)) will be used as $p(\Theta|D)$ in (3.11).

The resulting bounds on da/dN are wider when C and m are treated as independent random variables; under this assumption, the additional uncertainty will propagate through the crack growth model and will affect the resulting crack size distributions.
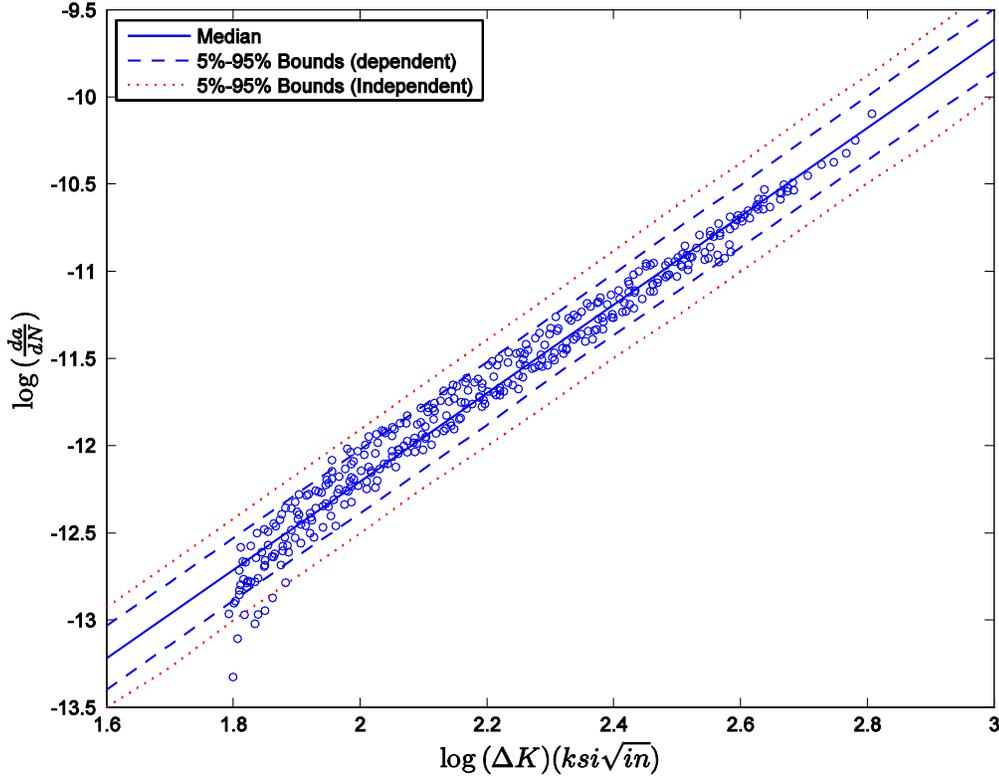
Figure 4.11 – Bayesian regression results with and without consideration for dependence between parameters

Once the uncertainties of all the inputs to the crack growth model are characterized, Monte Carlo simulation can be used to simulate the crack growth trajectories. To generate each crack growth trajectory, first a sample from the distribution of a_0 is drawn as the initial crack size. Next, a sample from the joint distribution of (C, m) is drawn and is set as the model parameters. At every iteration of the simulation, multiple samples are drawn from the distribution of ΔP to represent the uncertainty in the applied loading cycles. For every ΔP sample, a sample of ΔK corresponding to

75

that iteration is calculated. Finally, Paris equation (4.3) (with parameters chosen as described above) is used to calculate the corresponding samples of da/dN at that iteration. The crack growth trajectories can be obtained by summing over the amount of crack extension ($\Delta a = (da/dN).\Delta N$) at each iteration. The above process is then repeated for multiple initial crack sizes drawn from a_0 distribution.

The simulation result for crack growth in a CT specimen is shown in Figure 4.12 (left).
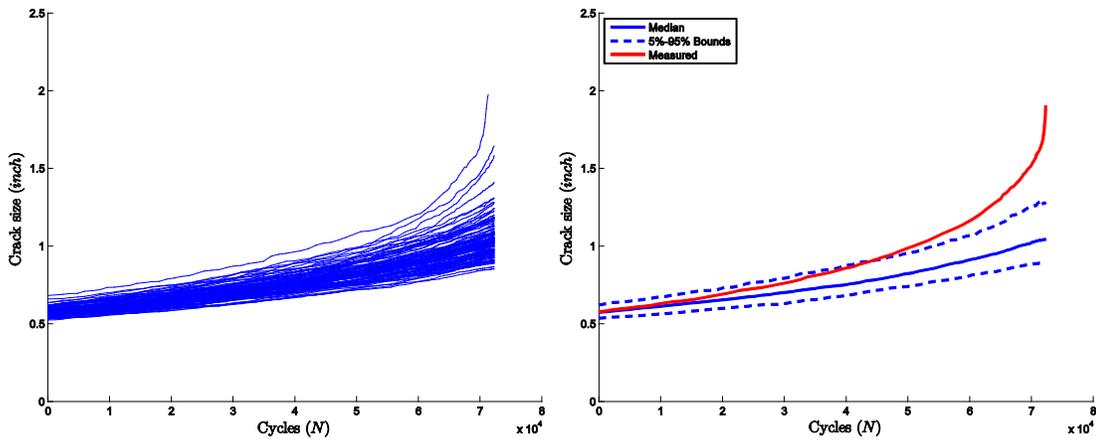
Figure 4.12 – Probabilistic crack growth simulation result: simulated trajectories (left), comparison with measured crack (right)

The comparison between simulation result and the actual measured crack size is shown in Figure 4.12 (right). The model in this case consistently underestimates the true crack size, and the difference grows towards the end of life of the component. This shows that the actual crack growth rate in the experiment was higher than what was predicted by the model. Several factors could contribute to the poor performance of the empirical model:

- Model uncertainty (structure): The simplest empirical crack growth model (Paris equation) was used to obtain the results presented here. Equation (4.3)

76

shows that this simplified model does not take into account other contributing factors that could affect the rate of crack growth. Other, more sophisticated models that account for factors such as applied loading ratio (the Walker model (Walker 1970) and the Forman model (Forman et al. 1997)) or the crack closure effect (the Closure model (Newman Jr 1981)) could be used to reduce the uncertainty due to model structure.

- Model uncertainty (parameters): The estimated crack size is very sensitive to the parameters of the empirical model. Any error in the estimation process of such parameters (e.g., using data from tests performed in a significantly different environment) could result in poor performance of the crack growth model.

- Effect of the "rogue" flaw: Empirical life models are developed based on average behavior of materials and fail to capture the contributing factors that are specific to an individual structure. The result presented here is from a test performed on one specific specimen that could have suffered from material flaws (e.g., a large undetected internal flaw) and therefore had a faster-than-average growth rate. Many more tests are required to reliably assess the performance of an empirical model.

The result presented here clearly shows that despite every effort made at the time of modeling, the outcome of the empirical models could be far from reality because of unpredicted factors that could affect the performance of any individual structure in a real-life application.

The model developed in this section will be used in the next chapter as a typical example of an empirical model that fails to predict the reality due to multiple sources of uncertainty that are not taken into account at the time of modeling. The chapter will then discuss how the additional feedback provided by structural health monitoring techniques could be used to update the model estimates in a systematic fashion.

4.5. *Summary*

Two new approaches were proposed for structural health management using AE monitoring: In the first approach, an AE-based risk measure, R_{AE}, is defined as the probability that the crack growth will transition from the stable to non-stable/rapid growth regime. The transition probability is equal to the probability that K_{max} exceeds the fracture toughness of the material, K_{Ic}. In the proposed approach, K_{max} is calculated as a function of real-time AE monitoring data using the calibrated model obtained in the previous chapter.

In the second approach, AE monitoring data is used to calculate the instantaneous distribution of crack growth rate, da/dN. For a given initial crack size and with crack growth rates obtained from AE monitoring, the crack size distribution is estimated as a function of elapsed fatigue cycles.

In this chapter, the process for developing an empirical probabilistic crack growth model was also presented. In the next chapter, the outcome of this model as well as its parameters will be updated using additional feedback provided by an AE-based structural health monitoring system.

Chapter 5: Multi-Source Bayesian Knowledge Fusion

5.1. *Introduction*

The ultimate goal in structural health management is to assess the integrity of a structure at the current time and to predict the long-term evolution of the damage based on the anticipated future usage profile.

The necessary information for developing a structural health diagnostic and prognostic solution is often obtained from various sources; this is similar to having a group of *experts* (with different credibility) that can each provide relevant information about certain aspects of the problem at hand. It is critical to be able to formally combine all these independent sources of information to achieve a more accurate assessment of the health of a structure.

Fusion of data and information can happen at different levels in an automated health management system, as shown in Figure 5.1. At each level, the outcomes of the previous layer are fused together with the objective to improve the overall performance of the SHM solution.
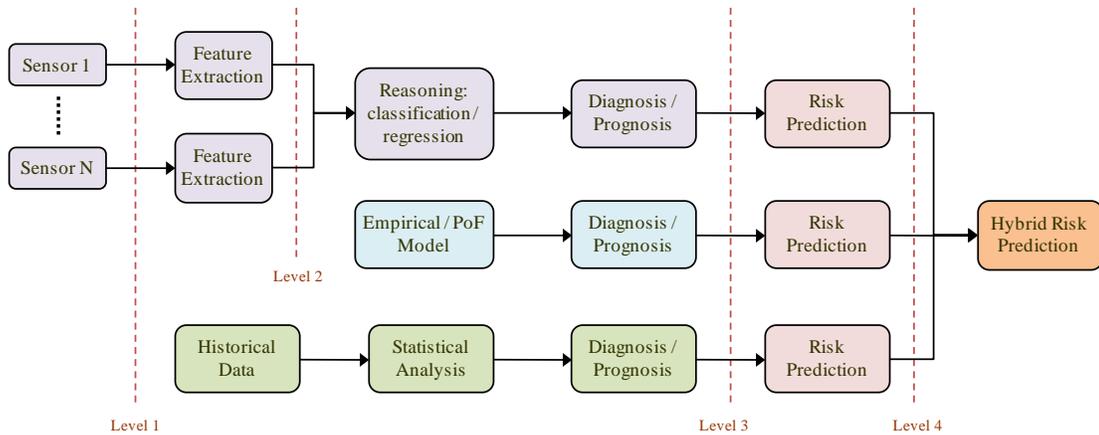
Figure 5.1 – Fusion architecture

At the lowest level, data coming from an array of sensors can be combined to validate the signals or to create possible new features. At level 2, feature extraction is performed on signals from individual sensors, and then the extracted features are combined to obtain better diagnostic and prognostic information. For instance, in AE monitoring, the AE count rate feature is calculated by first extracting the AE count feature directly from the raw signals and then calculating its rate of change with respect to elapsed fatigue cycles. Knowledge fusion could also be performed at a higher level (level 3) where fusion techniques are used to combine diagnostic and prognostic information obtained from various sources such as sensor readings and experimental approaches, empirical models, and statistical methods applied to historical data. Fusion could also be performed at level 4, where different measures of risk calculated at the previous layer (using different approaches) are combined to obtain a hybrid (unified) risk prediction.

The main goal in fusion is to obtain results that are superior to all the individual inputs that contribute to it. However, there is always the danger that the fusion process produces results that are worse than what was attainable from the best individual approach used in the fusion process. This can happen because poor

estimates can drag better ones if weights to each approach are not properly assigned. The only solution to this concern is *a priori* assessment of the credibility and performance of individual building blocks of a fusion model and weighing each block accordingly. Therefore, the ideal knowledge fusion process for a given application should be based on historical performance of individual models.

Various techniques are available for performing data, feature and knowledge fusion at different levels. Some of the most common fusion approaches include (Vachtsevanos et al. 2006):

- Bayesian Fusion

- Dempster-Shafer Fusion

- Fuzzy-Logic Inference Fusion

- Neural-Network Fusion

There is no hard rule for selecting the appropriate fusion technique for an application, and discovering the tool that best suits an application could be a daunting task. Each case should be individually assessed based on the level at which fusion is performed and the amount and type of available information. Of all these techniques, the focus in this dissertation will be on the Bayesian approach to fusion.

The approach presented here enables us to predict the posterior probability distribution function of the damage state using a dynamic state transition model and a measurement model. This methodology—which is based on recursive Bayesian estimation technique—allows for fusion of information from multiple sources in a principled manner. This is a robust framework for long-term prognosis, as it effectively accounts for uncertainties.

Recursive Bayesian estimation, also known as *Bayes filter*, is a probabilistic approach for estimating an unknown probability density function recursively over time using incoming uncertain observation (noisy measurements) and a mathematical process model that describes the evolution of the state variables over time.

The key state variable that we are interested in estimating in this study is the crack size in the structure. More specifically, we are interested in estimating the probability density of crack size at any point in time based on all available sources of information.

Prediction of future state of damage (i.e. prognosis) is an inherently uncertain process that relies on accurate estimation of the current state of damage as well as reliable modeling to describe the fault progression.

The damage progression model (process model) that will be used in this chapter is the probabilistic empirical crack growth model that was previously developed in Section 4.4. As was discussed before, the overall performance of the SHM solution can potentially be improved by fusing the outcome of this model with real-time NDI observations. Here, the crack size estimates predicted by this model will be updated recursively using two types of observations:

1. Observations of the crack size: these are direct observations of the damage state that may become available by periodic inspection of the structure. Like any other observation, these suffer from measurement error and other uncertainties that should be taken into account.

2. Observations of the crack growth rate: these observations are obtained from the online AE-based NDI technique developed in this dissertation. This type of evidence is indirectly used to update the estimate of the crack size.

The goal is to use the recursive Bayesian estimation technique to fuse the outcome of the empirical crack growth model with the crack size and the crack growth rate observations.

The sections below start with a high-level discussion of recursive Bayesian estimation and then continue with a more detailed discussion of Kalman filter and its extensions and how they can be implemented to address the fusion problem at hand.

5.2. *Recursive Bayesian Estimation*

Recursive (sequential) Bayesian estimation is a probabilistic inference process in which the hidden (unobserved) variables (states or parameters) of a dynamic system are estimated based on noisy and uncertain observations (Figure 5.2).
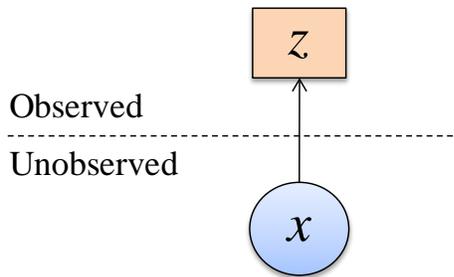
Figure 5.2 – Schematic diagram of probabilistic inference: Given a vector of noisy observations z, what can we infer about unknown system state x?

The focus here will be on discrete-time dynamic systems that can be described by a *dynamic state-space model*. A state-space model is a mathematical representation to describe the evolution of a dynamic system over time. The following set of equations describe a discrete-time, non-linear, state-space model,

$$x_k = f(x_{k-1}, u_k, w_k) \qquad\qquad\qquad (5.1)$$
$$z_k = h(x_k, v_k) \qquad\qquad\qquad\qquad (5.2)$$

where $f(\cdot)$ is the nonlinear state transition function that describes the evolution of system state x from time step $k-1$ to k. This is a non-deterministic transition in which the uncertainty is represented by the process noise, w_k. The term u_k is a known exogenous input to the system at time step k which may or may not exist. The function $h(\cdot)$ in (5.2) is the observation function that, at any time step k, relates the observation z_k to the true state x_k. v_k is the corresponding observation noise that corrupts the observation of the hidden state, x_k, through the observation function $h(\cdot)$.

Let $X_k = \{x_1, x_2, \dots, x_k\}$ represent a time-series of the state variable of interest where x_k is a random variable at the k-th time step. Similarly, $Z_k = \{z_1, z_2, \dots, z_k\}$ is a time-series of the observations on the same time horizon. Both the state and the observations are described by random variables due to the uncertainties involved. Our goal is to estimate the unobserved state x_k based on all observations $z_1, z_2, \dots, z_k$ as well as the process model that describes the evolution of x through time. In mathematical form, we are interested in calculating $p(x_k | z_k, z_{k-1}, \dots, z_1)$ which is the posterior density of x_k conditioned on all observations available up to time step k. In general, the complexity of computing this posterior density grows exponentially as the number of incoming observations increases over time. A number of assumptions are typically made to make such computations tractable; Bayes filters assume that the dynamic system that describes the state evolution is a Markov process. Because of the Markov assumption, the probability of the current true state given the immediately previous one is conditionally independent of the other earlier states.

$$p(x_k|x_{k-1}, x_{k-2}, \ldots, x_1) = p(x_k|x_{k-1}) \qquad\qquad (5.3)$$

The Markov assumption also implies that the measurement at the k-th time step is dependent only on the current state x_k and is conditionally independent of all other past states given the current state.

$$p(z_k|x_k, x_{k-1}, \ldots, x_1) = p(z_k|x_k) \qquad\qquad (5.4)$$

Equations (5.3) and (5.4) are the two key components of Bayes filters; equation (5.3) is known as the process model where $p(x_k|x_{k-1})$ describes the *system dynamics*—that is, how the system states change over time. The information about the system dynamics is usually available from the physics of the process that is being modeled. For a dynamic state-space model, the process model $p(x_k|x_{k-1})$ is fully defined by the state transition function $f(\cdot)$, the process noise density $p(v_k)$ and the initial distribution of the state variable $p(x_0)$. In the damage prognosis problem, a process model is needed that describes how one can obtain the damage state at current time step, x_k, given the state of damage at previous time step, x_{k-1}. The process model, in general, could be defined either explicitly or implicitly as a black-box model. In this dissertation, the nonlinear empirical crack growth model that was developed earlier will be used as the process model in defining the state-space model.
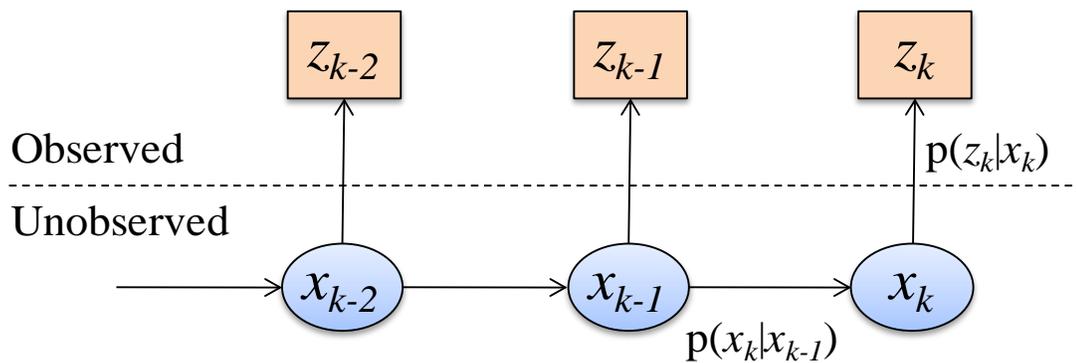
Figure 5.3 – Graphical representation of a dynamic state-space model.

Equation (5.4) is commonly referred to as the *observation model* or the *perceptual model*. The observation likelihood, $p(z_k|x_k)$, describes the likelihood of making observation z_k given the current state variable x_k (see Figure 5.3). The observation model is fully defined by the observation function $h(\cdot)$ and the observation noise, v_k (see (5.2)). The definition of the observation function is typically based on the properties of the sensor technology being used and should capture the error characteristics of the measurement system. Roughly speaking, the observation model answers the question: "What do the sensors observe if the true state of the system is x_k?" Both the accuracy (the proximity of the observations to the true value) and the precision (the repeatability of the observations) of the measurements play a role in defining the observation model (Figure 5.4). For instance, if based on previous experience, we know that our measurement system suffers from a systematic bias, that bias should be included in the definition of the measurement model. In this dissertation, we will assume that our measurements are accurate but not precise; the lack of precision is represented by the observation noise, v_k.
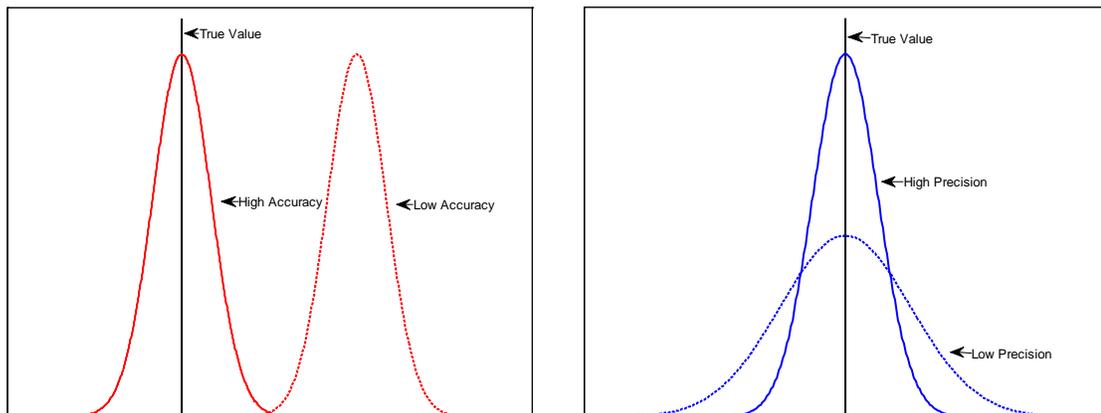
Figure 5.4 – The accuracy and the precision of measurements

Once the process model and the observation model are characterized, the next step is to derive the equations that allow the posterior density of the state variable to be recursively updated as new observations arrive. By making use of Bayes' rule and taking advantage of the conditional independence assumption, the posterior density can be derived as follows:

$$p(x_k|Z_k) = \frac{p(Z_k|x_k)p(x_k)}{p(Z_k)} \qquad (5.5)$$

$$= \frac{p(z_k, Z_{k-1}|x_k)p(x_k)}{p(z_k, Z_{k-1})} \qquad (5.6)$$

$$= \frac{p(z_k|Z_{k-1}, x_k)p(Z_{k-1}|x_k)p(x_k)}{p(z_k|Z_{k-1})p(Z_{k-1})} \qquad (5.7)$$

$$= \frac{p(z_k|Z_{k-1}, x_k)p(x_k|Z_{k-1})p(Z_{k-1})p(x_k)}{p(z_k|Z_{k-1})p(Z_{k-1})p(x_k)} \qquad (5.8)$$

$$= \frac{p(z_k|Z_{k-1}, x_k)p(x_k|Z_{k-1})}{p(z_k|Z_{k-1})} \qquad (5.9)$$

$$= \frac{p(z_k|x_k)p(x_k|Z_{k-1})}{p(z_k|Z_{k-1})} \qquad (5.10)$$

where Z_k is the set of all the observations up to time step k. Notice that in going from (5.7) to (5.8), Bayes' rule was used again on $p(Z_{k-1}|x_k)$. We also used the conditional independence of observations given the state in going from (5.9) to (5.10).

To gain more insight into the Bayesian estimation process, each term in (5.10) will be examined more closely; the term $p(z_k|x_k)$ is the observation likelihood as described by the observation model at time step k. This will be discussed in greater detail in the next section. The term $p(x_k|Z_{k-1})$ is the *prior* estimate for the state variable at time step k—that is, the predicted state value at time step k given all the

measurements up to the previous time step, $k - 1$. This term can be expanded using the chain rule as follows,

$$p(x_k|Z_{k-1}) = \int p(x_k|x_{k-1})p(x_{k-1}|Z_{k-1}) \, dx_{k-1} \qquad (5.11)$$

where $p(x_k|x_{k-1})$ is the process model as described before and $p(x_{k-1}|Z_{k-1})$ the *posterior* estimate of the state variable from previous time step, $k - 1$. The posterior from each time step is projected forward in time, using the process model, to obtain the prior estimate of the state for the next time step.

The denominator in (5.10) is the normalizing constant that—through the law of total probability—is given by

$$p(z_k|Z_{k-1}) = \int p(z_k|x_k)p(x_k|Z_{k-1}) \, dx_k \qquad (5.12)$$

The posterior $p(x_k|Z_k)$ is just a conceptual solution to the recursive estimation problem. In general, the multi-dimensional integrals (5.11) and (5.12) have no explicit analytical solution. This means, from a practical point of view, that one needs to resort to an approximate description of the posterior density of the state variables. There is one case, however, where a closed-form recursive solution for the posterior density exists. This occurs when the state-space equations $f(\cdot)$ and $h(\cdot)$ are linear and all the random variables are Gaussian. The solution in this case is given by the well-known *Kalman filter (KF)* (Kalman 1960). For most general real-world systems, however, the multi-dimensional integrals are intractable, and approximate solutions must be used.

Several approximate solutions to the recursive Bayesian estimation problem have been proposed in a variety of fields. These approximate methods are based on simplifying assumptions regarding either the form of the probability densities to be

estimated or the structure of the underlying system dynamics. These assumptions are made to allow for tractable and implementable estimation algorithms. The *extended Kalman filter (EKF)* (Jazwinski 1970) method is an example of an approximation of the underlying dynamics of the system; the EKF extends the application of the Kalman filter framework to nonlinear Gaussian systems by first linearizing the state transition and the observation equations using a first-order Taylor series approximation around the current estimate.

In the following sections, the KF equations and their interpretations are first described; next, a brief overview of recursive Bayesian estimation methods for nonlinear and non-Gaussian problems will be presented.

5.3. *The Kalman Filter*

The celebrated Kalman filter is the optimal closed-form solution to the recursive Bayesian estimation problem for a linear system with Gaussian random variables.

Since its original development (Kalman 1960; Kalman & Bucy 1961) the Kalman filter has been the subject of extensive research and has been applied successfully in numerous real-world applications. Owing mostly to its simple implementation and computational efficiency, the Kalman filter is established as a fundamental tool for analyzing and solving a broad class of estimation problems (McGee et al. 1985). Apart from being a Bayesian solution to a certain class of models, the Kalman filter has several other interpretations; see (West & Harrison 1997) and (B. D. O. Anderson & J. B. Moore 2005) for historical perspectives and a complete presentation of linear estimation theory.

In this section, the equations for the KF solution to recursive Bayesian estimation will be presented without proof. More details about the derivations of these solutions can be found in (Simon 2006; Welch & Bishop 1995; Crassidis & Junkins 2004).

The Kalman filter addresses the general problem of estimating the state variable, $x_k \in \mathbb{R}^n$, of a system described by a discrete-time linear state-space model based on observations $z_k \in \mathbb{R}^m$, at time step k. Such system is governed by the following equations:

$$x_k = Ax_{k-1} + Bu_k + w_k \qquad (5.13)$$
$$z_k = Hx_k + v_k \qquad (5.14)$$

which are the same Equations as (5.1) and (5.2), respectively, for the case of linear systems.

Here the noise processes w_k and v_k are both defined as white Gaussian noise—i.e., zero-mean, uncorrelated Gaussian random variables with known covariance matrices Q_k and R_K, respectively.

$$w_k \sim N(0, Q_k) \qquad (5.15)$$
$$v_k \sim N(0, R_k) \qquad (5.16)$$

The matrix $A_{n \times n}$ in (5.13) relates the state at the previous time step $k - 1$ to the state at the current time step k. The matrix $B_{n \times l}$ relates the exogenous input $u_k \in \mathbb{R}^l$ to the state x_k. The matrix $H_{m \times n}$ in (5.14) relates the measurement z_k to the state x_k at the current time step. In practice, A, B and H could all be functions of time and change with every time step, but in this dissertation they are assumed constant.

According to KF assumptions, the state variable is Gaussian; therefore, the posterior density $p(x_k|Z_k)$ can be fully specified by calculating its first and second moments.

Let $\hat{x}_k$ and P_k denote the first and second moments of the posterior state distribution (i.e., posterior mean and posterior covariance) at time step k:

$$\hat{x}_k = E[x_k]$$

$$P_k = E[(x_k - \hat{x}_k)(x_k - \hat{x}_k)^T]$$

and,

$$p(x_k|Z_k) = N(\hat{x}_k, P_k) \qquad (5.17)$$

It can be shown (Simon 2006; B. D. O. Anderson & J. B. Moore 2005; West & Harrison 1997) that the posterior mean $\hat{x}_k$ and the posterior covariance P_k can be calculated as follows:

$$\hat{x}_k = \hat{x}_k^- + K_k(z_k - H\hat{x}_k^-) \qquad (5.18)$$

$$P_k = (I - K_kH)P_k^- \qquad (5.19)$$

where,

$$K_k = P_k^- H^T (HP_k^- H^T + R)^{-1} \qquad (5.20)$$

$$\hat{x}_k^- = Ax_{k-1}^- + Bu_k \qquad (5.21)$$

$$P_k^- = AP_{k-1}A^T + Q \qquad (5.22)$$

Descriptions of all these terms are given in Table 5.1.

Table 5.1 – Description of key terms in Kalman filter equations

Term	Name	Description
$\hat{x}_k$	*a posteriori* state estimate	Mean of the posterior state density at time k. This is *a posteriori* because it has been updated with observation z_k.
$\hat{x}_k^-$	*a priori* state estimate	This is the state estimate at time k, solely based on the process model (5.13) as described by (5.21). The minus superscript denotes that this is an *a priori* estimate of the state based only on system dynamics and before updating with observation z_k.
P_k	*a posteriori* error covariance matrix	Covariance matrix of the posterior state density at time k. This is *a posteriori* because it has been updated with observation z_k. P_k is a measure of accuracy for the estimated state.
P_k^-	*a priori* error covariance matrix	Covariance matrix of the state density at time k, solely based on the process model as described by (5.22). The minus superscript denotes that this is an *a priori* estimate based only on system dynamics and before updating with observation z_k.
K_k	Kalman Gain	The Kalman gain is a blending factor used in Equations (5.18) and (5.19) to update (or adjust) the prior state estimate $\hat{x}_k^-$ and covariance estimate P_k^- based on new observation.
A, B, H, Q, R	N/A	Known matrices which define the state-space equations.

The term $(z_k - H\hat{x}_k^-)$ in (5.18) is known as observation *innovation*; the innovation reflects the discrepancy between the actual measurement z_k and the predicted measurement $H\hat{x}_k^-$. If the two are in complete agreement, the innovation corresponding to the observation at that time step will be zero, and therefore, no updating will take place. This happens if the observation z_k does not contain any new information about the system that is not already captured in the process model.

The easiest way to interpret the Kalman filter equations is to think of them as a two-step updating process (Welch & Bishop 1995):

1. Step 1 is the *time update* in which the process model (5.13) is used to project forward (in time) the state estimate x_{k-1}^- and the error covariance estimate P_{k-1} at the previous time step $k - 1$ to obtain the *a priori* estimates $\hat{x}_k^-$ and P_k^- at the current time step k.

2. Step 2 is the *measurement update* in which the most recent observation z_k is used to update the *a priori* estimates $\hat{x}_k^-$ and P_k^- to obtain the *a posterior* estimates $\hat{x}_k$ and P_k. The goal in this step is to use the additional information in the observation to improve the *a priori* estimates that were solely based on the process model.

The time and measurement update pair are repeated recursively for prediction at future time steps; the *a posteriori* estimate at the current time step will be projected forward to predict a new *a priori* estimate for the next time step, which will in turn be updated by the new measurements at that time step.

5.3.1. Extensions to the Kalman Filter

As discussed earlier in this chapter, the Kalman filter formulation is based on two limiting assumptions: (a) the process and observation models should be linear, and (b) the uncertainty of the state variables should be represented by Gaussian distributions. In this section, two extensions of the Kalman filter will be discussed: the extended Kalman filter (EKF) and the particle filter.

In the extended Kalman filter, the state transition and observation models need not be linear functions of the state; EKF is the nonlinear version of the Kalman filter that linearizes the system using a first-order Taylor series approximation around its current state. The idea of the EKF was originally proposed by Stanley Schmidt so that the Kalman filter could be applied to nonlinear spacecraft navigation problems (Bellantoni & Dodge 1967). This filter has undoubtedly been the most widely used nonlinear state estimation technique in the past few decades (Simon 2006).

Some higher-order approximation techniques have been proposed (e.g., the unscented Kalman filter (Julier & Uhlmann 1997)) to reduce the linearization errors that are inherent in the EKF. These techniques typically provide better estimation performance for highly nonlinear systems, but they do so at the price of higher complexity and computational expense (Simon 2006).

Unlike EKF and its higher-order extensions that are all approximate nonlinear filters, the particle filter is a completely nonlinear state estimator. The particle filter, also known as the Sequential Monte Carlo method (SMC), is a statistical, brute-force approach to estimation that works well for problems beyond the scope of the conventional Kalman filter (i.e., highly nonlinear systems and/or systems with non-

Gaussian state variables). There is, of course, a price to be paid for the higher performance of particle filters, and that is increased computational cost.

Particle filter is a simulation-based estimation technique that models the PDF of state variables using a set of discrete points called particles. The main idea of particle filtering is intuitive and straightforward: randomly generate samples from the PDF of the initial state, which is assumed to be known—the number of samples is chosen as a trade-off between computational effort and estimation accuracy. Next, use the process model of the system and a known distribution of the process noise to propagate each particle in time to obtain an *a posteriori* set of particles at the next time step. The next step is to compute the relative likelihood of each particle conditioned on the measurement at the current time step. The final step is to generate a set of *a posteriori* particles based on the calculated relative likelihoods. Any desired statistical measure of the posterior distribution of the state can be calculated from these *a posteriori* particles. For a detailed overview of the particle filter technique and its various applications, see (Doucet et al. 2001; Doucet & Johansen 2010). Particle filter algorithms and practical implementation issues are presented in (Simon 2006; Van Der Merwe 2004).

The particle filter is an alternative to EKF with the advantage that with sufficient samples, it can be made more accurate than the EKF (or any of the other approximate nonlinear techniques). However, when the simulated sample is not sufficiently large, the particle filter might suffer from sample impoverishment.

In this dissertation, EKF is used as the practical solution to the recursive estimation problem mainly because the process model used here (i.e., the empirical crack growth

model) is not considered highly nonlinear and also because the Gaussian assumption for the state variable was sufficient for the purpose of this dissertation. Details of the EKF equations and algorithms can be found in various references, including (Welch & Bishop 1995; Diard et al. 2003).

5.4. *State-Space Formulation for Crack Growth Problem with AE Observations*

In this section, the theory of recursive Bayesian estimation is applied to the specific knowledge fusion problem at hand. To do so, we set up a Bayesian inference problem in which all the pieces of knowledge available about the crack growth phenomenon are systematically fused together to produce an updated crack size distribution.

The available information about the crack growth phenomenon consists of the following:

1. An empirical crack growth model: our knowledge is embodied in the structure of the model as well as the model parameters.

2. Sparse crack size observations: these typically come from scheduled and non-scheduled maintenance events in which the structure is rigorously inspected for possible cracks.

3. Real-time crack growth rate measurement: the AE-based methodology developed in this dissertation is used to get an (indirect) continuous measurement of crack growth rate.

The model alone (Source 1) could be used to predict the crack size as a function of geometry and input stresses. But as discussed earlier, these models are often based on various simplifying assumptions and/or are based on limited empirical data, and as a

result, suffer from inaccuracy and imprecision. To account for such inaccuracies and to make the system robust to rogue cracks (unexpected large cracks that the model does not account for), it is of great interest to use other sources of information (Sources 2, 3) that directly originate from monitoring the particular target system. The feedback provided from the real system, when combined with the model estimate, will result in less uncertain condition assessment and more accurate prognosis.

In the context of the recursive Bayesian estimation framework described above, each of these pieces of information could be used to define and characterize a part of the state-space model or the observations used in the updating process. The first step in posing the fusion problem in the Bayesian estimation context is to define the state-space model. To do so the following must be defined:

- The state variable(s) to be estimated.

- A function that defines the evolution of state variables over time. (process model)

- A function that defines how various observations over time are related to the state variables. (observation model)

- The noise (uncertainty) in both the process model and the observation model.

Equation (5.23) describes the general form of the process model where X is the vector of state variables to be estimated.

$$x_k = f(x_{k-1}, u_k, w_k)$$ (5.23)

In a typical crack growth problem the state variable of interest is the crack size at time step k, denoted by a_k. In addition to a_k, the crack growth rate, $\dot{a}_k$, was chosen as the second state variable to be estimated, i.e. the state vector $x_k = \begin{pmatrix} a_k \\ \dot{a}_k \end{pmatrix}$.

We use the exogenous input u_k to map the time steps in our state-space model to the actual elapsed loading cycles, ΔN_k. The process noise is defined by $w_k \sim N(0, Q_k)$ the same as before. Note that here Q_k is a 2×2 covariance matrix, as we are estimating two state variables. We can now rewrite (5.23) as follows:

$$\begin{pmatrix} a_k \\ \dot{a}_k \end{pmatrix} = \begin{pmatrix} a_{k-1} + \dot{a}_{k-1}\Delta N_k \\ C(\Delta K_k)^m \end{pmatrix} + w_k \qquad (5.24)$$

Equation (5.24) consists of two equations that each describe the evolution of one of the state variables over time. The first equation is simply based on the difference relationship $\dot{a}_{k-1} = (a_k - a_{k-1})/\Delta N_k$ that defines the crack growth rate at time step $k-1$. Based on this relationship, the crack size a_k can be calculated based on the crack size at the previous time step, the crack growth rate at the previous time step, and the number of actual cycles elapsed since the last time step.

The second equation in (5.24) describes how the crack growth rate can be calculated at every time step k. Here the Paris equation is used to relate the crack growth rate $\dot{a}_k$ to the stress intensity factor range ΔK_k at every time step; that is, $\dot{a}_k = C(\Delta K_k)^m$ where C and m are the parameters of the Paris equation—any other empirical crack growth model could be used here as well.

As discussed in previous chapters, the stress intensity factor range at every time step k, ΔK_k, could be defined as a function of the geometry of the structure, applied loading cycle ΔP_k and the crack size a_k. For instance, ΔK_k for a standard CT specimen (ASTM E647-08 2008) is defined as follows:

$$\begin{aligned} \Delta K_k &= g(a_k) \\ &= \frac{\Delta P_k}{B\sqrt{W}} \frac{2\alpha}{(1-\alpha_k)^{3/2}} (0.886 + 4.64\alpha_k - 13.32\alpha_k^2 + 14.72\alpha_k^3 \\ &\quad - 5.6\alpha_k^4) \end{aligned} \qquad (5.25)$$

where α_k is the dimensionless crack size a_k/W, B and W are the width and the thickness of the specimen, respectively, and ΔP_k is the amplitude range of applied load at time step k.

Note that for a given geometry, the ΔK (and therefore, $\dot{a}$) can be calculated as a function of applied loading and the instantaneous crack size a. This completes the definition of the recursive relationship of the system states in (5.24).

The next step is to fully define the observation model (5.26):

$$z_k = h(x_k, v_k) \tag{5.26}$$

As mentioned before, here there are two types of observations; an observation vector $z_k = \begin{pmatrix} z_{1k} \\ z_{2k} \end{pmatrix}$ is defined where z_{1k} is the observation of crack size, and z_{2k} is the observation of crack growth rate at time step k.

$$\begin{pmatrix} z_{1k} \\ z_{2k} \end{pmatrix} = \begin{pmatrix} 1 & 0 \\ 0 & 1 \end{pmatrix} \begin{pmatrix} a_k \\ \dot{a}_k \end{pmatrix} + v_k \tag{5.27}$$

where $v_k \sim N(0, R_k)$ and R_k is a 2×2 covariance matrix. Here a linear form is assumed for the observation function $h(\cdot)$. It is also assumed that our observations are accurate (note the diagonal identity matrix in (5.27)) but imprecise (represented by the white Gaussian noise v_k).

These measurements are independent from each other and may take place at different frequencies. In practice, z_{1k}'s are sparse crack size observations that are measured less frequently whenever the structure is thoroughly inspected. At other times, when only one observation is available, the observation equation is reduced to

$$z_{2k} = (0 \quad 1) \begin{pmatrix} a_k \\ \dot{a}_k \end{pmatrix} + v_k \tag{5.28}$$

where $v_k \sim N(0, R_k)$ and R_k is a scalar representing the standard deviation of the observation noise.

5.5. *Results and Discussion*

In this section, the results of applying the aforementioned techniques to the experimental data are presented. First, the recursive estimation results are presented; next, we describe how parameters C and m can be estimated from experimental data. Finally, we describe the prognosis process is described and its results are presented. An overview of the estimation and prognosis process is shown in Figure 5.5.

Figure 5.6 shows the recursive estimation result for both state variables of interest. In the top figure, the estimated crack size trajectory is shown (in red) along with the true crack trajectory (in purple) measured in this case. The black markers show the specific points on the purple line that were used as sparse observations of the crack size in the estimation process. The blue line is the crack growth trajectory based solely on the process model developed in the previous section (fracture mechanics-based crack growth model). The green line represents the crack growth trajectory based solely on the AE-based crack growth model (i.e., using the AE model developed in previous sections gives an estimate of the crack growth rate, da/dN, as a function of AE count rate, dc/dN). The blue and green lines represent two extreme cases; in one case (blue line) no AE NDI information is used to calculate the crack size, and the estimation suffers from all potential model uncertainties (both in terms of model parameter and the model structure). In the second case (green line), the estimation is completely based on observed crack growth rate information obtained from AE monitoring and disregards the fracture mechanics-based model. This

100

approach suffers from the inaccuracies in all steps of the NDI process (e.g., data collection noise, modeling uncertainties and parameter estimation). By comparing these lines with the purple line (true crack trajectory), it is evident that in this specific experiment, the blue line consistently underestimates the crack size, whereas the green line consistently overestimates the crack size. The red line, which is the estimated crack size by taking into account both sources of information, is much closer to the true crack trajectory (purple line). It is important to note that this observation is based on results from limited experimentation and cannot be generalized. The fusion outcome is dependent on the performance of the individual techniques fused together. Obviously, if both the model and the AE observations overestimate the crack size in one application, the fused result will also be an overestimation of the true crack trajectory—i.e., new information is not created in the fusion process.

Figure 5.6 (bottom) shows the estimated values (in red) for the second state variable, da/dN, along with the sequential rate observations used in the estimation process.

The dashed lines in Figure 5.6 are the 5% and 95% confidence bounds of the predicted state values. As we saw before in equation (5.24), at every time step, a noise term w_k is added to the state estimate.

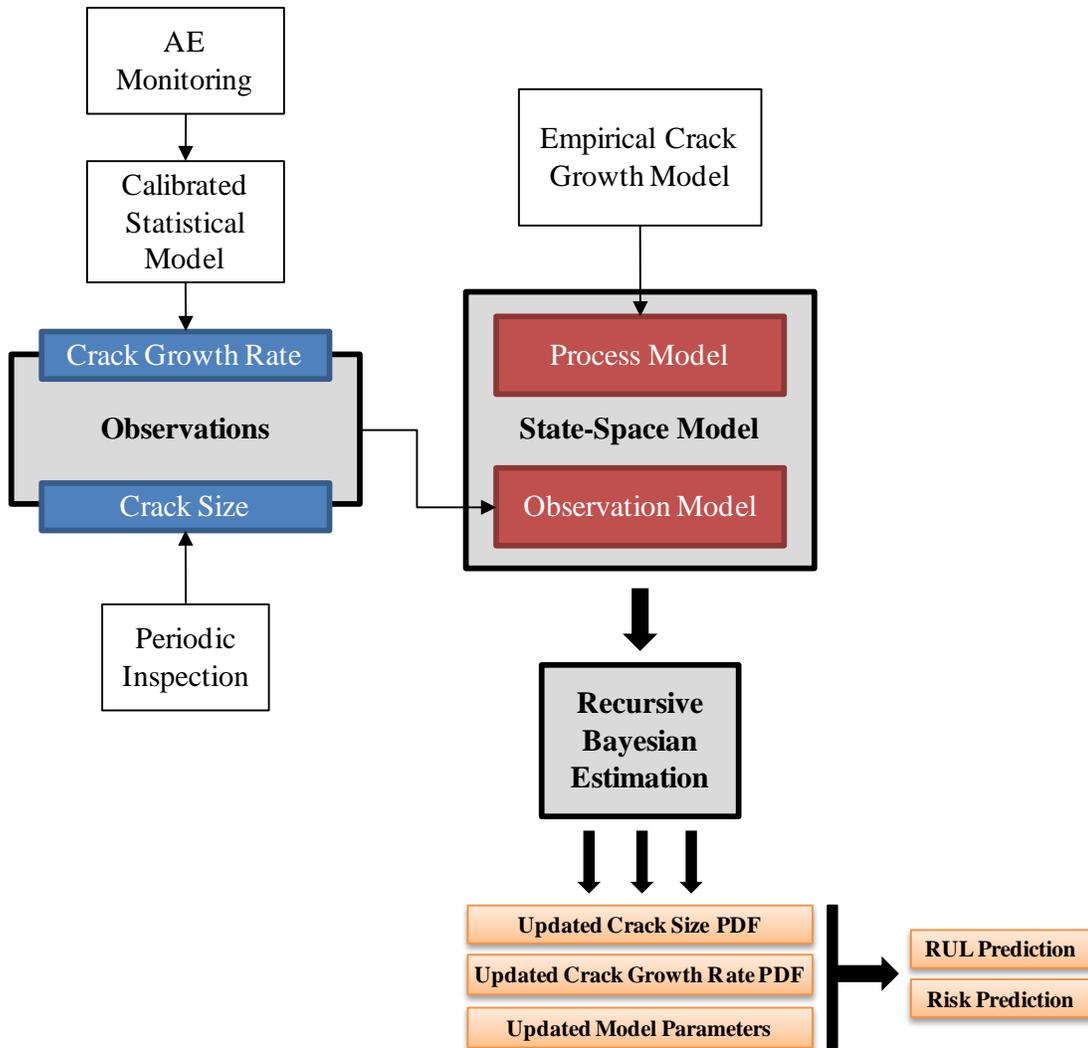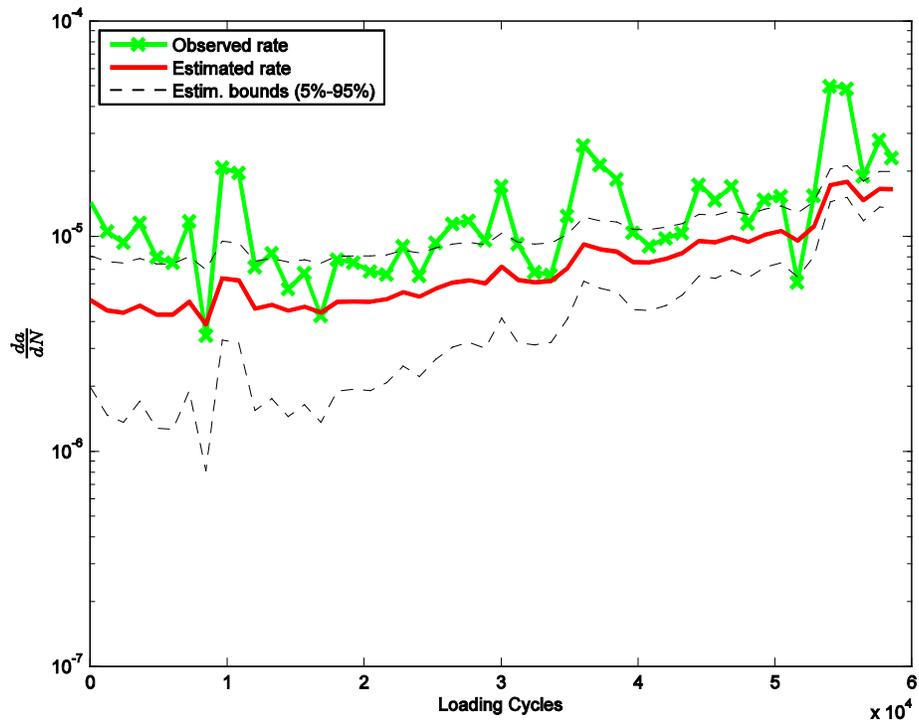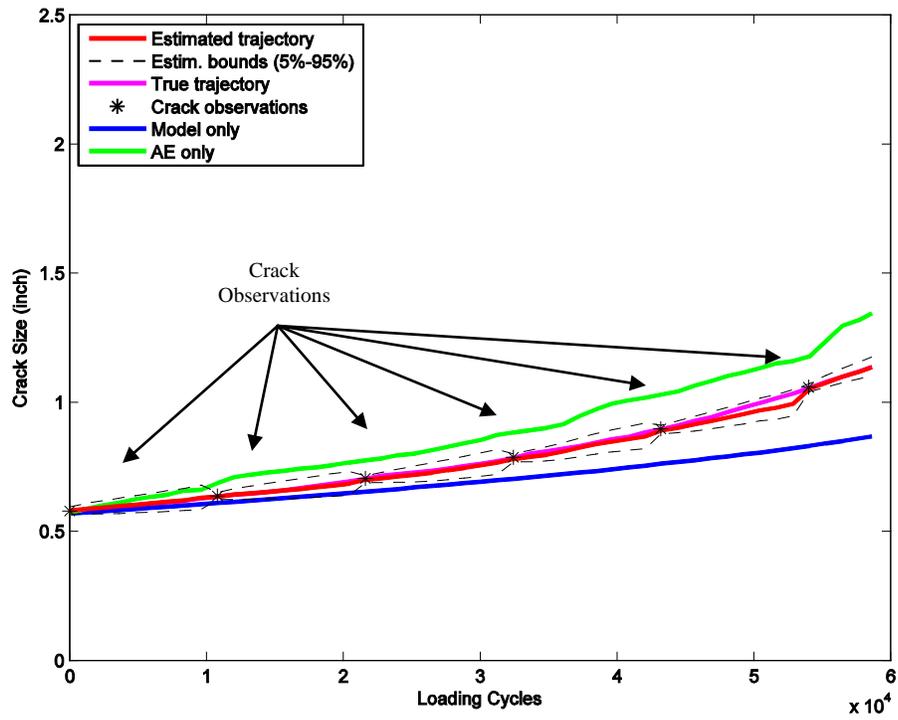Figure 5.5 – Overview of the recursive estimation and prognosis process

Figure 5.6 – Recursive Bayesian estimation of crack size (top) and crack growth rate (bottom)
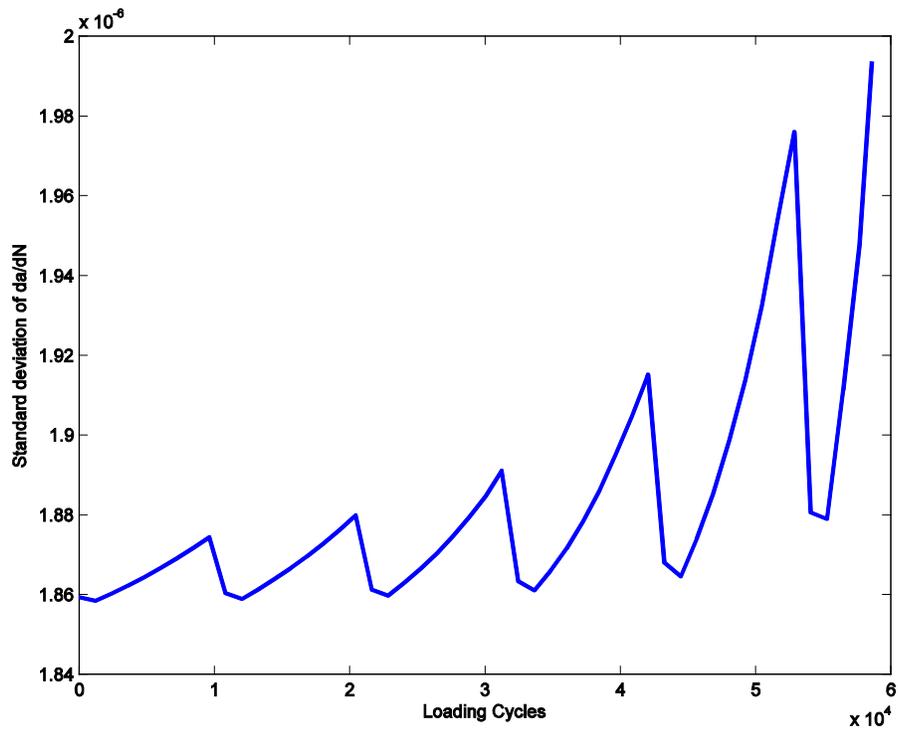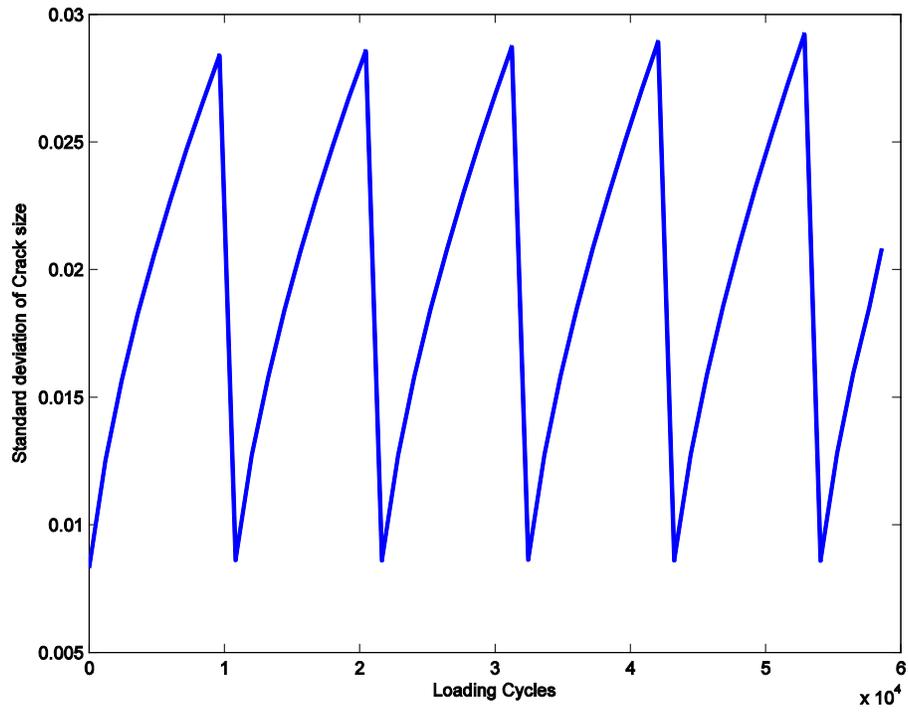using sparse crack observations and AE rate observations

Figure 5.7 – Estimated standard deviation of crack size (top) Estimated standard deviation of crack size (bottom). The uncertainty is reduced every time a new crack size observation is received.

In the absence of any observations, i.e., projecting forward the state variables using only the process model with no updating steps, the added process noise at every step accumulates over time, which results in diverging confidence bounds (see Figure 5.6 (top)) for the estimated state variables between observations. In Figure 5.7, the estimated standard deviation of the state variables is presented. This figure shows that the crack size observations (which directly correspond to the first state variable, a_k) affect the standard deviation of *both* states.

In section 5.3, it was discussed that the posterior mean $\hat{x}_k$ and the posterior covariance P_k can be calculated using equations (5.18) and (5.19). Notice in (5.22) that the *a priori* error covariance matrix at time step k, P_k^-, is calculated using the *a posteriori* error covariance matrix from the previous time step, P_{k-1}, plus Q which is the covariance matrix of the process noise. In the absence of the measurement updating step (5.19), P_k will continue to grow over time. When a new observation is received, first the appropriate Kalman gain for that observation is calculated according to (5.20). Next, the *a posteriori* error covariance matrix P_k is calculated according to (5.19) by updating the *a priori* error covariance matrix P_k^- based on the Kalman gain associated with the observations at current time step, k. In this step, because of the minus sign in (5.19) , the error covariance matrix shrinks. This can be clearly seen in Figure 5.7 for both the crack size (top) and the crack growth rate (bottom). Figure 5.7 (bottom) shows that the standard deviation of the crack growth rate is also reduced as a result of updating P_k using crack size observations. The root of this coupling effect between the states can be seen in the way the Kalman gain is defined in (5.20). The Kalman gain, K, is a $m \times n$ matrix where m is the dimension

of the state space and n is the dimension of the observation space. Each element k_{ij} in K can be thought of as a measure of influence that each observation z_j will have on the mean estimate of state x_i and the state error covariance matrix. In the crack growth problem presented here, the Kalman gain associated with the effect of the observations of the first state (a) on the second state (da/dN) is such that it is clearly influenced in the measurement update state, which results in the reduced confidence bounds in Figure 5.7 (bottom).

Figure 5.8 shows the crack size estimation result in a case with fewer crack observations. In real-life fleet management applications, this could correspond to less frequent ground inspections, which are of course desirable if the onboard NDI technologies reach the maturity level needed to support such non-conservative management decisions. As explained above, the uncertainty of the estimation accumulates over time in the absence of new observations but is reduced whenever new observations are received and used in the measurement update step. In Figure 5.8 (bottom) the increase in the estimated standard deviation of the crack size is shown for two cases with 3 and 6 observations. This figure clearly shows that more frequent (accurate and precise) observations would result in a more confident state estimation by not allowing the standard deviation to grow too large and by "anchoring" the mean state estimate using crack size observations.
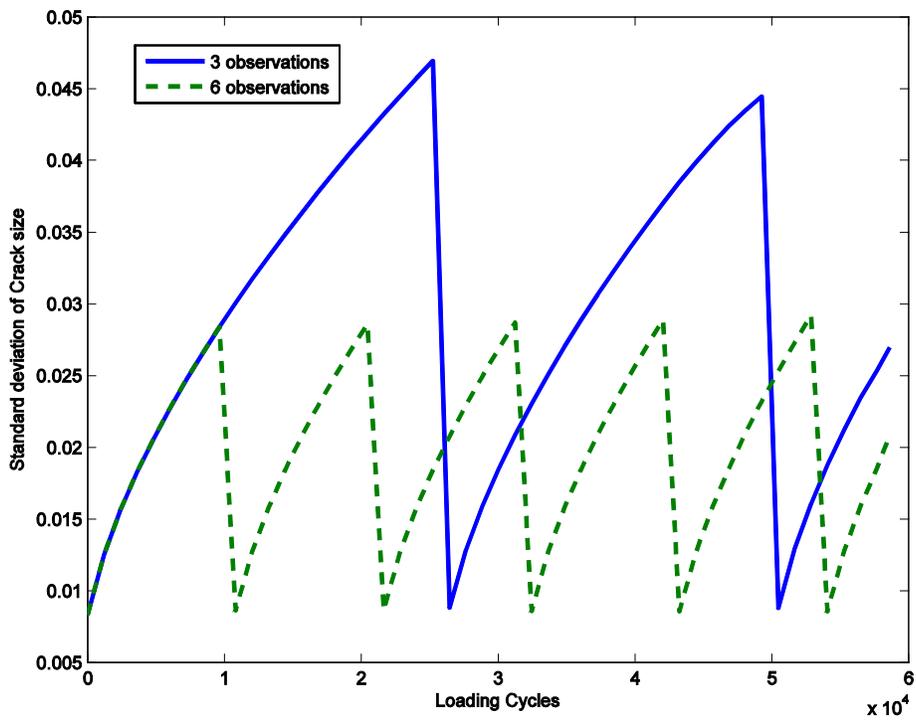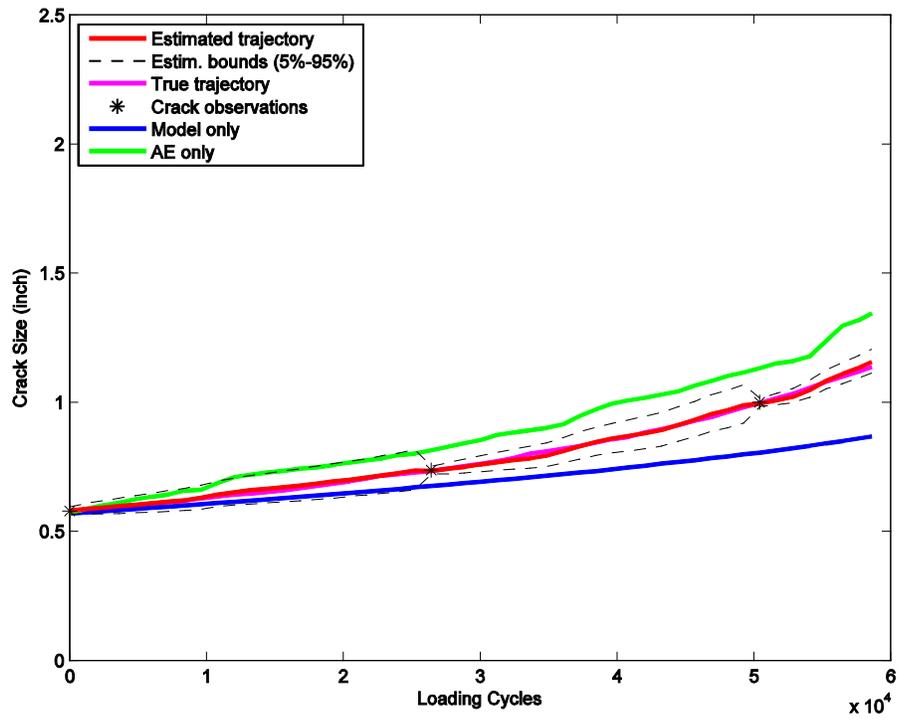
Figure 5.8 – Estimation of crack size using only 3 observations (top). Comparison of the estimated standard deviation of crack size using 3 and 6 crack observations (bottom).

Based on what has been presented so far, it is evident that the estimated states are in fact the result of a tradeoff between three competing sources of information: the crack growth model, the AE-based crack growth rate observations and the periodic crack size observations. What dictates the dominance of one over the other is the amount of uncertainty associated with each source of information. In the Kalman filter formulations, the uncertainties for all states and all observations are embodied in Q_k and R_k, which are the covariance matrices of the process noise w_k and the observation noise v_k, respectively. In general, the covariance matrix can change over time (denoted by subscript k), but in our problem we assume that their values are constant over time.

The values of Q and R are both inputs to the state estimation problem and should either be obtained from data or assumed based on engineering judgment. The covariance matrix of the measurement noise can be directly determined based on the precision of the measurement techniques used. For the crack size observations, the standard deviation of the error is selected based on errors in the digital imaging technique used for crack measurement. For simplicity, we assumed a constant measurement noise, whereas in reality, there is more uncertainty associated with measuring smaller cracks; as the cracks grow larger, they can be measured more accurately and with higher confidence. To account for this, a decreasing standard deviation term for the crack measurements could be assumed.

The observations of the second variable, $\dot{a}$, are not direct measurements: $\dot{a}$ observations are obtained by first measuring AE count rate and then using the model developed in previous chapter to correlate the AE count rate with crack growth rate.

There are two main sources of uncertainty in this process: first, the uncertainties involved in fitting a model to da/dN versus dc/dN data; and second, the uncertainty associated with the measurement, filtration, feature extraction and the processing of AE signals. Characterizing all these sources of uncertainty is itself a separate research problem that requires further experimentation under more controlled conditions. Here it was assumed that the scatter in the da/dN versus dc/dN data, as captured by parameter σ in the regression analysis, reflects all the uncertainties in the crack growth rate measurement. It was further assumed that this noise term is constant throughout the process. The covariance of the measurement noise was selected as $R = \begin{bmatrix} 9e^{-3} & 0 \\ 0 & 5e^{-6} \end{bmatrix}^2$ based on what was discussed above.

The process noise can be characterized based on the uncertainties associated with the model structure as well as the model parameters. In section 4.4 we showed how the uncertainty over model parameters C and m can be determined based on test data. Here it was assumed that the uncertainty over model parameters was the only factor that contributed to the process noise and therefore, the covariance of the process noise was selected as $Q = \begin{bmatrix} 0 & 0 \\ 0 & 2e^{-6} \end{bmatrix}^2$ accordingly. Note that the first element (q_{11}) that corresponds to the standard deviation of the process noise for a was selected as zero; in this formulation, the uncertainty over C and m will first affect the estimated $\dot{a}$ directly and then, propagate to the estimation of a due to the coupling of state variables as defined in (5.24).

The relative contribution of the process model and the observations to the final estimated states is determined based on the values in the Kalman gain matrix (see equation (5.20)). For instance, for a given state variable, a combination of noisy observations and a clean (less noisy) process model results in an estimated state that is mainly influenced by the process model. On the other hand, if the process model is too noisy and the observations are clean, the Kalman gain associated with those observations will have a large value, and therefore, the final estimated state would be highly influenced by these observations.

To demonstrate this, assume that $Q = \begin{bmatrix} 0 & 0 \\ 0 & 2e^{-6} \end{bmatrix}^2$ and $R = \begin{bmatrix} 9e^{-1} & 0 \\ 0 & 5e^{-5} \end{bmatrix}^2$ which means that the observations are noisier than what was first assumed (i.e., larger standard deviation for both a and $\dot{a}$ measurements), while the process noise is kept as before.

Noisier observations will play a weaker role in the updating process, since their corresponding Kalman gain value is negligible. This is clearly shown Figure 5.9 (top), where the red line, which is the estimated crack size, falls on top of the blue line, which is the crack growth trajectory solely based on the process model. Both the crack size observations and the crack growth rate observations have practically no influence on the estimated state. This is also clear from Figure 5.9 (bottom), where the estimated crack growth rate state (red line) is not influenced by the observed rate (green line). The red line in this figure shows the estimated rate as calculated according to the process model (equations (5.24) and (5.25)) without being updated by any AE-based observations. The estimated rate in this figure has an increasing

trend as the test progresses in time, which is expected because under constant loading condition the crack growth rate increases as the crack becomes larger in the specimen. Now we look at the other end of the noise spectrum, where the observations play a very strong role in the estimation process. To demonstrate this, consider the same estimation problem as before but with noise covariance matrices equal to $Q = \begin{bmatrix} 0 & 0 \\ 0 & 2e^{-5} \end{bmatrix}^2$ and $R = \begin{bmatrix} 9e^{-1} & 0 \\ 0 & 2e^{-6} \end{bmatrix}^2$. Similar to the previous example, the crack size observations have a large standard deviation and therefore weak influence on the estimated state. For the second state variable, a large process noise combined with small observation noise significantly increases the effect of crack growth rate observations on both the second and first state variables. The result for this combination of the process and the observation noise is given in Figure 5.10. In Figure 5.10 (top) the red line, which is the estimated crack size, falls on top of the green line, which is the AE-based crack growth trajectory. In other words, the estimated crack size here is based only on the observed (through AE) crack growth rates and not the empirical process model (Paris crack growth equation). Figure 5.10 (bottom) shows the estimated crack growth rate (red line), which closely matches the rate observations (green line) obtained through the previously developed AE method.
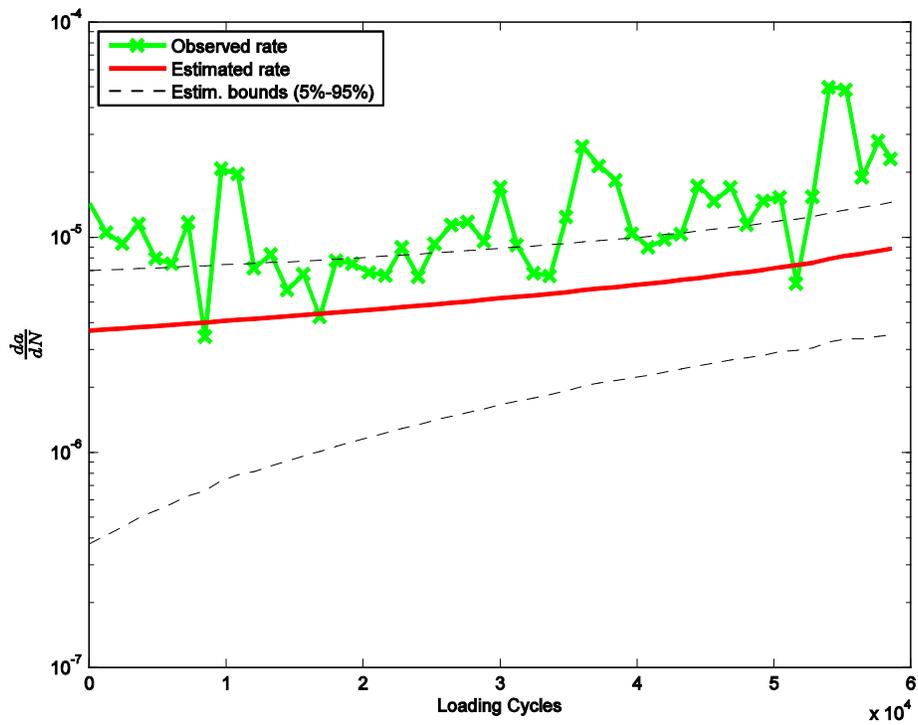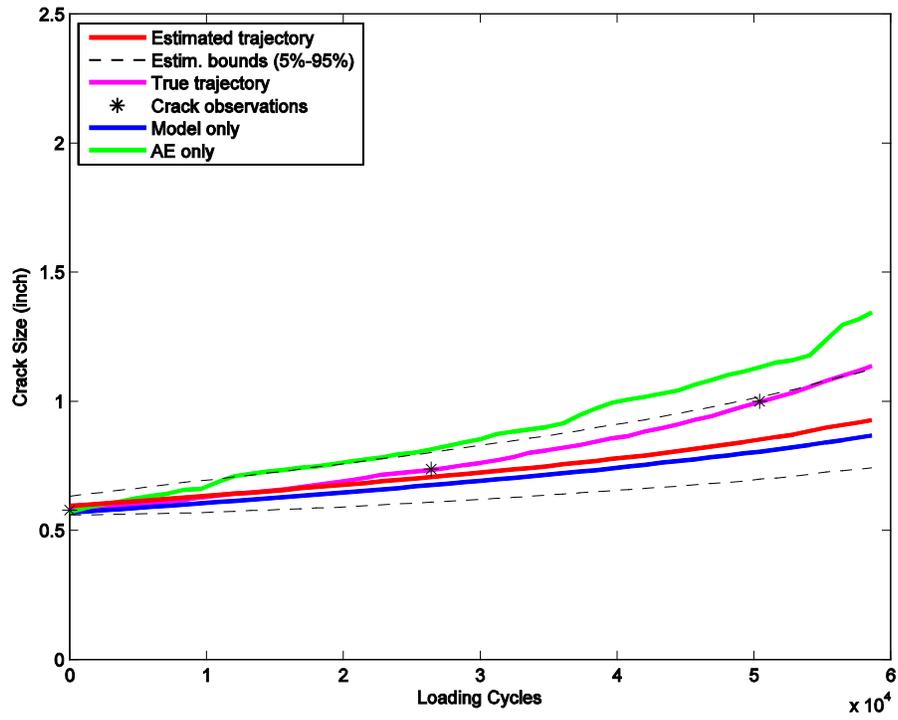
Figure 5.9 – The effect of excessive observation noise on the crack size estimation (top) and
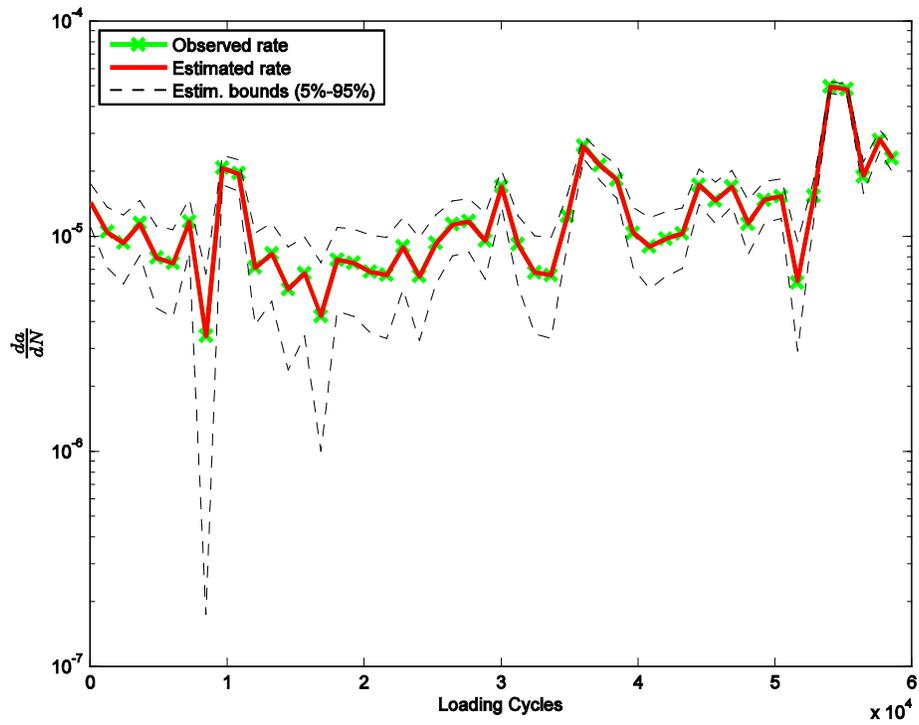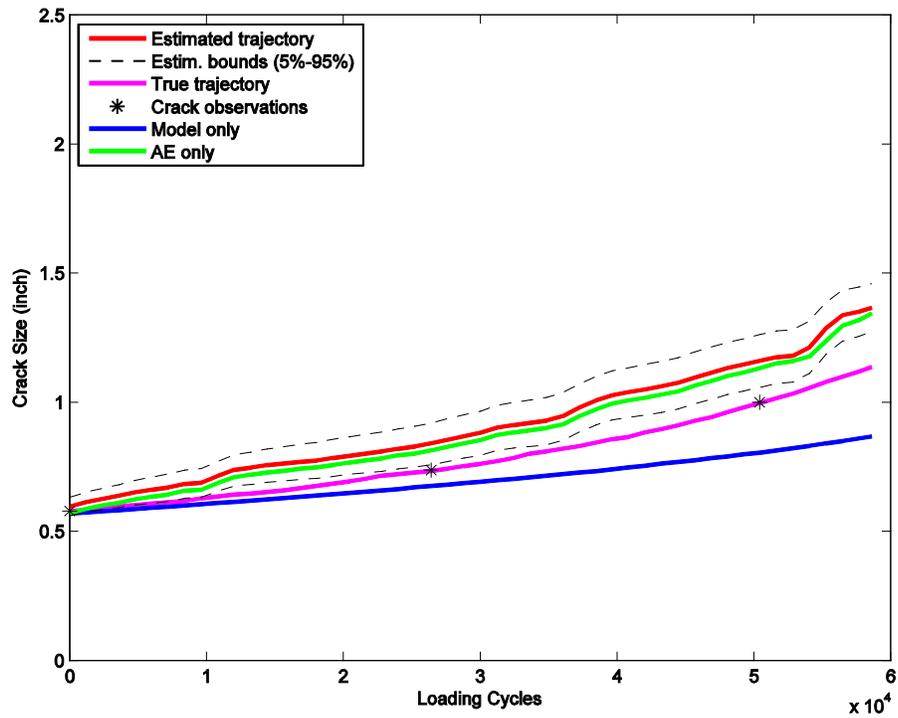the crack growth rate estimation (bottom).

Figure 5.10 – Results of estimation problem for the case where the estimated states are highly influenced by the AE-based crack growth rate observations.

In both examples above, the crack size observations were assumed to be highly uncertain and therefore did not influence the estimated states. Figure 5.11 shows the crack size estimation results for the above examples but this time with reduced uncertainty for the periodical crack size observations. The result in Figure 5.11 (top) is based on $Q = \begin{bmatrix} 0 & 0 \\ 0 & 2e^{-6} \end{bmatrix}^2$ and $R = \begin{bmatrix} 9e^{-3} & 0 \\ 0 & 5e^{-5} \end{bmatrix}^2$, while the result in Figure 5.11 (bottom) is based on $Q = \begin{bmatrix} 0 & 0 \\ 0 & 2e^{-5} \end{bmatrix}^2$ and $R = \begin{bmatrix} 9e^{-3} & 0 \\ 0 & 2e^{-6} \end{bmatrix}^2$. The only difference with previous examples is that the standard deviation for the crack size observations is reduced from $9e^{-1}$ to $9e^{-3}$, thereby increasing its effect in the estimation process. In Figure 5.11 (top), the rate of the crack growth follows that of the fracture mechanics-based process model between crack size observations (depicted by black stars). Whenever a new crack size observation is received, because of its low noise and therefore large Kalman gain value, the crack size estimate is updated to reflect the effect of these observations. A similar effect is shown in Figure 5.11 (bottom), but here the rate of the crack growth follows that of the AE-based crack growth model (i.e., based on rate observations) between crack size observations.

The examples above were presented to show the flexibility of the proposed fusion approach and how it performs in extreme cases. The last example also highlights the importance of periodic crack size inspections. The benefit of using crack growth rate observations in the fusion process is that the confidence in the crack size estimation between the periodic inspections is increased, and therefore, the frequency of such expensive inspections can be safely reduced.
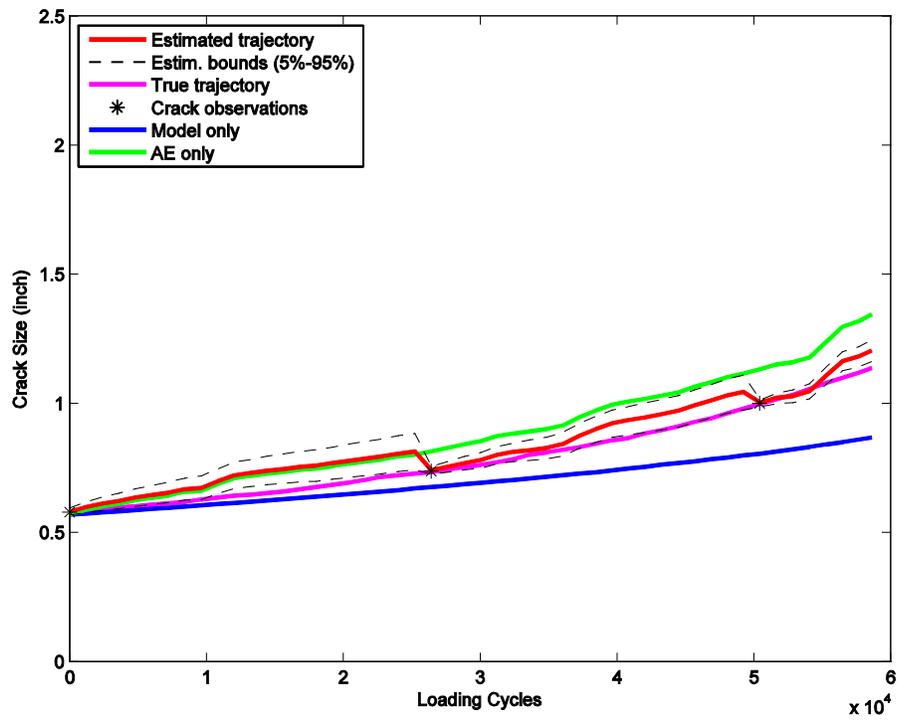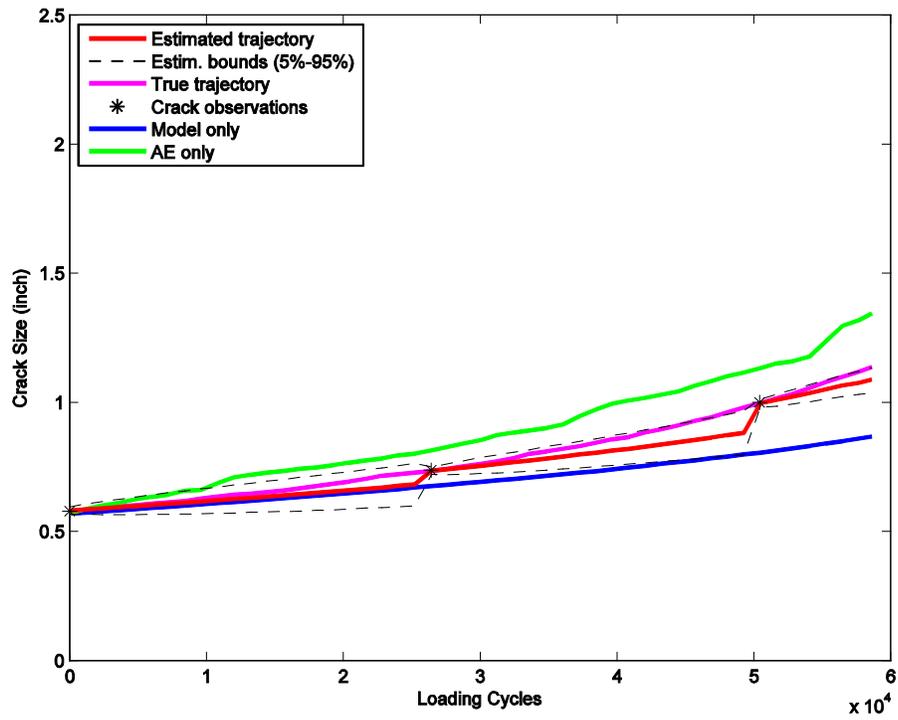
Figure 5.11 – Effect of periodic crack size observations on the estimated crack size for cases
where the crack growth rate observations have negligible (top) and strong (bottom) influence.

5.5.1. Prognosis approach

So far a formal approach has been presented for utilizing multiple sources of information (including theoretical and empirical models as well as periodic inspections and real-time health monitoring data) produce the best estimate for the state variables of interest: crack size and crack growth rate. The next logical step would be to predict how these states evolve in time (prognosis) and then extract useful features from such predictions that can be used for high-level decision support (e.g. fleet management).

The most straightforward method for prognosis is to use the process model and project forward in time the estimated values of the state variables. To do so, the same Kalman filter formulation as before can be used, but this time with no observations and therefore no updating steps. The Monte Carlo simulation method can also be used to predict future values of state variables given the current estimates of states and model parameters.

Here the Monte Carlo approach will be used because of its versatility; in Monte Carlo simulation, the normality assumption of state variables can be released, and the uncertainty in model parameters can also be accounted for via sampling. It is also easier to account for random amplitude loading scenarios in crack growth simulation. Of interest here is simulating the crack growth trajectory as a function of applied loading cycles. A schematic representation of this process is presented in Figure 5.12.

In order to predict the value of state variables at a future time, the crack size distribution at current time is needed (to be used as the initial crack size distribution in the simulation) as well as an updated (based on all past observations, Z_k) set of

model parameters. In other words, the effect of all past observations from the beginning until when the prognosis starts is manifested in the crack size distribution a_k and the updated model parameters that are passed on to the prognosis algorithm.
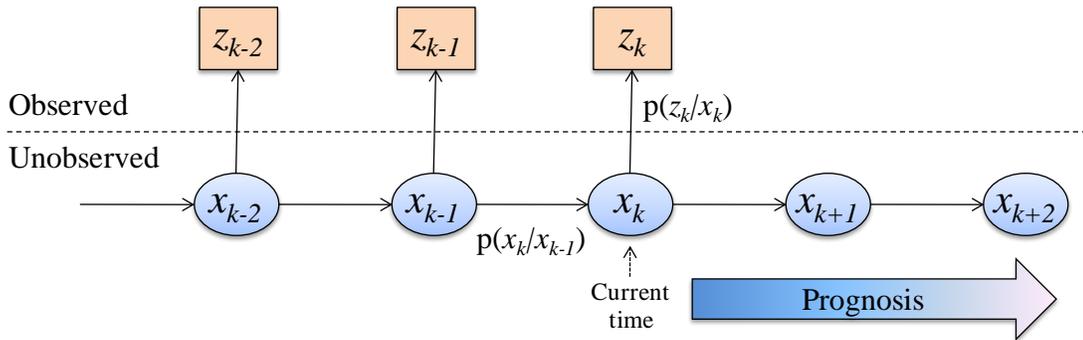

Figure 5.12 – Schematic representation of the state estimation plus prognosis process

Estimating model parameters C and m based on observations of a_k and $\dot{a}_k$

In this section we describe how one can recursively use the history of the estimated state variable, a_k and $\dot{a}_k$, to find the parameters C and m via regression.

For any crack growth trajectory that follows the Paris equation, the model parameters C and m are the intercept and slope of the regression line in the $\log da/dN$ versus $\log \Delta K$ plot. Therefore, at any given time, the history of estimated state variables a_k and $\dot{a}_k$ can be used to calculate the model parameters that, if used, would have resulted in the observed crack growth trajectory. We first use a_k to calculate the corresponding ΔK_k value and then use regression analysis to find the intercept C and the slope m of the $\log \dot{a}_k$ versus $\log \Delta K_k$ line. Both a_k and $\dot{a}_k$ are the outcome of the Bayesian updating process and therefore have been influenced by both the process model and past observations.

At the beginning of the test there are few data points, and therefore the outcome of regression is not reliable[13]. As the crack grows and more data points populate the $\log \dot{a}_k$ versus $\log \Delta K_k$ plot, the calculated C and m would be more accurate. This is depicted in Figure 5.13.
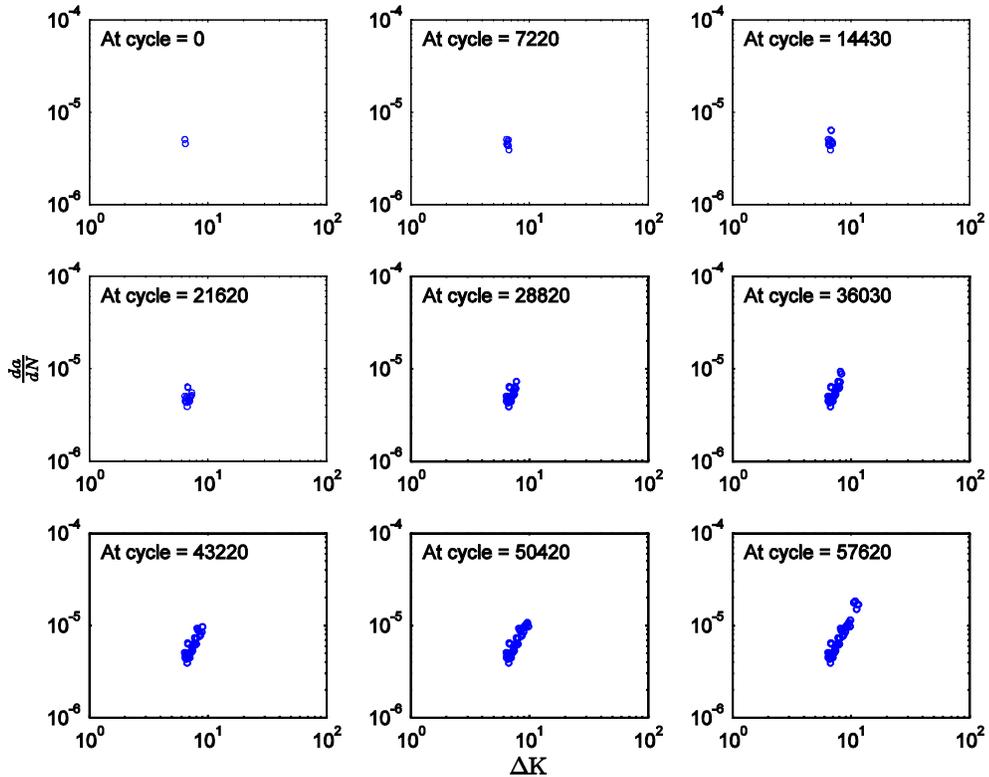
Figure 5.13 – $\log \dot{a}$ versus $\log \Delta K$ plotted at different elapsed cycles

The estimated model parameters as a function of elapsed cycles are plotted in Figure 5.14. It is evident that as the number of elapsed cycles increases, both parameters start to converge; the final parameter values represent a crack growth model that takes into account all sources of available information until that time step. The value of these parameters evolves through the updating process; the final

---

[13] Bayesian regression technique can be used here as well; in that case, the estimated uncertainty bounds of the parameters will be wide at the beginning and will shrink as more data is used in the regression process.

estimated values in this case were $C = 4.88e^{-8}$ and $m = 2.39$, while the initial values used in the process model (not influenced by any observations) were $C = 3.2e^{-8}$ and $m = 2.53$. In this particular case, the evidence (both a and $\dot{a}$ observations) indicated a higher growth rate than what was suggested by the initial model parameters (see Figure 5.6 (top)).
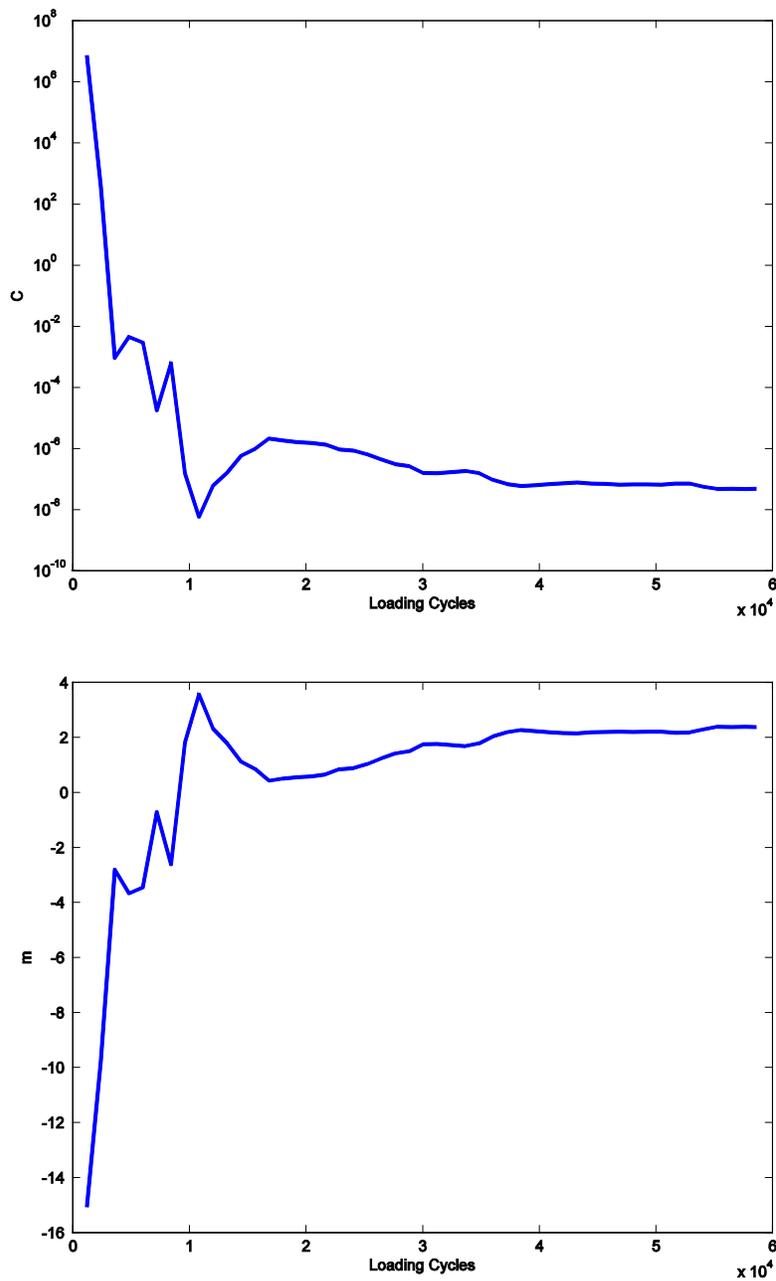

Figure 5.14 – Parameters C (top) and m (bottom) estimated as a function of elapsed cycles

Prediction of crack size distribution at future time steps

So far this dissertation has discussed how a combination of process model and various observations can be used to obtain an updated estimate of the crack size distribution. To use this information as a management decision tool (e.g., to optimize a maintenance policy based on the condition of the structure rather than on fixed conservative maintenance intervals), it is necessary to predict the future crack size distribution as a function of elapsed cycles.

At a given time step k, the process model can be used to simulate future crack growth trajectories (Monte Carlo simulation) starting from the updated crack size distribution, a_k , and using the updated model parameters. This process is demonstrated in Figure 5.15, in which the predicted future crack growth trajectory is shown by the cyan line. Results from Figure 5.6 and Figure 5.14 are used to define the initial crack size distribution and the updated model parameters used in this case.

Here the critical crack size—the size beyond which the crack growth becomes highly accelerated and non-stable and the structure could fail quickly afterwards—is selected as 2" and is shown with a horizontal red line.

Once the crack growth trajectory is predicted, it can be used in multiple ways to provide management decision support. The first piece of information that can be extracted from this result is the estimated RUL of the structure based on the current predicted growth trajectory and the selected critical crack size. This information is obtained by "slicing" the predicted crack growth trajectory (and its confidence bounds) horizontally at the selected critical crack size value. This results in a

probability distribution function representing the RUL at the selected critical crack size, as shown in blue in Figure 5.15.

The other piece of information often useful in decision making is the estimated probability of failure—i.e. the probability that the predicted crack size exceeds the critical limit—as a function of elapsed cycles (or any other measure of time or structural usage). This can be obtained by slicing the predicted crack growth trajectory (and its confidence bounds) in the vertical direction to obtain the crack size distribution as a function of elapsed cycles and then calculating the probability of exceedance (PoE) corresponding to the critical crack size. This probability is then compared with the maximum tolerable probability of failure to decide when the structure should be removed from service. Figure 5.17 shows the calculated PoE as a function of loading cycles based on the result in Figure 5.15. Note that in this case, the PoE goes from negligible values to very high values in a very short period of time (few thousand cycles); this is due to the high growth rate predicted by the prognosis module and the critical crack size as depicted in Figure 5.15.

The prognosis result strongly depends on the state of the system at the start of prediction. In Figure 5.16, the predicted RUL distribution is compared for two cases: case I where prognosis is started at around 35,000 cycles, and case II, where it starts later at around 60,000 cycles.
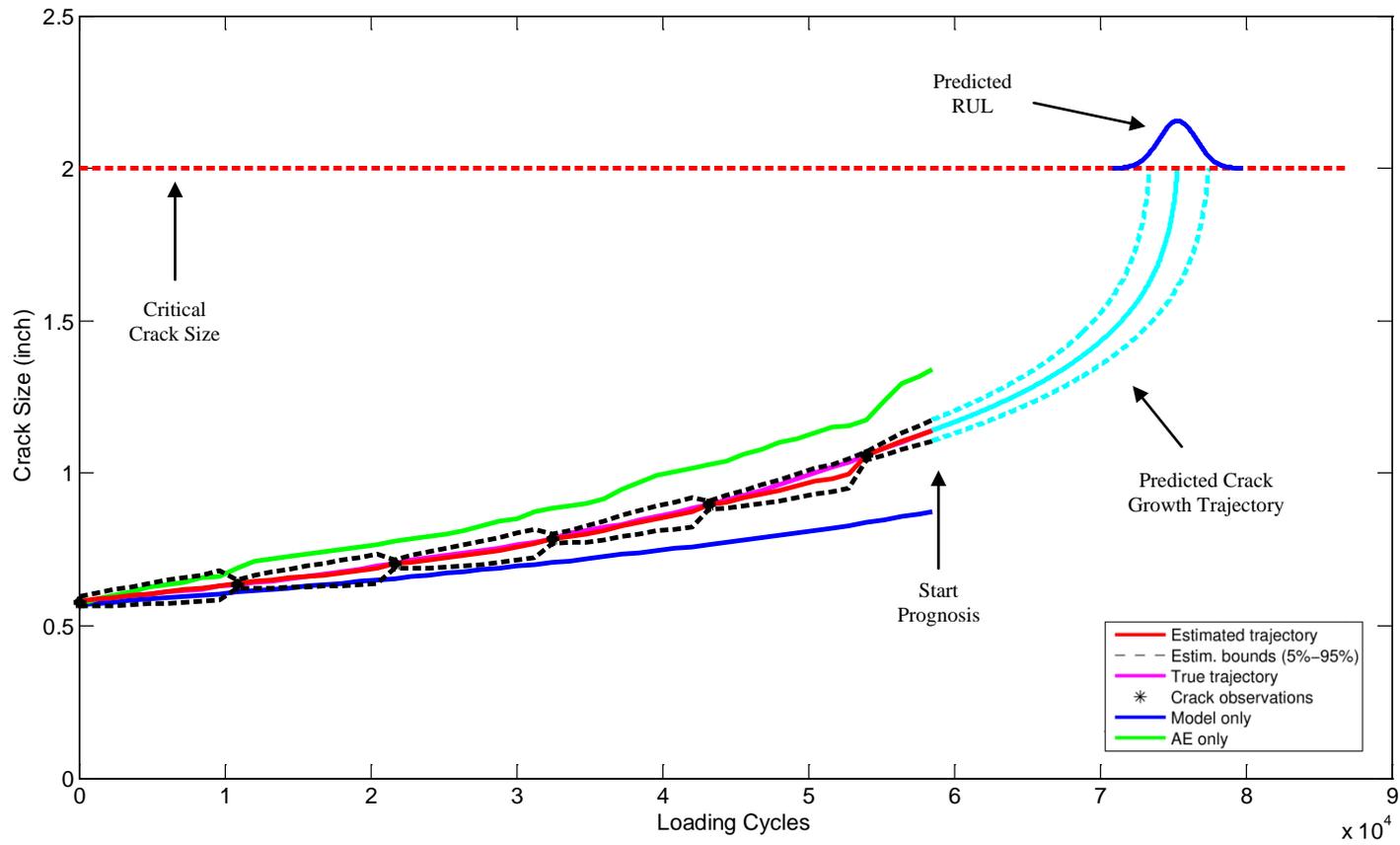
Figure 5.15 – Prognosis result: the estimation of crack size is projected forward and the remaining useful life distribution is obtained based on the assumed critical crack size.
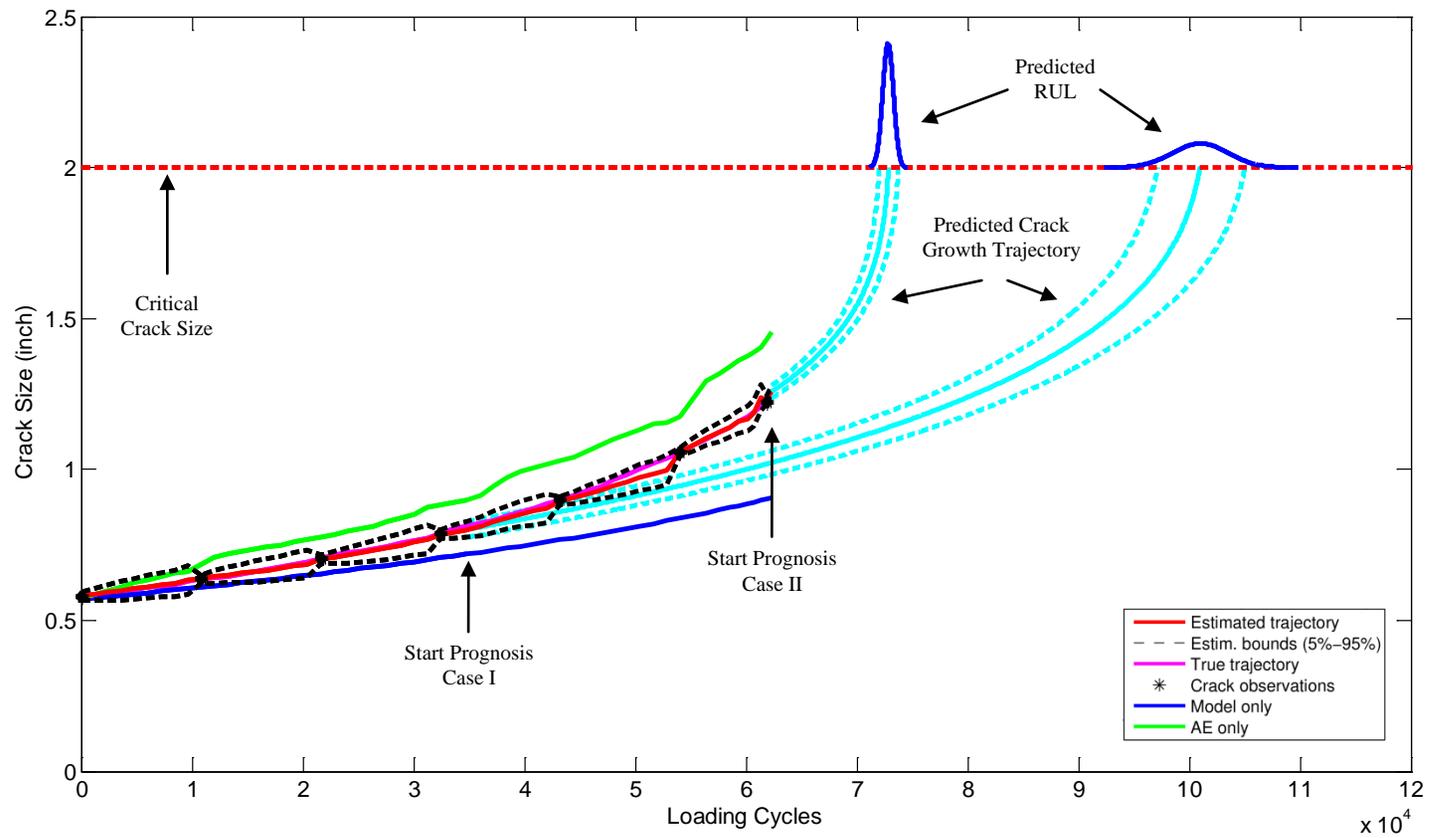
Figure 5.16 – Comparison of the prognosis results for early (Case I) and late (Case II) starting points.
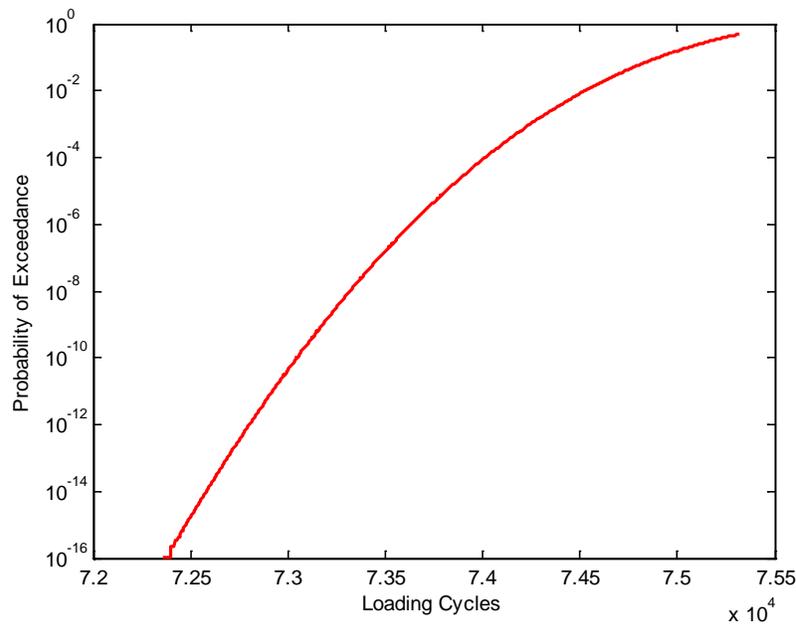
Figure 5.17 – Probability of Exceedance as a function of loading cycles

In case I, the prognosis starts early, and therefore, the estimated crack size distribution (used as initial state for prognosis) and the model parameters C and m are not yet updated with a significant number of observations. This is why the projected crack growth trajectory in this case is similar to what one would expect to see using only the process model. In case II, however, the prognosis starts later, when the estimated crack size distribution and the model parameters are updated with a significant portion of field and AE observations, which results in a higher predicted rate of crack growth. It is also clear from this figure that the RUL in case II has a tighter distribution, which is due to tighter confidence bounds on the initial crack size distribution at the beginning of the Monte Carlo simulation.

In general, it is expected that the predicted RUL distribution becomes tighter (more precise) as the starting prognosis time approaches the end of life. But whether or not this predicted value is in fact more accurate (closer to actual life) depends on the overall quality of the observations and the trade-off between the process model and

124

the observations. For example, if the observations suffer from systematic bias (e.g. always over-estimated by 20%) then the more the estimated states are updated, the farther the final prediction results will get from the true life of the structure.

5.6. *Summary*

This chapter started with a high-level discussion of recursive Bayesian estimation and then continued with a more detailed discussion of Kalman filter and its application in knowledge fusion.

In this chapter, recursive Bayesian estimation technique was used to fuse the outcome of the empirical crack growth model with crack size observations as well as the online crack growth rate observations.

A state-space formulation of the crack growth model was proposed with crack size, a, and crack growth rate, $\dot{a}$, defined as state variables. The state variables were recursively updated based on available observations from periodic NDI inspections and the AE-based SHM system. The approach was implemented and estimation results based on data from previous chapters of this dissertation were presented.

In the proposed framework, the model parameters were also updated to match the updated crack growth trajectory. The model with updated parameters was then used for prognosis; the RUL of the structure and PoE with respect to a critical crack size were calculated assuming a known future usage profile.

Chapter 6: Summary, Contributions and Suggested Future Research

6.1. *Summary*

Many aerospace and civil infrastructures currently in service are at or beyond their design fatigue-life limit. The ability to assess and predict the state of damage is critical in ensuring the structural integrity of such aging structures.

Structural health monitoring (SHM) is an emerging research area for online assessment of structural integrity using appropriate NDI technology. SHM could have a major contribution to the structural diagnosis and prognosis: when SHM is performed in coordination with existing offline NDI practices, the structural health monitoring information collected in between current inspection intervals would provide supplementary data that would help alleviate some the problems associated with conventional inspection practices.

This research focused on fatigue crack growth monitoring in metallic structures using AE technology. In the first part of the dissertation, crack growth experiments were performed on standard CT specimens in a laboratory environment; the AE signals generated during the crack growth process were collected using the sensors installed on the specimen. Various filtrations were applied to the AE data to distinguish crack growth-related signals from extraneous noise. The resulting data suggests a log-linear relationship between fracture parameters, da/dN and ΔK, with the AE feature dc/dN, which is consistent with the findings of other researchers in the field.

In order to use AE information for quantitative crack growth monitoring, a flexible statistical model was proposed to describe the relationship between the AE features and fracture parameters. The Bayesian regression technique was used to estimate the model parameters (and characterize their corresponding uncertainties) using the experimental data obtained in the first part.

The developed model was then used to calculate two important quantities that can be used for structural health management:

- An AE-based instantaneous damage severity index: the index was defined as the probability that a growing crack will transition from stable growth regime to rapid crack growth and ultimately failure.

- An AE-based estimate of the crack size distribution at a given point in time, assuming a known initial crack size distribution: in this approach, the rate of crack growth, da/dN, was directly estimated based on input AE data. The crack growth trajectory was calculated starting from a known initial crack size and using the estimated growth rate.

As the final step of this research, a formal Bayesian framework was proposed for knowledge fusion; in this framework the crack size distribution predicted by an empirical model was recursively updated using SHM monitoring information as well as periodic inspection results. The model parameters will also adapt to the data which will result in enhanced prognosis results.

6.2. *Contributions of this Work*

The main contributions of this work can be summarized as follows:

- The feasibility of crack growth monitoring using AE technique is demonstrated. A flexible statistical model is proposed to represent the relationship between select AE features and key fracture parameters. Model parameters, along with their associated uncertainties, are estimated using experimental data obtained as part of this research.

- A quantitative approach is developed for assessing the severity of structural damage due to existence of fatigue cracks, based on information from the AE monitoring system.

- A probabilistic approach is proposed to estimate the crack size distribution as a given time, based on structural health monitoring information provided by the AE technique (assuming an initial crack size distribution).

- A hybrid structural health management framework is proposed; in this framework, the probability distribution of crack size and the probability distribution of crack growth rate are estimated based on the information from the following sources: (a) empirical crack growth model, (b) structural health monitoring, and, (c) periodic NDI inspections.

  o The approach presented here can handle noisy observations received at arbitrary frequencies. It can also readily handle additional sources of information.

  o As part of this approach, the parameters of the empirical model are updated to reflect the new information; the updated model is then used

for prognosis, i.e., the remaining useful life (RUL) and the risk associated with further utilization of the structure is calculated as a function of applied loading cycles.

6.3. *Suggestions for Future Research*

At the beginning of this dissertation, it was mentioned that the scope of this research does not include addressing the challenges of implementing the approaches presented here in fielded applications. In this section some ideas for extending this work to more realistic structures and use cases are presented:

- An extensive set of experiments is required to confirm that the approach proposed here for using AE technique for crack growth monitoring is valid for: (a) smaller crack sizes, (b) more complex geometries, and, (c) random amplitude loading profiles.

  The main challenge, as always, will be to filter out the extraneous signals to distinguish crack-related AE signals—this becomes considerably more difficult in complex geometries.

- The correlation between fracture parameters and other non-conventional AE parameters (besides count rate) should be investigated. New features can be extracted from AE waveforms that could potentially be less sensitive to the change in the environment, and therefore, perform better in field applications.

- An optimization problem can be set up to find the optimum thresholds for filtering AE signals based on their feature values; the threshold values can be selected such that features extracted from the filtered signals will have the

maximum correlation with the fracture parameters of interest. Genetic Algorithm (GA) is a good candidate for solving this problem.

- The outcome of this research could be used directly to optimize the periodic inspection intervals. The optimum inspection intervals can be determined by solving a multi-objective optimization problem to minimize the risk while maximizing the time between inspections.

- One technique suggested in the literature to estimate the size of a crack using AE is to use triangulation to locate the AE source (i.e. the tip of the crack) using multiple sensors. If implemented, the crack size information obtained from this method could be used as an additional source of information in the proposed Bayesian fusion framework.

Bibliography

Anderson, B.D.O. & Moore, J.B., 2005. *Optimal Filtering*, Dover Publications.

Anderson, T.L., 1994. *Fracture Mechanics: Fundamentals and Applications, Second Edition* 2nd ed., CRC.

ASTM E647-08, 2008. *Standard Test Method for Measurement of Fatigue Crack Growth Rates*, ASTM International.

Bassim, M.N., St Lawrence, S. & Liu, C.D., 1994. Detection of the onset of fatigue crack growth in rail steels using acoustic emission. *Engineering Fracture Mechanics*, 47(2), pp.207-214.

Bellantoni, J.F. & Dodge, K.W., 1967. A square root formulation of the Kalman-Schmidt filter. *AIAA Journal*, 5(7), pp.1309-1314.

Berkovits, A. & Fang, D., 1995. Study of fatigue crack characteristics by acoustic emission. *Engineering Fracture Mechanics*, 51(3), pp.401-416.

Besuner, P.M., 1987. Probabilistic fracture mechanics.

Boller, C., 2001. Ways and options for aircraft structural health management. *Smart materials and structures*, 10(3), pp.432-440.

Cowles, M.K., 2004. Review of WinBUGS 1.4. *The American Statistician*, 58(4), p.330–336.

Crassidis, J.L. & Junkins, J.L., 2004. *Optimal estimation of dynamic systems*, CRC Press.

Diard, J., Bessiere, P. & Mazer, E., 2003. A Survey of Probabilistic Models Using the Bayesian Programming Methodology as a Unifying Framework.

Doucet, A., De Freitas, N. & Gordon, N., 2001. *Sequential Monte Carlo methods in practice*, Springer Verlag.

Doucet, A. & Johansen, A.M., 2010. A tutorial on particle filtering and smoothing: Fifteen years later. *Handbook of Nonlinear Filtering*.

Dowling, N.E., 1998. *Mechanical Behavior of Materials: Engineering Methods for Deformation, Fracture, and Fatigue* 2nd ed., Prentice Hall.

Fang, D. & Berkovits, A., 1993. Fatigue damage mechanisms on the basis of acoustic emission measurements. In *Novel experimental techniques in fracture mechanics: presented at the 1993 ASME Winter Annual Meeting New Orleans, Louisiana November 28-December 3, 1993*. American Society of Mechanical Engineers, p. 219.

Forman, R.G., Kearney, V.E. & Engle, R.M., 1997. Numerical analysis of crack propagation in cyclic-loaded structures.

Gamerman, D. & Lopes, H.F., 2006. *Markov chain Monte Carlo: stochastic simulation for Bayesian inference*, Chapman & Hall/CRC.

Gelman, A. et al., 2003. *Bayesian Data Analysis, Second Edition* 2nd ed., Chapman & Hall.

Gilks, W.R. et al., 1996. *Markov chain Monte Carlo in practice*, Chapman & Hall/CRC.

Giurgiutiu, V., 2008. *Structural health monitoring with piezoelectric wafer active sensors*, Academic Pr.

Hamel, F., Bailon, J.P. & Bassim, M.N., 1981. Acoustic emission mechanisms during high-cycle fatigue. *Engineering Fracture Mechanics*, 14(4), pp.853-860.

Hastings, W.K., 1970. Monte Carlo sampling methods using Markov chains and their applications. *Biometrika*, 57(1), p.97.

Holford, K.M. et al., 2009. Acoustic emission for monitoring aircraft structures. *Proceedings of the Institution of Mechanical Engineers, Part G: Journal of Aerospace Engineering*, 223(5), pp.525-532.

Huang, M. et al., 1998. Using acoustic emission in fatigue and fracture materials research. *JOM*, 50(11), pp.1-14.

Jazwinski, A.H., 1970. *Stochastic processes and filtering theory*, Academic Pr.

Julier, S.J. & Uhlmann, J.K., 1997. A new extension of the Kalman filter to nonlinear systems. In *Int. Symp. Aerospace/Defense Sensing, Simul. and Controls*. p. 26.

Kaiser, J., 1950. *Investigation of acoustic emission in tensile testing*. Munich, Germany: Technische Hochschule München.

Kalman, R.E., 1960. A new approach to linear filtering and prediction problems. *Journal of basic Engineering*, 82(1), p.35–45.

Kalman, R.E. & Bucy, R.S., 1961. New results in linear filtering and prediction theory. *Journal of Basic Engineering*, 83(3), p.95–108.

McGee, L.A., Schmidt, S.F. & Center, A.R., 1985. *Discovery of the Kalman filter as a practical tool for aerospace and industry*, National Aeronautics and Space Administration, Ames Resarch Center.

Miller, R.K. & McIntire, P., 1987. *Nondestructive testing handbook*, American Society for Nondestructive Testing.

Mix, P.E., 2005. *Introduction to nondestructive testing: a training guide*, Wiley-Interscience.

Modarres, M., Kaminskiy, M. & Krivtsov, V., 1999. *Reliability engineering and risk analysis: a practical guide*, CRC Press.

Moore, N.R. et al., 1992. Probabilistic failure risk assessment for structural fatigue. *Jet Propulsion Laboratory*.

Morton, T.M., Harrington, R.M. & Bjeletich, J.G., 1973. Acoustic emissions of fatigue crack growth. *Engineering fracture mechanics*, 5(3), p.691–692.

Newman Jr, J.C., 1981. A crack-closure model for predicting fatigue-crack growth under aircraft spectrum loading. *Methods and Models for Predicting Fatigue Crack Growth Under Randomloading-Stp 748*, p.53.

Ntzoufras, I., 2009. *Bayesian Modeling Using WinBUGS*, Wiley.

Paris, P. & Erdogan, F., 1963. A critical analysis of crack propagation laws. *Journal of Basic Engineering*, 85(4), p.528–534.

Pollock, A.A., 1988. Practical Guide to Acoustic Emission Testing. *Physical Acoustics Corporation Publication*.

Provan, J.W., 1987. Probabilistic fracture mechanics and reliability. *Martinus Nijhoff Publishers, P. O. Box 163, 3300 AD Dordrecht, The Netherlands, 1987. 467*.

Rabiei, M., Modarres, M. & Hoffman, P., 2009. Probabilistic Structural Health Monitoring Using Acoustic Emission. In Annual Conference of the Prognostics and Health Management Society 2009. San Diego, CA.

Rabiei, M., Modarres, M. & Hoffman, P., 2010. Towards Real-Time Quantification of Fatigue Damage in Metallic Structures. In Aircraft Airworthiness & Sustainment (AA&S 2010). Austin, TX.

Rahman, S. & Rao, B.N., 2002. Probabilistic fracture mechanics by Galerkin meshless methods–part II: reliability analysis. *Computational mechanics*, 28(5), p.365–374.

Rich, T.P., 1977. *Case Studies in Fracture Mechanics.*, Watertown, MA, USA: Army Materials and Mechanics Research Center.

Roberts, T.M. & Talebzadeh, M., 2003. Acoustic emission monitoring of fatigue crack propagation. *Journal of Constructional Steel Research*, 59(6), pp.695-712.

Schütz, W., 1996. A history of fatigue. *Engineering Fracture Mechanics*, 54(2), pp.263-300.

Shantz, C.R., 2010. *Uncertainty Quantification in Crack Growth Modeling Under Multi-Axial Variable Amplitude Loading*. Vanderbilt University.

Shinozuka, M. & Yang, J.N., 1969. Optimum structural design based on reliability and proof load test. *Annals of Assurance Science, Proc. of Reliability and Maintainability*, 8, p.375–391.

Simon, D., 2006. *Optimal State Estimation: Kalman, H Infinity, and Nonlinear Approaches*, Wiley-Interscience.

Talebzadeh, M. & Roberts, T.M., 2001. Correlation of Crack Propagation and Acoustic Emission Rates. *Key Engineering Materials*, 204-205, pp.341-350.

Vachtsevanos, G.J. et al., 2006. *Intelligent fault diagnosis and prognosis for engineering systems*, Wiley Online Library.

Van Der Merwe, R., 2004. *Sigma-point Kalman filters for probabilistic inference in dynamic state-space models*. Citeseer.

Walker, K., 1970. The effect of stress ratio during crack propagation and fatigue for 2024-T3 and 7075-T6 aluminum. *Effects of environment and complex load history on fatigue life*, p.1–14.

Wang, X. et al., 2009. A probabilistic-based airframe integrity management model. *Reliability Engineering & System Safety*, 94(5), pp.932-941.

Wang, X. et al., 2008. A probability-based individual aircraft tracking approach for airframe integrity. In Aging Aircraft 2008. Phoenix AZ.

Welch, G. & Bishop, G., 1995. An introduction to the Kalman filter. *University of North Carolina at Chapel Hill, Chapel Hill, NC*.

West, M. & Harrison, J., 1997. *Bayesian forecasting and dynamic models*, Springer.

Yang, J.N., Salivar, G.C. & Annis Jr, C.G., 1983. Statistical modeling of fatigue-crack growth in a nickel-base superalloy. *Engineering Fracture Mechanics*, 18(2), p.257–270.

Yang, J.N. & Trapp, W.J., 1974. Reliability analysis of aircraft structures under random loading and periodic inspection. *AIAA Journal*, 12, p.1623–1630.